S. Casalbuoni, A.-S. Müller,
and F. Zimmermann (eds)

Beam Tests and Commissioning of Low Emittance Rings

Proceedings ARIES-ICFA Workshop KIT Karlsruhe, 18-20 February 2019

Editorial Series on ACCELERATOR SCIENCE

Institute of Electronic Systems
Warsaw University of Technology — Warsaw 2020

The work is vol. LIV in the Editorial Series on Accelerator Science and Technology.
The series is associated with the EU H2020 ARIES Project — Accelerator Research and Innovation for European Science and Society.
The H2020 ARIES Project is coordinated by CERN. Additional information about the Editorial Series on Accelerator Science and Technology can be found at CERN ARIES web site: https://aries.web.cern.ch/ (Results, Publications) and at the web site of the Warsaw University of Technology Publishing House: http://www.wydawnictwopw.pl.
Previous volumes in the series were published with the EU FP7 Project EuCARD2 — Enhanced European Coordination for European Research and Development: http://eucard2.web.cern.ch/science/monographs.

Cover design

Danuta Czudek-Puchalska

The main cover shows normalised emittances in present, next and next-next generation storage ring light sources. Courtesy R. Bartolini (modified)

Back cover image — group photo in front of the Karlsruhe palace (© KIT Karlsruhe)

ISBN 978-83-8156-030-6

Internet bookshop of the Warsaw University of Technology Publishing House (OWPW):
http://www.wydawnictwopw.pl; e-mail: oficyna@pw.edu.pl
phone 48 22-234-75-03; fax 48 22-234-70-60

Printed and bound by OWPW,
ul. Polna 50, 00-644 Warszawa, Poland, phone 48 22-234-70-30, 1st edition, order no 012/2020

Abstract:

The ARIES Workshop: “Beam Tests and Commissioning of Low Emittance Storage Rings”, was held at the KIT Campus South in Karlsruhe from 18 to 20 February 2019. The workshop, also organized under the auspices of the ICFA Beam Dynamics Panel, was part of ARIES Work Package 7, RULE, and co-supported by ARIES Work Package 6, APEC.

A workshop focus was on beam tests and commissioning of low emittance rings such as MAXIV and SuperKEKB, as well as on preparation procedures, components and tests necessary for commissioning of the upcoming low emittance rings, like ESRF-EBS, SIRIUS, HEPS, ALS-U, PETRA-IV etc. Similarities and synergies with future circular colliders were evidenced.

The present proceedings consist of summaries from the chairs of the seven workshop sessions, which are accompanied by individual contributions.

Preface

From 18-20 February 2019, more than 80 world experts gathered at the Karlsruhe Institute of Technology (KIT) for the ARIES-ICFA Workshop on "Beam Tests and Commissioning of Low Emittance Rings" to discuss the best methods for running-in an utterly complex modern research facility: the low emittance storage ring. Figure 1 shows many of the 84 workshop participants.

This particular ARIES workshop was organized under the auspices of the International Committee for Future Accelerators (ICFA). Researchers hailing from 29 scientific laboratories in 16 countries (Germany: 27, France: 12, Switzerland: 8, USA: 7, Italy: 6, China: 5, Russia: 5, UK: 3, Japan: 2, Poland: 2, Sweden: 2, Australia: 1, Canada:1, Denmark: 1, Korea: 1, Spain: 1) discussed suitable technologies and procedures to master the rising complexity of particle accelerators, in view of the advent of new large-scale facilities with ever-increasing demands on stability and efficiency. Over the next 10 years, most synchrotron light sources around the world will carry out expensive upgrades, and close international networking is becoming increasingly important in this area of science.

Opening speaker Emanuel Karantzoulis from ELETTRA, Trieste, recalled that some experts had thought that the 4th generation light sources would be the FELs. He stressed that no prediction could have been wronger! FELs are complementary but, for the moment, they do not have the high repetition rate, reproducibility and stability required, and they cannot simultaneously serve many beam lines. A whole range of experiments requiring low intensity at the sample and high-repetition rate brought about a renaissance of storage ring light sources. It took 26 years from the pioneering proposal of a multibend achromat lattice to the commissioning of the first of these novel machines.

The new light sources offer higher brilliance (implying a smaller emittance), higher transverse coherence, small photon beam size, small photon beam divergence, and cleaner spectral flux. In addition they might provide short electron pulses (for time resolved measurements) and round beams.

New technologies include high gradient magnets small apertures (100 T/m 12.5 mm), longitudinal gradient dipoles and strong gradient dipoles, advanced short period undulators, NEG pumping (no harm seen for impedance!), fast pulsed kickers and on-axis injection (feedbacks, higher-harmonic cavities, …). A lot of design and technology synergies were evidenced between the next generation of ultralow emittance storage rings, and future low-emittance ring colliders like FCC-ee and FCC-hh. As shown at the workshop, their energy-normalized "invariant optical emittances" are indeed quite comparable.

The workshop featured 37 presentations and 7 summary talks distributed over 8 sessions: 1. Motivations, lessons and projects overview; 2. Injectors and injection; 3. Insertion devices; 4. Diagnostics, controls, automation, and feedbacks; 5. High current effects; 6. Low emittance; 7. Optics design, measurements and correction; and 8. Summary.

These workshop proceedings contain individual contributions from many of the speakers along with summaries from all of the sessions except the one on optics.

Figure 1: Group photo in front of the Karlsruhe palace.

List of ARIES-ICFA Workshop Participants

name	first name	institute
Agapov	Ilya	DESY
Aiba	Masamitsu	PSI
Barabin	Sergey	ITEP
Blednykh	Alexei	BNL
Böge	Michael	PSI
Boltz	Tobias	KIT
Brosi	Miriam	KIT
Bründermann	Erik	KIT
Carmignani	Nicola	ESRF
Carver	Lee Robert	ESRF
Casalbuoni	Sara	KIT
Chaikovska	Iryna	LAL
Chao	Hung-Chun	DESY
Charles	Tessa	U. Melbourne
Cleva	Stefano	ELETTRA
Delerue	Nicolas	LAL
Drago	Alessandro	INFN-LNF
Duan	Zhe	IHEP
Ehrlichmann	Heiko	DESY
Einfeld	Dieter	ESRF
Emery	Louis	ANL
Fernandes Tavares	Pedro	Lund U.
Gamelin	Alexis	SOLEIL
Ghasem	Hossein	DIAMOND
Grau	Andreas	KIT
Gurov	Sergei	BINP
Härer	Bastian	KIT
Hagelstein	Michael	KIT
Han	Jang-Hui	PAL
Hellert	Thorsten	LBNL
Huttel	Erhard	KIT
Iriso	Ubaldo	ALBA-CELLS

List of ARIES-ICFA Workshop Participants cont'd

name	first name	institute
Ji	Daheng	IHEP
Kallestrup	Jonas	PSI
Karantzoulis	Emanuel	ELETTRA
Keil	Joachim	DESY
Koval	Adam	U. Dundee
Krecic	Stefano	ELETTRA
Kubytskyi	Viacheslav	LAL
Kuske	Peter	HZB
Lindberg	Ryan	ANL
Liuzzo	Simone Maria	ESRF
Loulergue	Alexandre	SOLEIL
Malygin	Anton	KIT
Marendziak	Andrzej	NSRC Polaris
Martin	Ian	DIAMOND
Meshkov	Oleg	BINP
Mexner	Wolfgang	KIT
Mezentsev	Nikolay	BINP
Milardi	Catia	INFN-LNF
Mochihashi	Akira	KIT
Müller	Anke-Susanne	KIT
Nagaoka	Ryutaro	SOLEIL
Nielsen	Jørgen S.	Aarhus U.
Nuel Gavaldà	Xavier	DESY
Ohmi	Kazuhito	KEK
Papash	Alexander	KIT
Qin	Qing	IHEP
Richter	Sebastian	CERN/KIT
Riemann	Bernard	PSI
Ruprecht	Robert	KIT
Saez de Jauregui	David	KIT
Sajaev	Vadim	ANL
Scafuri	Claudio	ELETTRA

List of ARIES-ICFA Workshop Participants cont'd

name	first name	institute
Schlott	Volker	PSI
Schreiber	Patrick	KIT
Schuh	Marcel	KIT
Smaluk	Victor	BNL
Steinmann	Johannes	KIT
Tarawneh	Hamed	MAX IV Lund U.
Tian	Kai	SLAC
Tordeux	Marie-Agnes	SOLEIL
Torino	Laura	ESRF
Wawrzyniak	Adriana	NSRC Polaris
Wesolowski	Pawel	KIT
White	Simon	ESRF
Xu	Gang	IHEP
Xu	Haisheng	IHEP
Yamamoto	Naoto	KEK
Zhang	Jie-Xi	DESY
Zimmermann	Frank	CERN
Zisopoulos	Panagiotis	CERN

Table of Contents

7. Optics Design, Measurements and Correction

*A paper was not submitted to the proceedings. However, the slides presented are available in electronic form at *https://indico.cern.ch/event/772326/contributions/3318431/*.

Session 1: Projects Overview

Summary: Motivations, lessons and projects overview I

D. Einfeld
ESRF, Grenoble, France

***Abstract*—This is a summary of the first part of the session entitled "Motivations, Lessons and Projects Overview".**

***Keywords*—Fourth generation storage rings, Multi-Bend-Achromat, Accelerator Commissioning**

I. Introduction

The subsection included a presentation describing the steps from the 3rd to 4th Generation light source:

- From 3rd to 4th Generation light sources – Emanuel Karantzoulis (Elettra Sincrotrone Trieste) The lessons learnt during the commissioning of the first 4th Generation Light Source Max IV:
- Lessons learnt from MAX IV – Pedro F. Tavares (MAX IV - Lund)

Two presentations about the plans for the commission-ing of the 4th Generation light sources ESRF-EBS and SLS-II:

- Baseline system specifications for Low Emittance storage ring commissioning – Michael Boege (Swiss Light Source)
- Commissioning strategies and plans for the ESRF-EBS – Simone Luzzio ESRF)

II. From 3^{rd} to 4^{th} Generation Light Sources – Emanuel Karantzoulis (Elettra Sincrotrone Trieste)

- Generations and characteristics: 36 light sources do exist with energies from 0.5 to 8 GeV and circumference from 50 to 2300 m.
- The 3^{rd} generation light sources are based on 2 and 3 Bend Achromat's, large dynamic aperture, non complicated, non-linear dynamics, mainly off – axis injection (kicker bumps), easy and fast commissioning, most used boosters, fewer Linac as main injec-tors, top up injection, etc. The emittance of the 3rd generation light sources is larger as 1 nmrad. In general the 3rd generation is very successful and very productive.
- The 4^{th} generation light sources are based on Multiple Bend Achromat's with 5 to 7 and more bending magnets in an achromat in order to reach emittance down to 100 pmrad and if possible going in the direction of a Diffraction Limited Storage Ring (DLSR). For a DLSR an emittance of 16 pmrad is required for a photon energy of 12.4 keV (1 Å).
- The types of lattices of the "Diffraction Limited Storage Rings (DLSR)" are:
  - Multi-Bend-Achromat, detuned theoretical minimum emittance (TME) cells with small dynamic apertures
    TME: MAX IV, SIRIUS, ALS-U
    TME + Reversed Bends + Longitudinal Gradient Bends LGBs: SLS II
  - H-MBA (Hybrid)
    LGBs +Dx bump + paired sextupoles
    HMBA: ESRF- EBS
    HMBA + Reversed Bends: APS-U, IHEPS
  - M-MBA (Modified)
    With mid – straights sections in the arcs with M = even
    Elettra 2.0 (S6BA), Diamond II, SLiT-J, KEK-LS
  - M-MBA + Revers + LGBs
    Final version of Elettra 2.0 lattice (S6BA-E)
- The present status of the different DLSR projects are:
  - MAX IV in operation (250 mA in top up)
  - ESRF off in Dec 2018 for installation; back in operation summer 2020
  - Sirius (Brazil) under construction; commissioning 2019
  - Elettra 2.0 and SLS-II completed CDR by 2017
  - Elettra 2.0 project financed by the government 2018
  - APS-U (US) has passed CD2
  - ALS-U, HEPS (China) got money for R&D programms
- Challenges of the DSLR projects:
  - Accelerator engineering: magnets
  - Needed tools for optimization of DLSR lattices
  - Off (On)-axis injection route
  - Longitudinal (on-axis) injection
  - Short pulses, why SR
  - Controlling the electron pulse
  - Round beam

III. Lessons Learnt from MAX IV – Pedro F. Tavares (MAX IV)

- 3 GeV Ring achieved performance:
  - 500 mA stored current in multibunch mode demostrated during accelerator studies
  - Regular delivery to beamlines at 250 mA (RF power limitations)
  - 9 mA stored current in single bunch
  - 20 Ah lifetime×current from gas scattering
  - 90% injection efficiency
  - Emittance: $\epsilon_x = 32{\pm}18$ pmrad;$\epsilon_y = 6.5{\pm}0.1$ pmrad

- RMS orbit stability (up to 100 Hz) better than 1.3/5.5% of beam size (H/V)
    - Beta beats $< \pm 2\%$
    - Residual Vertical Dispersion < 0.6 mm RMS
- Commissioning Challenges / Our share of pain:
    - Beam commissioning was preceded by a comprehensive sub-system test campaign.
    - Most sub-system issues were discovered and solved early on during subsystems test, but a few could only be addressed at the very end of sub-systems tests or even early into the beam commissioning phase
    - Main commissioning challenges were related to "simple" problems that risked a slow down progress rather than fundamental issues.
- Things that went particularly well:
    - Several turns obtained with all correctors OFF.
    - Vacuum Chamber Conditioning was fast.
    - Accumulation with single kicker (no closed bump).
    - Accumulation with Multipole Injection Kicker (MIK) gave just as high a stacking rate.
    - No magnet polarity errors in initial commissioning, despite some initial suspicions.
- Lessons Learned Summary:
    - Invest time and effort in sub-system testing prior to beam commissioning.
    - Perform subsystem-tests as much as possible using the final control system configuration and GUIs. Use subsystem-tests as an opportunity to drive the control system development and deployment schedule.
    - Design subsystem tests to reproduce as much as possible real operating conditions.
    - Allow time for correcting errors found during those tests.
    - Make sure radiation safety understands and agrees to the commissioning.
    - Allow plenty of time for RF cavity conditioning.
    - Have spare parts on-site during commissioning.
    - Have an on-line model of the accelerator for quick testing.
    - Be ready to improvise.

IV. BASELINE SYSTEMS SPECIFICATIONS FOR LE STORAGE RING COMMISSIO-NING - MICHAEL BOEGE (SWISS LIGHT SOURCE)

- For the Commissioning 5 phases can be identified:
    - Phase 0: before commissioning (time of final system installation and alignment).
    - Phase 1: injection into LE ring / getting stored beam.
    - Phase 2: characterization of LE ring using stored beam at low current $\rightarrow$ realignment to optimize the alignment error distribution in favor of machine performance.
    - Phase 3: commissioning with multi-bunch filling and high current.
    - Phase 4: commissioning of systems vital for user operation (Fast Orbit Feedback) running at design parameters.
    - Phase 5: after commissioning (insertion device and beamline commissioning) and final operation with friendly users.
- Phase 0: before commissioning (time of final system installation and alignment):
    - One main prerequisite for going through phase 1 is a LE ring within specifications (magnets and alignment), correct cabling.
    - Measurement of BPM to Quadrupole offsets after final alignment.
    - Check of the correct polarity of all magnets and search for forgotten or wrong magnet cabling.
- Phase 1: injection into LE ring / getting stored beam:
    - If some beam can be stored, characterization and correction of the LE rings optics, BBA and orbit correction can be immediately done $\rightarrow$ Phase 2.
    - If NOT.... Try as much as you can by playing with the different elements and going from sector to sector around the machine to get a stored beam.
- Phase 2: characterization of LE ring using stored beam at low current:
    - Tune measurement.
    - Average beta function measurement.
    - Measurement of amplitude dependent tune shifts
    - LOCO based on BPM / corrector response matrices
    - Betatron coupling / dispersion minimization with dedicated skew quadrupoles
    - Orbit Feedback (Hz) for orbit standardization (zero orbit = golden orbit)
- Phase 3: commissioning with multi-bunch filling and high current:
    - Filling pattern and commissioning of FP feedback.
    - Top-up operation by doing frequent injections with small single bunch currents.
    - Commissioning of multi-bunch feedbacks.
    - Harmonic cavity tuning for bunch lengthening $\rightarrow$ lifetime improvement.
    - Longitudinal bunch profile characterization with streak camera.
    - Orbit noise identification with BPMs running in narrow bandwidth (a few kHz) mode (power spectral densities) $\rightarrow$ preferable noise suppression by source suppression.
    - Final commissioning of the BPM system for preparation of the first Fast Orbit Feedback operation.
    - Commissioning of the first photon monitors (PBPMs)
    - Measurement of open loop transfer functions of fast correctors $\rightarrow$ determine bandwidth limitations of the correction system.
- Phase 4: commissioning of systems vital for user operation / running at design parameters:
    - Correction up to > 100 Hz (0 dB point) $\rightarrow$ a few BPM bandwidth.
    - Suppression of all ID induced orbit distortions ($\sim$ typically a few Hz, transparent ID operation.

- Suppression of residual noise (typically LS have $< 1\mu$m orbit stability!).
- Reference orbit manipulations for ID's (Demands for "Fast Orbit Feedback").

- Phase 5: after SR commissioning, beamline commissioning and finally operation with user:
  - Creation of ID Feed Forward tables keeping photon beam stable during ID operation.
  - Correction of local beta beat induced by ID operation (tune stabilization).
  - Operation of fast ($\sim$Hz) tune feedback acting on tuning quadrupoles.
  - PBPM based photon position feedbacks to stabilize the photon beam in the beamlines on the sample (sacrifice electron orbit stability!)
  - Operation with friendly users (close collaboration between machine and beam line in order to achieve the ultimate stability)
  - Consolidation of procedures in order to allow for 24/7 beam operation, fast machine setup and refilling.

V. COMMISSIONING STRATEGIES AND PLANS FOR ESRF-EBS - SIMONE M. LU-ZIZO (ESRF)

The next 4th Generation Light Source which goes into operation is the upgrade of the ESRF (ESRF-EBS). The ESRF was switched off in December 2018 and the commissioning will start one year later in December 2019. In March 2020 will start the operation for friendly users and the user operation begins in August 2020.
The goals of the machine commissioning are:
A) Hardware set up, tuning and conditioning for the booster synchrotron and the storage ring, as well
B) Reach best possible beam parameters.

- Hardware set up, tuning and conditioning: Magnets, RF, vacuum, diagnostic, timing, absorbers, collimators, etc.
- Reach best possible parameters: emittance, injection efficiency, lifetime stability, Mean Time Between Failure (MTBF) , etc.

The commissioning steps are divided in "Low Current" and "Ramp Current":

- Low Current: Make first turn: orbit steerers, tune correction, few turns $\rightarrow$ RF on, SY-SR RF, beam accumulation, orbit, tunes, BPM-QUAD offsets, chromaticity, response matrix (optics/coupling), close collimators/optimize losses.
- Ramp Current: Implement SB, 2PW optics adaptations, ID commissioning, bunch-by-bunch feedback, optimize injection efficiency as soon as possible, optimize lifetime, high-current per bunch.

Beam Parameters Goal:
A) Parameters ensuring that no major problem remain in the new hardware or tuning of the new machine. Goal: to be exceeded by 01-March-2020. Parameters have to be achieved simultaneously.
B) Parameters that could allow "comfortable" USM operation. Goal: to be exceeded by 24-August-2020.
C) Design EBS parameters. Goal: to be exceeded by Dec 2021.

TABLE I
BEAM PARAMETERS GOAL OF ESRF-EBS.

	A)	B)	C)
Total current	> 50 mA	200 mA	200 mA
MTBF	> 12 h	> 30 h	> 50 h
Up-time	$> 90\%$	$> 95\%$	$> 97\%$
Inj. Eff.	$> 50\%$	$> 70\%$	$> 80\%$
Lifetime	> 5 h	> 10 h	> 20 h
H emittance	< 250 pm	< 150 pm	~ 135 pm
V emittance	< 50 pm	< 20 pm	< 10 pm
Stability	$< 0.2\ \sigma$	$< 0.1\ \sigma$	$< 0.05\ \sigma$

Summary: Motivations, lessons and projects overview II

P. F. Tavares
MAX IV Laboratory, Lund, Sweden

***Abstract*—This is a summary of the second part of the session entitled "Motivations, Lessons and Projects Overview".**

***Keywords*—4th generation storage rings, MBA, accelerator commissioning.**

I. Introduction

The subsection included presentation describing plans for commissioning of new storage rings that are currently in the design stag, all using variants of the multi-bend achromat lattice in order to achieve ultra-low emittances.

- Commissioning strategies and plans for APS-U – Louis Emery (ANL)
- Commissioning strategies and plans for ELETTRA2 – Emanuel Karantzoulis (Elettra)
- Lattice design, commissioning and operation challenges for PETRA IV - Joachim Keil (DESY)
- Simulation of HEPS storage ring commissioning – Daheng Ji (IHEP)

Common to all of these presentations is that the current plans foresee commissioning (up to a level where beamline commissioning is possible) in a time similar to 3rd generation sources ($\sim$ 3 months), despite tighter optics and on-axis injection schemes. It is also clear that new tools will be needed for commissioning before first turn is achieved: BPM offsets, optics correction, etc. In the next section, we highlight specific aspects of each presentation.

II. Commissioning Strategies and Plans for APS-U – L. Emery (ANL)

- Roughly 3 months commissioning will be required achieve 50-100 mA.
- Not fully operational longitudinal feedback / Harmonic Cavity systems in initial stages.
- No partial installations: make efficient use of beam time.
- IDs installed already during early commissioning (considered to be low risk).
- Diagnostics to be made ready as much as possible before introducing beam.
- Time for commissioning diagnostics along with beam or beam optics.
- Dealing with the extracted beam presents a challenge.

III. Commissioning Strategies and Plans for ELETTRA2 – E. Karantzoulis (ELETTRA)

- History: ELETRA 1 commissioning was very fast.
- For ELETTRA 2:
  - Downtime limited to 18 months (14 months for the accelerator)
  - Dissassembly in 4 months (partly overlap with installations)
  - Accelerator Commissioning in 3 months
  - Beamlines and Accelerator commissioning in parallel in the last 3 months
  - Long time for vacuum conditioning (100 A.h)
  - Magnet quality is crucial.

IV. Lattice Design, Commissioning and Operation Challenges for PETRA IV – J. Keil (DESY)

- On-axis swap-out injection
- Start-up procedure simulations indicate too tight alignment tolerances (5-10 μm) would be needed without corrections. Procedure includes:
  - All elements with independent normally-distributed errors.
  - Stepwise increase of sextupoles + octupoles.
  - Single pass correction of trajectory for each step.
  - After ramp: tune + orbit correction.
  - Assumptions: Initial threading can be done; tune & orbit can be determined from TBT data (without stored beam).
- Stability Challenges: Tunnel temperature, emittance change due to IDs, injection perturbations.
- Stability Challenges: Tunnel temperature, emittance change due to IDs, injection perturbations.
- Dealing with the extracted beam presents a challenge.

V. Simulation of HEPS Storage Ring Commissioning - Daheng Ji (IHEP)

- Commissioning simulations foresee 4 stages
- Stage 0: Beam Accumulation
- Stage 0.5: Transition
- Stage 1: Good beam performance (high current)
- Stage 2: IDs
- At start-up: 100 μm quad alignment error, BPM errors (incl. offset) up to 600 μm. Iterative procedure to get first turn and ten many turns.
- In simulation, BBA allows reduction of BPM offsets to 30 μm.
- Conventional optics correction complemented by physically moving sextupoles (sextupoles on movable stands).

- Compromise with vibrational stability deemed acceptable.

Summary: Motivations, lessons and projects overview III

Q. Qin
IHEP, China

***Abstract*—This is a summary of the third part of the session enti-tled "Motivations, Lessons and Projects Overview".**

***Keywords*—Assembling, large low-emittance ring, preparation, commissioning, operation.**

I. Introduction

Two presentations are included in the subsection, focusing on the magnets and vacuum chamber assembling of ESRF-EBS, and beam commissioning and operation of low emittance rings at CERN, LEP & LHC.

- Lessons learned from the ESRF magnets and vacuum chamber assembling – Sergei Gurov (BINP)
- Commissioning Large Low-Emittance Rings: LEP and LHC – Frank Zimmermann (CERN)

General comments on preparation of low emittance rings: magnets and vacuum chambers assembly in one girder, careful installation, tests for individual element and each sector of the machine, software check, are all important to the smooth commissioning on first beam and early operation, and can greatly reduce the time of pre-operation.

II. Lessons Learned from the ESRF Magnets and Vacuum Chamber As-sembling (S. Gurov, BINP)

- An MBA lattice consists of large number of magnets, with various kinds of nth-pole, permanent and electro-magnets, in one normal cell. The ESRF-EBS cell has 34 magnets in total, which means a very tight space between magnets along the cell. Crosstalk of magnets need to be concerned.
- Before assembling, careful preparations, such as storage places and assembly areas with well-arranged schedule, are necessary.
- Pre-installation with higher accurately measurement and check, well designed templates for magnet and well-packaged assemblies will help the assembly efficient and safe.
- The temperature control at the assembly areas is crucial to the quality of assembling.
- Magnets need to be aligned at each girder first, and girders should be surveyed after magnets are installed.
- Surveyor team participates the assembly of vacuum chambers.
- To purchase components, including thermo-switches, electrical terminal blocks, and hoses, for all magnets at once or at least define its in technical specifications, is helpful to assembly and installation.

III. Commissioning Large Low-Emittance Rings: LEP and LHC (F. Zimmermann, CERN)

- Well-prepared hardware and software before the LEP commissioning before 30 years ago ensured that only one month was spent from the single turn of the first beam up to the first stable beam for physics experiment.
- The experience of LEP commissioning is a good refer-ence to any future lepton collider like FCC-ee or CEPC.
- Software, commissioning procedures, planning and tests are main preparation work for LHC commissioning.
- The control system was tested on the other machines of CERN before the LHC commissioning.
- The stable operation team has experiences from LEP, which consists of physicists, engineers and operators, is well trained and knows the limit of the machine, obtaining and sharing experiences during operations.
- Different from lepton machine, the LHC commissioning relies on more hardware preparations, with an availability much less than light sources.

Commissioning strategies and plans for ESRF EBS

Simone Liuzzo
ESRF, Grenoble, France

***Abstract*—This paper lays out the list of actions that will be taken during ESRF-EBS beam commissioning. The planning will also be addressed.**

***Keywords*—Beam; commissioning; optics; planning**

I. General strategy

The strategy for commissioning the ESRF-EBS [1] upgrade is set as follows. Initially re-commissioning of electron gun, linac, transfer lines and booster will take place. Hardware will be tested and commissioned, followed by injectors timing and injectors beam commissioning. Concerning the Storage Ring tuning the procedure will be divided in two parts as follow:

itemize

Low current

- make first turn : orbit steerers, tune correction
- few turns, RF on, SY-SR RF, beam accumulation
- orbit, tunes, BPM-QUAD offsets, chromaticity
- response matrix (optics/coupling)
- close collimators / optimize losses

Ramp current

- implement SB, 2PW optics adaptations
- ID commissioning -by-bunch feedback
- optimize injection efficiency as soon as possible
- optimize lifetime
- high-current per bunch

A. Injectors

Booster tuning will be initially aimed to extract beam only, without optimizations. The lattice will be shorter to match the length of the new storage ring. To reduce the emittance the working point will be changed and operated off energy (40kHz). Timing of RF, pulsed magnets, injection and extraction will have to be revisited. Cleaning will have to be restored by the end of commissioning.

B. Injection in the Storage Ring (SR)

Injection into SR (see figure 1) will be initially aimed to inject beam only, without optimization. Pulsed elements timing/synchronization will have to be redefined. Transfer line booster to storage ring will require steering, alignment and optics matching. Tuning of S1-2 S3 septa and kickers strengths for injection will be performed along with the search for first turns. Figure 1 shows the injection layout, and it is possible to see that 2 sextupoles are inside the injection bump. Perturbation damping will take place using among others, sextupole correctors.

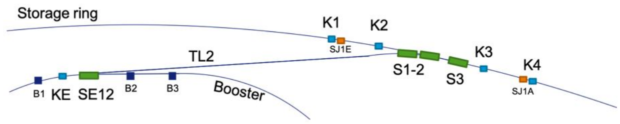

Fig. 1. Layout of extraction from booster and injection in storage ring.

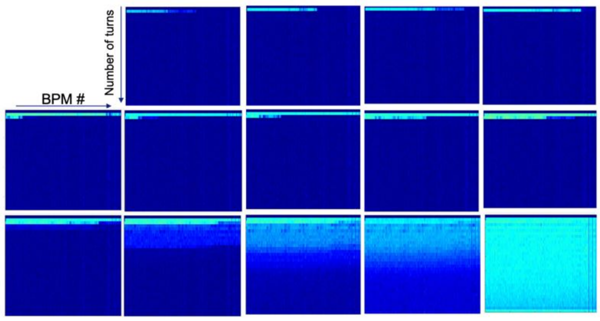

Fig. 2. Measurements during first turn search in the ESRF storage ring (2018).

C. Low current

1) Beam accumulation: Injection on axis (static bump) or off axis (fit injected beam oscillation) will be possible. The plan is to start from injection off axis. To obtain first turns, we power orbit steerers to achieve first turn. From simulations, beam survives about 3-4 cells without orbit steering, if magnets and alignment are within tolerances. During this procedure we established tools to check for quadrupole and steerer polarity or calibration errors. Once a few turns are available, an initial measurement of tune (most relevant for off-axis injection) will be possible. Once 50 turns are obtained, RF will be switched on to search for correct frequency and phase, until beam accumulation is reached.

2) Test and measurement of first turns: Several test where performed with the old ESRF storage ring to establish first turns in increasingly realistic conditions. Figure 2 shows the evolution of the measurement form less than one turn, to beam accumulation (RF already set).

The EBS control system simulator is being used with great profit to prepare these measurement.

3) Optics tuning: Once a few mA are stored in the storage ring response matrix measurement and beam-based alignment will take place.

A scan for the optimal tune working point will also be performed to find optimal emittance and lifetime. Chromaticity will be measured and corrected.

Dynamic aperture will also be measured to compare with the model and help solve possible issues.

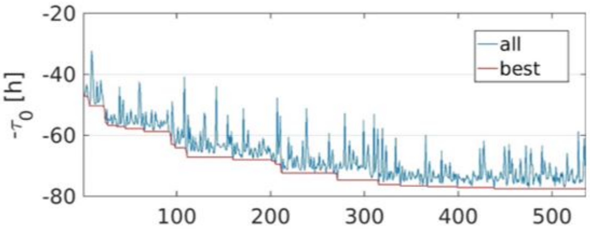

Fig. 3. Optimization of lifetime in the ESRF storage ring (2017).

Specific optics tuning as the measurement and correction of phase advance between sextupoles will also be put in place.

Losses tuning using the collimators will take place when needed while ramping current to keep 80% of the losses located on the collimators.

The installation of 2-pole wiggler and Short Bend magnets will follow the description in [2].

Fast orbit feedback and bunch-by-bunch feedback will be put in operation as early as possible to speed up current ramp and vacuum conditioning.

High current per bunch modes will be prepared for operation before user service mode starts.

Impedance and collective effects characterization will be performed as soon as possible.

Top-up and injection perturbations will be also soon in place to help with vacuum conditioning and beamlines commissioning.

ID commissioning will look at the impact of gaps closure on closed orbit, losses and emittances as soon as possible, in particular starting from in-vacuum undulators.

Injection efficiency and lifetime require online optimization, as shown in figure 3. Many knobs allow large room for optimization but also need a very long time. Automated optimizers and resonance correction knobs will be available, as today. Lifetime optimization will profit from the beam loss detectors measurements.

D. Planning

Fully dedicated beam commissioning will last about 3 months see Figure 4. 12h/day and 5days/week are considered. Extra hours and weekends are kept as buffers. Proper shutdown period for interventions are included in the planning. The present time dedicated to commissioning is in line with the programme.

Minimal goal for the commissioning is to achieve beam parameters compatible with the beamlines commissioning needs. Intermediate goals are described in Figure 5. Beam commissioning will continue in shared mode during the 5 months of beamlines commissioning with 3 dedicated 8hrs shifts/week.

REFERENCES

[1] "ESRF upgrade programme phase II", ESRF, December 2014.

[2] S.M. Liuzzo, et al., "Optics Adaptations for Bending Magnet Beam Lines at ESRF: Short Bend, 2-Pole Wiggler, 3-Pole Wiggler", MOPIK062, IPAC'17, Copenhagen, Denmark (2017).

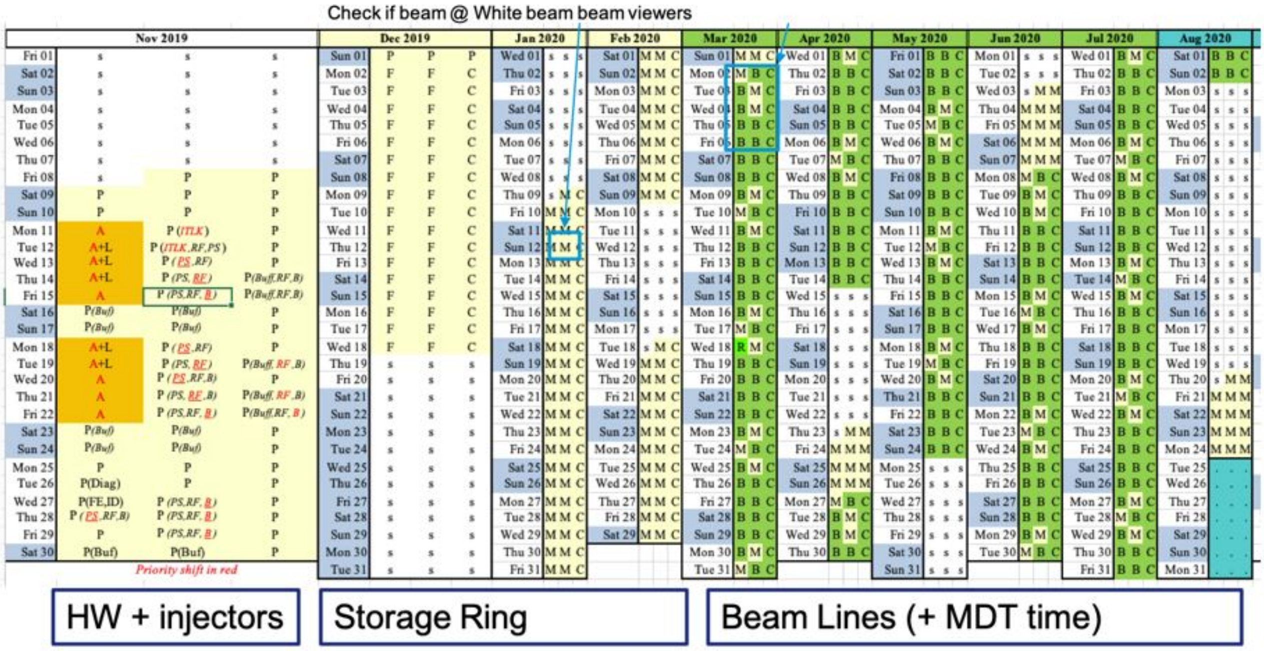

Fig. 4. Commissioning planning.

to be exceeded by	01-March-2020	01-March-2020	01-March-2020
Total current	> 50 mA *	200 mA	200 mA
MTBF	> 12h	> 30h	> 50h
Up-time	> 90%	> 95% **	> 97%
Inj. Eff.	> 50%	> 70%	> 80%
Lifetime	> 5h	> 10h	> 20h
H emittance	< 250 pm	< 150 pm	~ 135 pm
V emittance	< 50 pm	< 20 pm	< 10 pm
stability	< 0.2 σ	< 0.1 σ	< 0.05 σ

Fig. 5. Commissioning minimal parameters.

Commissioning Plan for APS-U

Louis Emery
Argonne National Laboratory

***Abstract*—Though the beam commissioning of the Advanced Photon Source Upgrade (APSU) is planned for March 2023, we make some initial preparations and adopt some principles in order to assure the completion of beam commissioning under a schedule of three months. We give an overview of the critical or novel features of the ring that produce commissioning challenges. We list the requirements for commissioning, and the beam activities during commissioning.**

***Keywords*—IEEEtran, journal, LaTeX, paper, template**

I. Introduction

THE Advanced Photon Source Upgrade (APSU) consists of a hybrid 7-bend achromat (Hybrid 7BA) derived from a concept originated from the ESRF upgrade [1], a cell of which is pictured in Figure 1 The cell includes several weak reverse bends [2], [3] to control the dispersion and further reduce the emittance from 67 nm to 42 nm. Commissioning with beam is the gradual introduction of beam around the magnetic lattice, following conventional methods. APS-U has however many novel and challenging aspects, which require special attention during commissioning and which we will cover here.

We state our goals for the 3 months of commissioning, then make some generalization of our approach. We require almost all equipment to be ready in advance of beam commissioning, which is not too surprising. We finally give a list the commissioning activities themselves, pointing out the ones that distinguish the APS-U.

II. Challenging aspects of ring

The quadrupoles and sextupoles are necessarily very strong and trajectory and orbit needs to be corrected in a bootstrap manner. See [4] for an overview of the algorithms.

The injectors are required to produce a 17-nC pulse to swap out the 4.2 mA bunch stored in APS-U. The booster emittance of 60 nm, even with -0.6% momentum error, is relatively large compared to the SR aperture. The booster will be upgraded before the dark time with a frequency ramp that will vary during the energy ramp to meet the circumference requirement at each end of cycle and to target one of the 1296 rf buckets in the ring.

On-axis “swap-out” injection [5]–[7] is an alternative to accumulation. Each injector shot replaces an existing stored bunch. A pre-kicker for inflating the target stored bunch will pulses 50 turns before extraction. The bunch inflation is required to prevent beam dump damage from the expended beam.

Work supported by the U.S. Department of Energy, Office of Science,Office of Basic Energy Sciences, under Contract No. DE-AC02-06CH11357.
(e-mail:lemery@anl.gov)

To prevent the whole stored beam from damaging the vacuum chamber the positioning of the collimators and beam dumps is critical. There are five horizontal collimators for Touschek scattering in the rf and injection sectors. Whole beam aborts (4400 J), will most certainly damage surfaces and the collimators will require refreshment. There are vertical beam bumps for absorbing 17 nC (100 J) bunches from swap out. The vertical beam dumps also absorbs bunch-by-bunch “slow” beam aborts with pre-kicker.

III. Goals for the 3 Months of Commissioning

We want to achieve at least the threshold “Key Performance Parameters” but plan to do a little more than that in the 3 month of commissioning. We would like to make beam available for any beam line ready to take it during that time. We would also prepare for operations in the last week of commissioning. The full 200 mA is not expected at end of three months, perhaps only 50 to 100 mA.

IV. Principles for scheduling and commissioning

In order to make beam time efficient there should be no partial installations, i.e. all equipment should have been tested/commissioned without beam. For example, the IDs are to be installed with gaps open or powered off for the initial low-charge beam tests, as risk for damage is thought to be low. This is to avoid commissioning pauses for their installation. In the detailed plan, we would interleave time between optimizing diagnostics performance and commissioning beam optics. We specify threshold currents or charge for different phases of commissioning, e.g. small amounts of charge that should be safe to dump anywhere or sufficient current to make some measurements. We give time for beamlines to take synchrotron light near end of commissioning period. We select a fixed day (maybe two) of the week for tunnel intervention if necessary. Two control room operators (technicians) would be on shift, with possibly a third one qualified for searches. And finally two physicists per shift on most shifts.

V. Equipment requirements before beam time

Essentially we ask that all equipment be installed before beam time. To be specific: complete vacuum system installed and vacuum $<$ 10 nT N2 equiv. including HHC and LBF kicker cavities; all magnets and power supplies; main rf system and 12 cavities ready to support the range 15 to 50 kW/cav; injection kickers (striplines) and DC septum; booster to storage ring synchronization system operational; much of the diagnostics, which are: all bpms ready to report single pass and turn-by-turn for, say, 1 nC, beam current monitors, tune measurement system, H and V diagnostics kickers, and

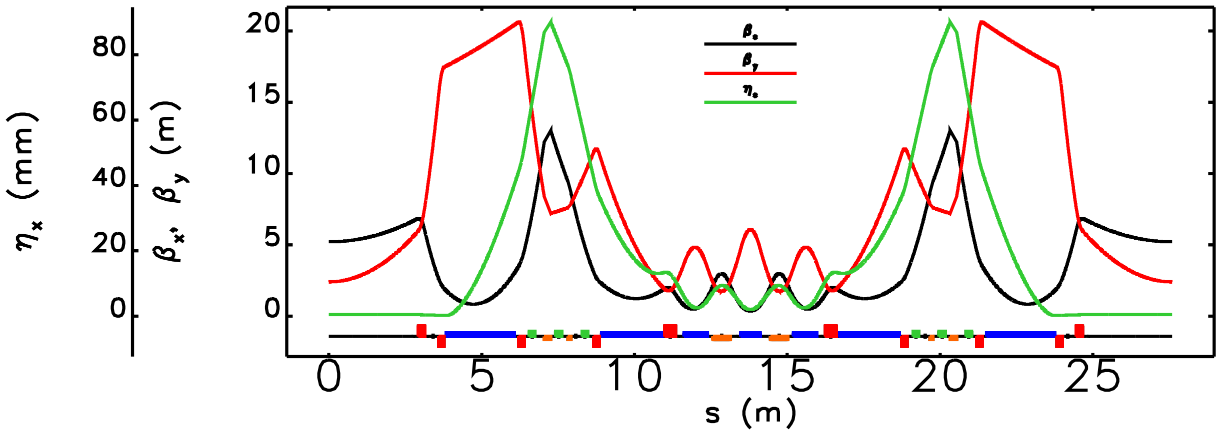

Fig. 1. Hybrid 7BA lattice with reverse bends for the APS. The natural emittance is 42 pm. Blue blocks represent normal-direction dipoles, orange blocks represent reverse-direction dipoles, red blocks represent quadrupoles, and green blocks represent sextupoles. Courtesy M. Borland

BTS (transfer line) emittance diagnostics. In terms of software: control system for all of the above plus vacuum, water, tunnel temperature, etc.; alarm handlers; high-level applications to be reviewed, re-written or created.

We ask that all IDs to be installed and aligned, including the SC undulators and SC HHC, which should be cooled down. The ID gap/current control would be needed ∼1 month into commissioning. The decoherence kicker and swap-out system should be ready to validate with beam. A rudimentary way of doing slow orbit feedback using rf bpms (e.g. workstation) should be ready. Other requirements are: tunnel air regulation of at least 2 deg F; vacuum chamber water cooling operational; data loggers for EPICS PVs running; beam swap-out and abort systems operational; beam dumps and collimators installed, inserted to nominal positions; synchrotron light monitor ready to show a beam image.

Once stored beam has been achieved, we require: orbit feedback ready to operate at some reasonably high bandwidth (say 100 Hz) using the rf bpms; beam-position limits detectors fully validated ; rf system conditioned and ready to support high beam current ramp; beam size monitor ready to resolve 0.4 pm vertical emittance and to confirm 42 pm horizontal emittance; rf cavity low-level control ready for current ramp up; x-ray bpms operational; hydrostatic leveling system operational; HHC ready to support ramp up to full beam current; Transverse and longitudinal bunch-by-bunch feedback ready for commissioning with beam.

VI. Beam time activities

The beam time activities, taking 3 months, are separate tasks completed roughly in sequence. The first tasks are single bunch injection and storage, then followed by multiple bunch injections and stores. For single bunch: verify booster functioning after dark time; commission new BTS line (trajectory only); first turn (plus rf bpm check-out), multiple turn trajectory, stored beam, one bunch; shielding validation with injected beam spills; characterize lattice (rf bpm offsets, which is critical for optics correction); swap out single bunch; position the vertical and horizontal collimators; fine-tune the optics of the new BTS line (the booster emittance is not small compared to SR aperture); Booster-SR synchronization (booster running with frequency ramp for selecting buckets and for lower emittance);

For multiple bunches, store beam in many bunches (>10 mA); ramp current for vacuum conditioning; characterize lattice (same as before but with higher current, measure lifetime and losses); test all undulator beams with shutters closed to setup feedforward orbit and tune corrections; fast orbit feedback; photon diagnostics; emittance-ratio (coupling) control; test various bunch patterns; HHC cavity check-out for some voltage generation; transverse feedback operational; longitudinal feedback operational, single rf system; bremsstrahlung shielding validation for beamlines; undulator beams for beamline checkout; HHC operational for some bunch pattern and current (optional).

VII. Conclusion

We presented the general goals and principles of APS-U beam commissioning with critical items identified. We provided a list of system readiness requirements and beam activities. Future preparations include more accurate time table of current ramp, say, from doing a vacuum conditioning simulation (see ESRF's contribution of this proceedings), and developing shift-by-shift calendar schedule, similar to ESRF's for Dec 2019.

Acknowledgment

The commissioning requirements list were created originally by M. Borland and V. Sajaev. Thanks to M. Borland, G. Decker and R. Connatser for discussions.

References

[1] L. Farvacque et al, *Proc. of 2013 PAC*, 2013, p. 79.
[2] J. Delahaye and J. P. Potier, *Proc. PAC89*, 1990, pp. 1611–1613.
[3] A. Streun, *NIM A*, vol. 737, pp. 148–154, 2014.
[4] V. Sajaev, *These proceedings*.

[5] E. Rowe *et al.*, *Part. Accel.*, vol. 4.
[6] R. Abela *et al.*, *Proc. EPAC 92*, 1992, pp. 486–488.
[7] L. Emery and M. Borland, *Proc.of PAC 2003*, 2003, pp. 256–258.

Lattice Design, Commissioning and Operation Challenges for PETRA IV

Joachim Keil
Deutsches Elektronen-Synchrotron DESY, Hamburg, Germany

***Abstract*—For the upgrade of the 6 GeV storage ring PETRA III into a diffraction limited storage ring PETRA IV different lattice options, the impact of collective effects, and error tolerances have been studied. The emittance of PETRA IV is in the range of 1030 pmrad and would be two orders of magnitude smaller compared to the natural emittance of 1.3 nmrad of PETRA III now. With such an ultra-small emittance the machine would be nearly diffraction limited at a wavelength of 1 Å. The status of the lattice design, collective effects, and commissioning and operational challenges of PETRA IV are presented and discussed.**

***Keywords*—PETRA IV; diffraction limited storage ring**

I. Introduction

The 6 GeV synchrotron radiation source PETRA III is in operation since 2009 [1]. With a natural emittance of 1.3 nmrad the machine has currently the smallest emittance of all synchrotron radiation sources in the energy range of 6 GeV and above. PETRA III is routinely running in top-up mode with a beam current of 100 mA and a current variation of 1%. Two different filling patterns are in use: In the continuous mode 960 (or 480) bunches are filled and in the timing mode 40 bunches. The typical lifetime in continuous mode is 10 h and in timing mode 1.5‘h. In timing mode losses due to Touschek scattering dominate the lifetime.

Currently 21 beamlines are in operation at PETRA III. They use radiation solely from insertion devices (IDs). Since the start of user operation, 14 beamlines were installed in a nearly 300 m long experimental hall (Max v. Laue Hall) in one octant. In this octant the FODO structure of PETRA was replaced by nine double bend achromats. For an additional emittance reduction, 20 damping wiggler were installed in two straight sections in the west and north straight sections of PETRA. Due to demands for more beamlines by users the lattice of the machine was changed in two arcs in the year 2014. In these two arcs a part of the FODO cells were replaced by DBA cells. This allowed 10 more beamlines in two new halls (A. Yonath Hall and Paul P. Ewald Hall).

The pioneering work of MAX IV based on the multi-bend achromat (MBA) concept has initiated many upgrade projects at other synchrotron light sources with lattices of extremely small emittances. Due to the large circumference of 2304 m of PETRA, the use of MBAs can decrease the emittance of PETRA dramatically by more than two orders of magnitude. This results in a huge increase in brightness and coherent fraction in the hard X-ray region. Design work for

joachim.keil@desy.de

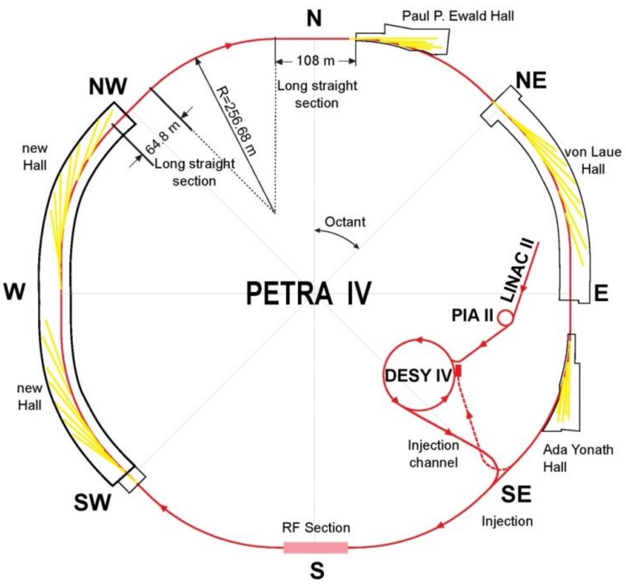

Fig. 1. Layout of the PETRA IV facility.

an upgrade of PETRA III into a diffraction limited storage ring at 10 keV was started in 2016; some aspects of lattice design, collective effects, and commissioning and operational challenges of PETRA IV will be discussed in the next sections.

II. Lattice Design

For the lattice design the special layout of PETRA has to be taken into account. It consists of eight arcs with four long and four short sections in between. The layout of the PETRA IV facility is shown in Fig. 1 with the existing three halls in north, northeast and east. For PETRA IV a new large hall in the west for additional beamlines is planned.

A. Linear Optics

The lattice design of the PETRA IV achromat is based on the hybrid multi-bend achromat (HMBA) of the ESRF-EBS [2] (Fig. 2). Each of the 8 arcs are composed of 8 achromats with a length of 26.2 m. The phase advance of each arc has an integer value in both planes to construct a higher order achromat [3]. One long straight section in south is used for the installation of RF cavities; a short straight section in southeast is used for the injection and extraction elements for on-axis swap-out injection (see later).

In total, space for 29 insertion devices is provided in the lattice. In the arc sections 25 undulators can be installed in

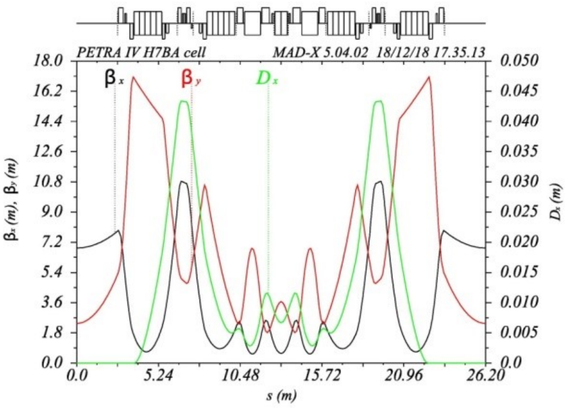

Fig. 2. Optical functions of the hybrid multi-bend achromat of PETRA IV.

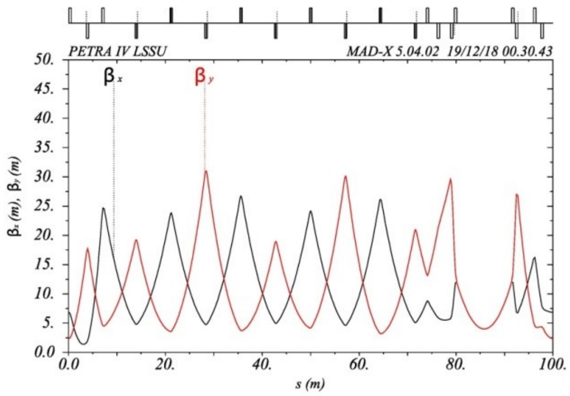

Fig. 3. Optical functions in one of the long straight sections with space for a 10 m undulator.

ID straights which have a length of 5 m. In four long straight sections space for long IDs (up to 10 m) with optimized beta functions in both planes of β^*=4 m is provided (Fig. 3). The layout of arcs with identical designs allows further upgrades for more beamlines in the future.

The small bending angles and strong quadrupoles with gradients up to 92 T/m leads to a very small natural emittance of 17 pmrad (with open undulators). However, the maximum of the dispersion function is only 4.4 cm (Fig. 2). This requires very strong sextupole magnets for compensation of the large negative chromaticity of the lattice. Even with the sextupole configuration of the HMBA with a I transport matrix between interleaved sextupoles installed at the dispersion maxima the dynamic acceptance is only $\approx$ 1.1 mmmrad in both planes. The local momentum acceptance is between 1.82.5%.

B. Beam Parameters without IBS

To compensate the energy loss of 4 MeV per turn a RF system with 500 MHz frequency and a voltage of 8 MV has been designed. It is planned that the RF system currently in use with twelve five-cell RF cavities will be replaced by HOM-less single-cell cavities based on the BESSY design. In total 24 cavities would be necessary. In addition, a 3rd harmonic RF system with a voltage of 2.3 MV is also required which consist also of 24 RF cavities.

Beam parameters of PETRA IV are shown in Table 1. They were computed without the effect of intra-beam scattering (IBS) which strongly influence beam parameters (see next section). The left column shows the values with open IDs, the right column shows the value if 29 IDs with a length of 5 m, 32 mm period length and a peak field of 0.91 T are closed.

TABLE I
PARAMETERS OF PETRA IV WITHOUT IBS EFFECTS.

Parameter	Without IDs	With 29 IDs closed
Energy E	$>$ 6 GeV	6 GeV
Nat. emittance ϵ_0	17.4 pmrad	7.6 pmrad
Tune Q_x, Q_y	164.18, 68.27	164.18, 68.27
Nat. chromaticity ξ_x, ξ_y	-230, -185	-230, -185
Damp. part. number J_x	1.54	1.18
Mom. comp. factor α_c	1.485 10^{-5}	1.485 10^{-5}
Rel. energy spread σ_E	0.678 10^{-3}	0.903 10^{-3}
Bunch length σ_z	1.24 mm	1.52 mm
Energy loss per turn U_0	1.32 MeV	4.02 MeV
β_x, β_y at IDs	6.86 m, 2.36 m	6.86 m, 2.4 m
D_x at IDs	0 m	0 m

C. Collective Effects

Because of the ultra-small emittances of PETRA IV the impact of IBS on beam parameters is very strong. Emittances,

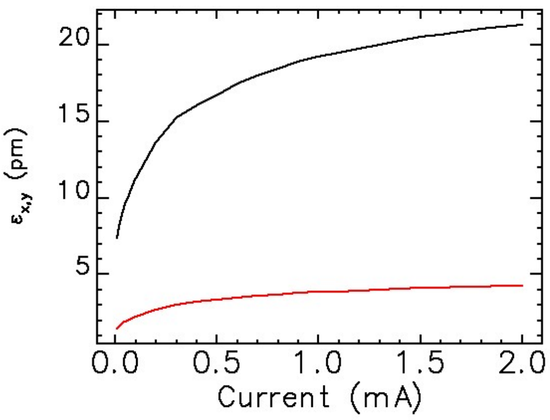

Fig. 4. : Emittance as a function of single bunch current (ϵ_x in black, ϵ_y in red).

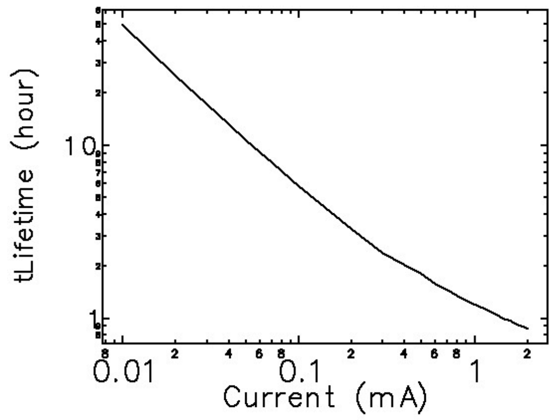

Fig. 5. Touschek lifetime as a function of single bunch current.

energy spread and bunch length increase with the single bunch current. Hence, two operation modes are planned:

- A brightness mode with ultra-small emittances and a total current of 200 mA. In brightness mode 1600 bunches with 80 bunch trains and 20 bunches per train are filled.
- A timing mode with emittances and energy spread slightly larger and a total current of 80 mA. In this mode 80 bunches are filled with a bunch distance of 96 ns. It is used for time resolved experiments.

In brightness mode and especially in timing mode losses by Touschek scattering dominate the lifetime. Bunch lengthening due to impedances (based on a preliminary impedance model of PETRA IV) is not enough to get an acceptable lifetime above 0.5 h in timing mode. An active third harmonic RF cavity system is necessary to lengthen the bunch. This helps also to increase the single bunch current limit which would be below 1 mA with the fundamental RF system alone. As an increase in the emittance ratio helps to achieve a larger Touschek lifetime and a vertical emittance below ≈ 4 pmrad is already below the diffraction limit an emittance ratio of 20% has been assumed for both modes.

The change of emittance with a third harmonic cavity system of 2.3 MV including additional bunch lengthening by impedance effects is shown in Fig. 4. The emittances with all effects included is 13.7 pmrad in brightness mode and 19.3 pmrad in timing mode. The Touschek lifetime is 4.7 hours in brightness mode and 1.2 h in timing mode (Fig. 5). All values are valid for an ideal machine without field and alignment errors. The use of damping wigglers to mitigate the influence of IBS on beam parameters like emittance and energy spread was investigated. The natural emittance and the increase of the emittance with single bunch current would be significantly lower. However, more RF voltage would be necessary to compensate the higher energy loss per turn and the energy spread would also increase. Simulations with the program SPECTRA [4] have shown that for the emittance range of PETRA IV the energy spread will reduce substantially the brightness especially for the higher harmonics of the undulator radiation. As closing the gaps of the undulators of the users already has a damping effect and will reduce the emittance already by a factor of 2 (see Table 1) no damping wiggler are included in the lattice design.

Beam parameters with IBS, bunch lengthening by impedance effects and an active third harmonic RF system with a voltage of 2.3 MV are shown in Table 2.

TABLE II
BEAM PARAMETERS OF PETRA IV WITH IBS EFFECTS INCLUDED AND A HARMONIC CAVITY SYSTEM.

Parameter	Brightness Mode	Timing Mode
Total current I	200 mA	80 mA
Nat. emittance ϵ_0	17.4 pmrad	7.6 pmrad
Number of bunches N_b	1600	80
Single bunch current I_b	0.125 mA	1.0 mA
Hor. Emittance ϵ_x	11.6 pmrad	19.2 pmrad
Ver. Emittance ϵ_y	2.3 pmrad	3.8 pmrad
Bunch length σ_z	13.7 mm	19.3 mm
Rel. Energy Spread σ_E	0.96 10^{-3}	1.56 10^{-3}
Touschek lifetime τ_{TL}	4.7 h	1.2 h

D. Injection Scheme and Pre-Accelerators

Due to the strong sextupoles the dynamic acceptance is only 1.1 mmmrad in both planes for a machine without alignment and field errors. Simulations with realistic errors have shown that the dynamic acceptance would be too small for off-axis injection even if the horizontal beta function is increased at the injection point in one of the long straight sections to a larger value (e.g. 100 m). Therefore, a swap-out on-axis injection is planned in the short straight section southeast with injection of either a single bunch or a bunch train of 20 bunches.

For an on-axis injection the pre-accelerator chain has to deliver in timing mode about 51010 particles per single bunch with an acceptable charge stability. It seems to be possible, that a modified gun and the LINAC can deliver the necessary number of particles. The accumulator ring PIA is not needed anymore. Furthermore, it is planned to increase the energy of the LINAC from 450 MeV to 700 MeV which would increase the injection efficiency in the booster.

PETRA III is using currently a fast ramping booster synchrotron (DESY II) as the pre-accelerator. With an emittance of 335 nmrad at extraction energy of 6 GeV, the emittance is too large for an efficient injection into the small dynamic aperture of PETRA IV. A new booster synchrotron (DESY IV) has been designed which has an emittance of only 19 nmrad and a repetition rate of 2 Hz. It is using a compact design with dipole, quadrupole and sextupole fields combined in a common magnet. Additional quadrupoles and sextupoles are needed to compensate for tune and chromaticity changes during the ramp.

III. Commissioning Challenges

The alignment tolerances of the magnets of PETRA IV have to be within very tight limits for a successful commissioning. According to preliminary simulations, an automatic first turn trajectory steering and an automatic closing of the first turn is required. This means, that reliable BPMs with a high accuracy in single turn mode are necessary. Measurements at PETRA III have shown, that the best achievable turn-by-turn resolution of the BPM system currently in use at PETRA III (Libera *Brilliance* from Instrumentation Technologies) is 30 μm which is a factor of two higher than required. The successor model *Brillance+* can fulfil these high demands on resolution.

A. Alignment Tolerances

The strong quadrupole and sextupoles magnets of the achromat require tight tolerances for the misalignments of these magnets. Similar to PETRA III magnets have to be installed on girders. The preliminary girder concept assumes that all strong magnets are installed together on a common girder. According to first simulations an alignment tolerance on the girders of $\sigma_{x,y} = 30\mu$m is needed for quadrupoles, sextupoles and octupoles and $\sigma_{x,y} = 50\mu$m for dipoles. The girder to girder tolerance has to be $\sigma_{x,y} = 50\mu$m.

B. Simulation of Start-up Procedure

A simplified start-up procedure to get circulating beam was simulated to determine the required alignment tolerances mentioned above. After assigning normal distributed errors to elements (with a 3σ cut) the sextupole and octupole strengths were increased in steps and a single pass trajectory correction was done with a BPM resolution of 20 μm for each step. After ramping up the non-linear magnets the orbit and the tune were corrected. This procedure assumes that the initial trajectory correction is possible and orbit and tune can be determined from turn-by-turn data without stored beam.

Simulations show, that for misalignments of $\sigma > 70$ μm the procedure starts to fail for some portion of the seeds and 70 μm alignment tolerances for the quadrupole and sextupole magnets is necessary to achieve adequate acceptance (Fig. 6). The beta functions of $\beta_x = 21.7$ m and $\beta_y = 3.7$ m are similar to the beta functions at the injection point. Note that the dynamic aperture can be recovered partly by optics correction, coupling correction and nonlinear tuning of the lattice with stored beam.

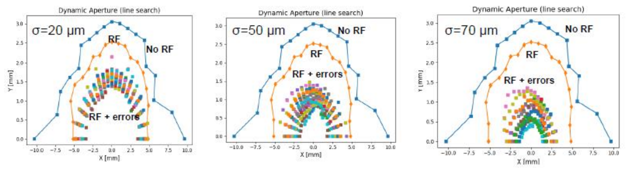

Fig. 6. Dynamic aperture for different misalignments of elements on girders.

IV. Operational Challenges

Compared to PETRA III the operation of PETRA IV has higher demands in several aspects. Some important topics are the stability, the reliability of the operation with a large mean time between failure (MTBF) and machine safety aspects due to small beam size of the stored beam, which would destroy components hit by the beam.

A. Stability

At PETRA III the tunnel temperature drops after a beam dump due to the sudden reduction of the heat load of synchrotron radiation even with a water-cooled vacuum chamber. Temperature changes are also observed during maintenance days when magnets are switched off. This is not acceptable for PETRA IV and a far better temperature stability is required in the old tunnel sections. In the accelerator tunnel of the large experimental hall (Max von Laue) the stability is sufficient with ± 0.1 K. This is not the case for the old tunnel sections and requires a better temperature stability. It is planned to heat the tunnel during maintenance days to keep the temperature fixed.

Simulations have shown that the emittance is changing substantially if the gaps of IDs are moved during operation. Closing all IDs reduce the emittance by a factor of two (Table 1). It is foreseen, that some additional damping undulators are needed for compensation.

Another aspect is the orbit stability during swap-out on-axis injection. By using a long stripline kicker pulse and injection of bunch trains with either 20 bunches in brightness mode or a single bunch in timing mode, a better stability can be achieved. As a drawback, the filling pattern has gaps necessary for the rise and fall time of the stripline kickers.

B. Reliability of Operation

The availability of PETRA IV should not be worse compared to PETRA III. For PETRA III the dominating sources for the reducing of the availability are trips of power supplies and trips of the RF system.

To keep the availability of PETRA III is a challenging goal for PETRA IV. The number of power supplies for magnets of PETRA IV will be substantially higher compared to PETRA III. More individually powered quadrupole magnets are required for a better optics correction and more corrector magnets are needed to achieve the tight goal for closed orbit deviations in the high gradient quadrupoles and sextupoles magnet in the achromats.

For the baseline design of PETRA IV it is planned to power as much magnets in series as possible. As an alternative, a few power supplies delivering the base current could be used and additional coils for each quadrupole for setting the individual current of each magnet. These additional coils would be fed by low current power supplies. Such a design is working successfully at PETRA III for dipole magnets in the DBA octant. From experience at PETRA III the mean time between failures (MTBF) of these power supplies with lower currents is far better compared to power supplies in the 100-200 A range. Nevertheless, coupling effects between power supplies by the magnetic fields have to be carefully investigated to check if the required current stability can be reached.

The RF system of PETRA III is using 2 klystrons and 12 five-cell cavities in two groups to provide a total voltage of 20 MV. In case of a failure of one RF system the beam is lost. Due to the lower momentum compaction factor of PETRA IV a lower RF voltage of 8 MV is necessary. A system using solid-state amplifiers and cavities which are individually powered offers a larger MTBF and the beam could survive the failure of one system without beam loss.

C. Machine Safety

Due to the ultra-low emittances of 11.6 / 2.3 pmrad of the electron beam, the small beam size of the swapped-out bunch or bunch train has to be enlarged before extraction. Otherwise, the local energy density would be too high at the entrance face of the beam dump and would damage it. It is planned to pre-kick the bunches before they are extracted into the dump.

In addition, a concept is needed for an emergency dump of the complete filling in the brightness mode with 200 mA total current which corresponds to a charge of 1500 nC. A possible way would be to use one of the short straight sections of PETRA IV and add weak dipole magnets to produce a large horizontal dispersion bump in this section. At the dispersion maximum an absorber block would be installed to dump the enlarged beam after switching of the RF. A pair of vertical sweeper magnets producing a local bump in this section would increase also the vertical beam size. This emergency beam dump is currently under investigation.

V. Summary and Outlook

A design has been worked out for an upgrade of PETRA III into a diffraction limited storage ring at 1 Å. The achromat design of PETRA IV is based on the ESRF-EBS HMBA achromat. It can provide a horizontal emittance in the range of 1020 pmrad including IBS effects. A third harmonic RF system is needed to achieve a reasonable lifetime in the timing mode with higher single bunch currents. Magnet strengths of quadrupoles and sextupoles are at the limit, but are technical feasible. Due to the strong sextupoles the dynamic aperture is small but adequate for on-axis injection. Of main concern are the high demands for alignment tolerances of the strong magnets of 30 μm on girders and of 50 μm between girders. According to simulations, these alignment tolerances would be acceptable for machine start-up. In addition, temperature stability and mechanical movements of the floor of the old tunnel segments is problematic and has to be improved. Still many challenging issues have to be solved. Presently, a conceptual design report for the PETRA IV project is in preparation and will be ready this year.

Acknowledgment

The author would like to thank the PETRA IV design team (I. Agapov, R. Brinkmann, H.-C. Chao, Y.-C. Chae, X. Nuel Gavaldà, R. Wanzenberg, J. Zhang) and the members of the technical groups of DESY involved in the PETRA IV design for material for this contribution. In addition, the author would like to thank the ESRF team for kindly providing the ESRF-EBS HMBA lattice.

References

[1] K. Balewski et al., PETRA III: A Low Emittance Synchrotron Radiation Source, Technical Design Report, DESY 2004-035, DESY, 2004.
[2] R. Dimper et al., ESRF Upgrade Programme Phase II (2015-2022), Technical Design Study (The Orange Book), 2014.
[3] PETRA IV: the ultralow-emittance source project at DESY, J. Synchrotron Rad. **25** (2018) 1277.
[4] T. Tanaka and H. Kitamura, SPECTRA: a synchrotron radiation calculation code, J. Synchrotron Rad. **8** (2001) 1221.

Session 2: Injectors and Injection

Summary Injectors and Injection

Volker Schlott[1] and Peter Kuske[2]
[1] Paul Scherrer Institute, Villigen, Switzerland
[2] Helmholtz Zentrum Berlin, Berlin, Germany

***Abstract*—In this summary an overview of low emittance ring projects and their proposed injectors and injection schemes will be given. Often the acceptance of these rings is too small for the traditional off-axis injection so that novel on-axis injection schemes have to be developed and employed. In any case, the performance of injectors and transfer lines today has to be improved for efficient injection into future low emittance rings. An attempt is made to summarize the important aspects presented and discussed during the workshop session in view of the commissioning process.**

***Keywords*—Injector, injection scheme, transfer line, commissioning**

I. Introduction

There were 4 contributions in this session of the workshop:

1) Transfer line from injector to LESR (Peter Kuske)
2) On axis injection (Masamitsu Aiba)
3) Injector requirements for LE storage ring upgrade projects (Zhe Duan)
4) Booster modifications and commissioning (Nicola Carmignani/Simon White)

The brief summaries of these contributions are part of the ARIES monograph of this workshop. The injector in combination with the injection scheme should allow for a highly efficient and transparent top-up operation. The transparency is essential for a perturbation free continuous measurement at colliders and at synchrotron light sources. Top-up is important for reaching and keeping the thermal equilibrium of optical components or achieving a high average luminosity in colliders. The high efficiency of injections will keep the radiation damage of insertion devices based on permanent magnet (PM) materials or in the future in PM-based lattice magnets at the lowest possible value. PM lattice magnets require less space at the same field strength / gradients and can achieve higher gradients with smaller apertures than traditional electromagnets. In this respect, they will be needed for lattices with even smaller emittances as foreseen today. In colliders the background will be smaller with higher injection efficiency.

II. Overview of Projects and Proposed Injection Schemes

Figure 1 shows the normalized horizontal acceptance of some of the already existing and proposed low emittance storage rings. The figure reflects the situation at the end of the 2^{nd} Workshop on Injection and Injection Systems, hosted by PSI in April 2019. The trend is clear: the smaller the emittance

peter.kuske@helmholtz-berlin.de

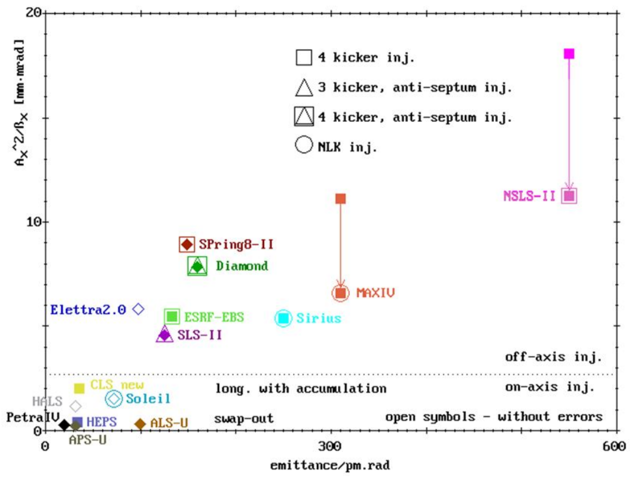

Fig. 1. Normalised horizontal acceptance as a function of emittance. For the two operating facilities (NSLS-II and MAXIV) the arrows point from the predicted to the measured acceptance. The smaller the emittance the smaller the acceptance. Off-axis injection is still an option if the acceptance is above 2-3 mmmrad and has been chosen by many facilities. If the acceptance is too small then transverse on-axis injection schemes have to be employed: either in the form of swap-out with and without accumulation or with a longitudinal injection scheme and accumulation in the storage ring.

the smaller the transverse acceptance, and the traditional off-axis injection schemes will be more and more inefficient. The dotted line separates the proposals for off-axis from on-axis injection schemes. Off-axis injection schemes with the traditional 4 kicker injection bump scheme have been chosen by NSL-II, ESRF-EBS, SPring8-II and with a 3 or 4 kicker bump in combination with an anti-septum by SLS-II and Diamond II. Off-axis injection based on a single non-linear injection kicker magnet promises to be more transparent and is the choice for MAXIV and also for Sirius. If the transverse acceptance becomes too small then on-axis injection schemes have to be used. Some are based on swap-out with dumping or accumulating the spent beam (APS-U or ALS-U, HEPS), some will employ longitudinal injection schemes which offer accumulation in the ring (Soleil, HALS). For more details, see contribution by M. Aiba. Longitudinal injection appears very attractive because in smaller emittance rings the momentum, or better the phase acceptance, does not reduce as drastically as the transverse acceptance.

Each of the different injection schemes demands certain features of the injector and requires different optimal matching conditions for the Twiss-parameters at the end of the transfer line (see contributions by Z. Duan and P. Kuske). On-axis injection prefers matching of Twiss-parameters whereas off-axis injection schemes usually favour a smaller ß-function at the end of the transfer line in comparison with the values in the ring. The best choice for NLK-based injection schemes depends on the placement of the kicker with respect to the injection point. For many upgrade projects the bottle neck remains the injector itself. The design or upgrade of the injector will be influenced by the choice of the injection scheme and the required target parameters. Only a few facilities have the chance to use a full energy injection LINAC which would be ideal for nearly all injection schemes (MAXIV and Spring8-II) or have the advantage of a low emittance booster synchrotron like e.g. SLS and ALBA. In most cases more economical synchrotrons with a small circumference are used as injectors and the emittance of the injected beam is quite large. The damping partition can be modified by operating these synchrotrons off-momentum which results in a smaller emittance at the cost of an enlarged bunch length, which can lead to particle losses, see N. Carmignani's contribution. Swap-out injections in the few bunch timing mode needs a high charge to be injected. A challenge which has not yet been mastered. Low charge injectors require accumulation in the storage ring and also this makes the on-axis, longitudinal injection schemes so attractive. This scheme works best with a smaller longitudinal emittance in comparison to the ring. A summary of key performance parameters of injectors related to injection scheme can be found in Table 1. In summary – the injection into next generation low emittance storage rings requires injectors delivering an emittance as low as offered by the current generation of rings.

TABLE I
DESIRED PERFORMANCE OF INJECTORS FOR DIFFERENT INJECTION SCHEMES

Injection Scheme **Energy spread**	**Emittance**	**Bunch Length**
4 kicker bump as in SR	as small as possible (emittance exchange)	as in SR
3 kicker bump + as in SR anti-septum	as small as possible (emittance exchange)	as in SR
non-linear kicker as in SR	as small as possible (emittance exchange)	as in SR
on-axis swap-out as in SR	small vertical (vertical injection)	as in SR
on-axis swap-out smaller longitudinal	small vertical (vertical injection)	shorter

Whatever the injection scheme will be, the chosen scheme has to be capable of injecting on-axis. All commissioning strategies discussed during the workshop assume that beam is injected on-axis. Circulating beam will be achieved by stepwise improvements of steering, linear and non-linear optics adjustments. This approach calls for quite sophisticated diagnostics which has to offer high resolution and accuracy for turn-by-turn beam position measurements already at low beam currents, which applies to storage ring, injector, and transfer line. In order to guarantee good performance the beam position must be measured and kept stable with high precision. Monitoring the efficiency of the injection process and preventing particle losses requires charge monitors and beam loss monitors distributed along the injection chain. Due to relatively low lifetimes and the request for top-up operation, injectors and injection are very important for the success of next generation light sources based on diffraction limited, low emittance storage rings. One should not try to save money by sacrificing diagnostics because this would not only slow down the overall commissioning but also threaten the general performance and reliability of such facilities.

Transfer Line from Injector to LESR

Peter Kuske*, Felix Kramer, Falk Hoffmann
Helmholtz Zentrum Berlin, Berlin, Germany

***Abstract*—Injecting, storing, and accumulating beam in future low emittance storage rings, LESR, will be more challenging than today. The lower the emittance the smaller the acceptance of the ring will be. The speedy commissioning of the injection transfer line resulting in the perfect matching of the injected beam parameters to the small acceptance of these rings will be essential for the success of any facility based on such rings. Aspects for the design, the commissioning, and experience with the modelling of transfer lines will be presented.**

***Keywords*—Transfer line commissioning, optics modelling, optics matching**

I. Design Philosophy for Transfer Lines

The design of the transfer line should allow for a fully transparent top-up injection with very high efficiency. This requires a design which offers:

- Stable and efficient beam transport
- Matching of the beam parameters in position and in size in all dimensions with a certain flexibility
- Measurements of relevant parameters: single pass BPMs, ideally with bunch-by-bunch resolution; a couple of beam size monitors based on optical transition radiation (OTR) for separating energy spread and emittance; charge monitors, beam loss monitors (BLM); monitoring of pulsed magnets (peak, width, pulse shape)
- Archiving all parameters
- Energy control, as part of the top-up safety interlock

II. Matching of Beam Parameters

There is always an optimal parameter set where the injection works best in terms of efficiency and transparency. The task of the transfer line commissioning is to find and keep the corresponding adjustment parameters. In some cases the linear analysis of the injection process can predict which parameters to choose, in general, the modelling of the non-linear dynamics in the storage ring is required in order to theoretically estimate the best matching conditions, see Ref. [1]. The results will depend on the selected injection scheme. With the traditional 4 kicker injection bump the ß-function at the end of the transfer line should be a factor of 2 to 3 smaller than in the ring, see Ref. [2], for a scheme based on a single non-linear injection kicker (NLK) the optimum would be a much larger ß-function at the end of the transfer line if a natural phase advance between the injection septum and the NLK is used. This is shown in Fig. 1 for the installation of the NLK at BESSY II where the kicker is located one symmetry cell downstream of the injection point. The situation is once again different if septum and NLK are located in the same straight section where the best choice for the ß-function is similar to the 4 kicker injection bump scenario.

In reality, all relevant parameters have to be optimized in order to achieve the highest injection efficiency. As a rule of thumb the emittance of the injected beam should be smaller than a tenth of the hard edge acceptance of the corresponding beam dimension, even for perfectly matched Twiss-parameters. In the first place this is a challenge for the injector, especially in case of upgrade projects and the desire to use existing hardware components, see Ref. [3]. The transfer line has to provide the necessary good matching.

III. Commissioning of Transfer Lines

The commissioning of any component of an accelerator complex can be split in the part without and with beam. Very often the time for commissioning with beam is very short especially for transfer lines. Therefore a careful and detailed pre-commissioning is mandatory.

A. Commissioning without beam

All hardware components should have undergone acceptance tests at the factory, FAT, and at the site, SAT. This has to be followed by:

- Integration tests after installation and alignment (controls, interlocks, diagnostics, polarity)
- Development of high level application software for fast error recognition (correlate BPM channel signals with steering actions to find polarity, cabling, control system errors)
- Develop software for basic commissioning tasks (image analysis of screens, quadrupole scans for emittance determination, develop strategy to separate emittance from energy spread, software for orbit response measurement and optics analysis, beam-based alignment with respect to quadrupole magnets, and software for automated optimization based on observations)
- Perform extended integration tests (test of hard- and software with simulated signals and responses, test software for basic features like save/restore, conditioning of magnets, logging and storing data, electronic log-book) , see Ref. [4]

B. Commissioning with beam

This requires the stable operation of the injector, which is usually not the case. The next steps in the commissioning should be:

- Optimization of extraction (timing, pulse shapes – easier to adjust with a shielded dump line)

*peter.kuske@helmholtz-berlin.de

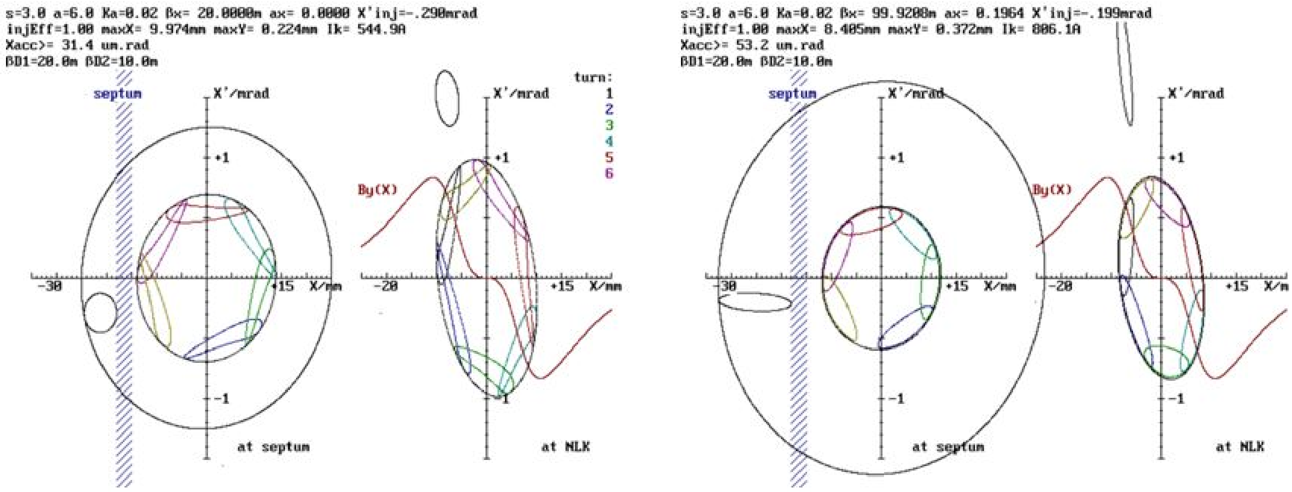

Fig. 1. Optimized Twiss-parameter matching for the injection scheme based on a single non-linear kicker and as realized at BESSY II.

- Hardware and diagnostics checks
- Beam transmission without any quadrupole magnet (should be possible with low emittance injector)
- Adjustment of orbit, control of dispersive orbit, beam steering, and beam-based alignment
- Quadrupole scans for emittance determination
- Optics determination and adjustment to target values
- Optimization of final injection conditions (injection septa, kicker, timing, position of injected beam – with first turn measurements in the ring or injection efficiency)
- Test automated optimization procedures (transmission, injection efficiency, injection bump closure)
- Archive results and use machine learning to further improve performance

IV. Practical experience

The implementation of top-up operation with high injection efficiency at BESSY II required a recommissioning of the transfer line which connects the booster with the storage ring. During the optimization of the transfer line many difficulties were encountered which will be presented in order to illustrate the challenges. In the very early days of commissioning one has to expect polarity errors, wrong cable connections, and other hardware defects. This is usually less important for upgrade projects where many of these typical initial errors have been rectified already in the past.

A. Non-linear effects at the beginning of the transfer line

In Fig. 2 the particle distribution of the extracted beam on a fluorescent screen is shown as a function of the vertical position at the beginning of the transfer line. Banana-shaped distortions are most likely the result of non-linear coupling effects in the septum magnets and finally the vertical beam position in the synchrotron was chosen to reach a flat beam in the transfer line.

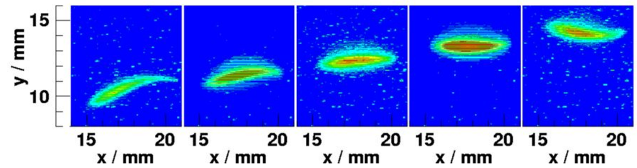

Fig. 2. Beam on a fluorescent screen downstream of the extraction septum as a function of the vertical position of the beam in the magnets at the start of the transfer line.

B. Finite resolution of screens

Our best screens are based on optical transition radiation, OTR. The resolution of these screens with their imaging system can be deduced by focusing the beam with two quadrupole magnets with different distances to the screen. The typical result of such quadrupole scans is shown in Fig. 3 and the finite resolution of as little as 22 μm has a noticeable impact on the quality of the fit and the resulting beam parameters. For most other screens in the transfer line the resolution is on the order of 100-200 μmm which makes it extremely difficult to accurately determine the small vertical emittance delivered by the booster.

C. Analysis of horizontal beam size measurements

The horizontal beam size contains contributions from the emittance and the energy spread. While the value of the dispersion at the screen can be determined by a separate experiment, the energy spread is an additional unknown parameter which cannot be extracted from a simple single quadrupole scan. However, many scans allow you to disentangle all contributions. A result of simultaneously fitting of the 6 unknown parameters to a set of quadrupole scans in the horizontal plane is shown in Fig. 4 for different operating conditions of the injector.

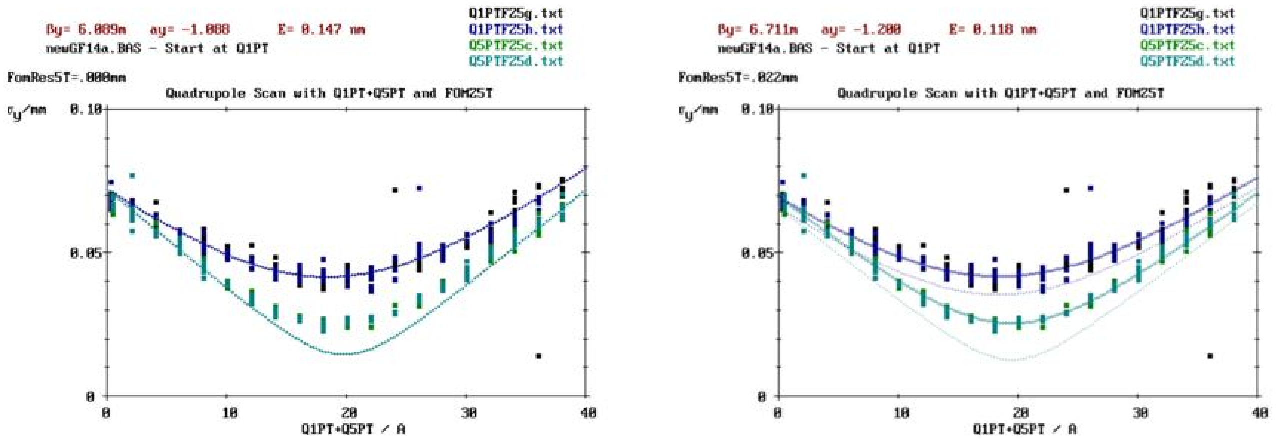

Fig. 3. Least square fit of the measured vertical beam size as a function of two quadrupole magnets close (blue) and further away (green) from the OTR-screen. Left without resolution limitation and right with finite resolution. The thin lines show the real beam size and as measured with a perfect screen and imaging system.

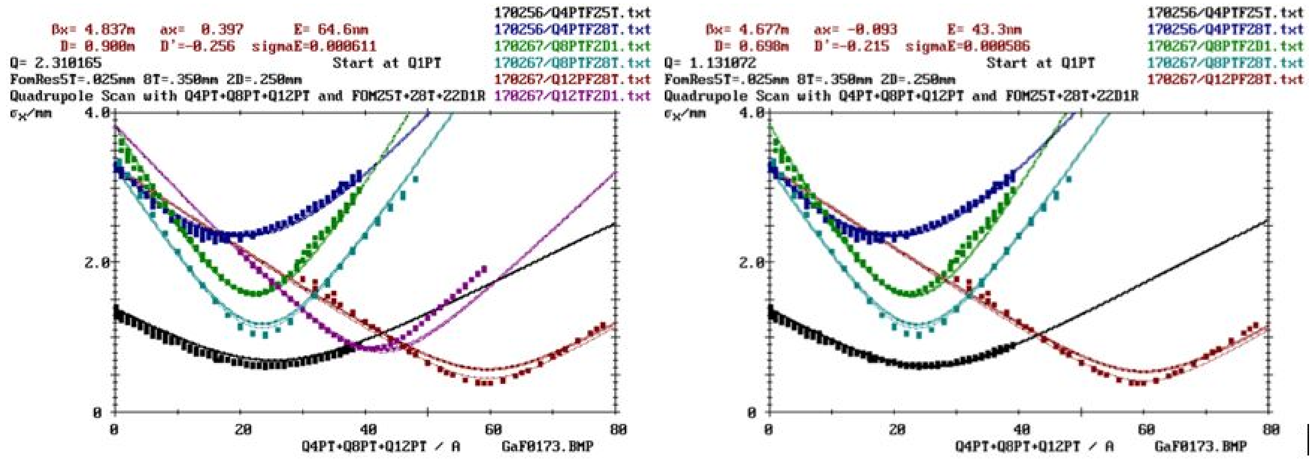

Fig. 4. Result of simultaneously fitting all six unknown parameters at the beginning of the transfer line to sets of horizontal quadrupole scans. Only the scanned quadrupole magnets are powered, all others are turned off. Left – for the nominal workingpoint in the booster, far away from the coupling resonance, and at the early extraction time where the horizontal emittance is still 20-30% smaller than expected for radiation equilibrium and right – on the coupling resonance at the later extraction time where the horizontal emittance is in equilibrium. All parameters, except the Twiss-parameters, are found to agree with the expectations based on the booster parameters.

D. Dispersive orbits

The transfer line at BESSY II is comparatively short and the emittance delivered by the booster is around 60 nm·rad. The extracted beam can be guided to the end of the transfer line without any quadrupole magnets. In such cases it is recommended to start with measurements of the dispersive orbits in order to assess the quality of the lattice modelling. Fig. 5 shows the very surprising experimental results which disagree with the model predictions. The disagreement is large for the dispersion measured by changing the frequency of the RF-system in the booster. This is the traditional way in order to vary the energy in a longitudinally damped circular accelerator. If the extraction timing is varied instead then the agreement is a bit better. The BESSY II booster operates with 10 HZ-White-circuits and the extraction energy is reached after 38 ms. A time long enough for the accelerated ensemble of particles to be damped longitudinally, however, short enough to still have adiabatic damping in the transverse planes, which results in a smaller transverse emittance.

The observed deviation of the dispersive orbits can be explained by a strong defocusing effect seen by the extracted beam in the last quadrupole magnet of the booster and in the two septum magnets. It is well known that the gradient in the quadrupole magnet will fall off if the beam orbit reaches the region between the pole pieces. The extracted beam just has to do that and in addition has to pass through the septum very close to the septum sheet where the field already falls off and in lowest order acts also as a defocusing gradient. This can explain the poor agreement of the measured dispersive orbits with the theoretical expectations. There was actually never a doubt about the Twiss-parameters in the booster because the lattice is very simple and the two K-values can be determined or checked with the help of tune measurements.

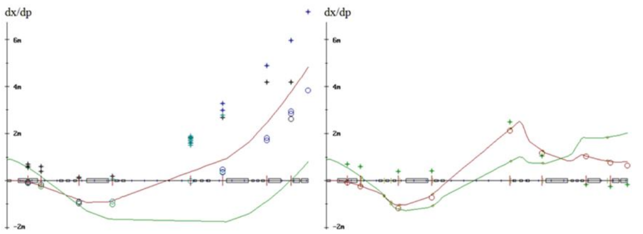

Fig. 5. Comparison of measured and expected dispersive orbits (red and green), left – without any quadrupole magnet and right – with the nominal settings of the magnets. The red curve should be compared with the experimental results presented in circles and the green curve should follow the crosses. The dispersion in the booster at the extraction point is 0.8 m, this corresponds to the green curve.

Based on the observations the model of the transfer line now includes defocusing gradients in the last quadrupole magnet and in the two septum magnets. The achieved agreement between model predictions and measurements is sufficient. Fine adjustments of the optics are performed with empirical techniques using the injection efficiency as the target parameter.

E. Optimal beam position

The best beam position for the injection has to be found by following the injected beam in the storage ring. All injected particles should be captured and the beam motion of injected and stored beam should be as small as possible or not measurable at all for a transparent injection. For the usual injection in the horizontal plane a rather large number of pulsed elements is involved and the stability of these pulsed elements plays a crucial role for the efficient and transparent injection. Thus a constant monitoring of all pulsed elements and the archiving of the relevant information is mandatory for a smooth and continuous top-up operation. The archived data will allow for preventive maintenance based on early indications of deteriorated performance.

Figure 6 shows the stability of the injection efficiency and the position of the beam just before the injection septum over a period of 4 weeks. At BESSY II the efficiency remains on average around 95%, and the vertical position of the beam is quite stable. The small vertical shot-to-shot jitter is also due to the measurement error. Because of the pulsed elements the jitter is much larger in the horizontal plane where the beam positon slowly drifts and shows a day-by-day (temperature) variation. The measured vertical position depends on the number of injected bunches – a single or a few (3 or 5) bunches are injected. The reason is unknown.

V. Summary

Transparent and efficient top-up injections should be the goal for the design and finally the commissioning of any future facility based on low emittance storage rings, LESR. Transfer lines have to match the beam parameters of the injected beam to the very small acceptance of these rings. Thus commissioning of transfer lines is an essential part of the successful LESR commissioning. It relies on the performance of the injector

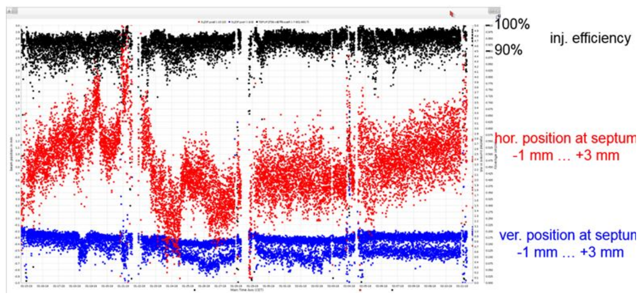

Fig. 6. Long term stability of some injection parameters over 4 weeks – in part related to the pulsed magnets of the transfer line. The injection efficiency (in black) remains on average around 95%. The horizontal position of the injected beam (in red), just in front of the storage ring septum, shows a large shot-to-shot jitter, 24 h oscillations, and a slow drift. Note, all pulsed elements bend the beam horizontally. The beam is more stable in the vertical plane (in blue). The measurements indicate a vertical position which shows a dependency on the number of injected bunches (1 or 3 and more). The accuracy of the single bunch, single shot measurement is 20 μm with a charge of 0.4 nC.

and for many fine adjustments a fully optimized storage ring is needed. Commissioning and optimization of transfer lines is an integrated task which includes many subsystems and should be repeated from time to time or as frequently as needed.

The allocated time for commissioning, and not exclusively for the transfer lines, is very short. Careful planning, hardware and software developments, and tests have to be done before hand in order not to waste any of the precious time for the commissioning with beam. Despite all the efforts to eliminate mistakes and errors before the actual start of the commissioning be prepared to encounter surprises. The correct modelling of the transfer line optics can be a challenge. As long as the model predictions are poor, alternative techniques should be considered which are based on trial and error.

References

[1] S.M. Liuzzo, priv. com., Injection Review, Grenoble, $29^{th} - 30^{th}$ March 2017.
[2] Andreas Streun, SLS booster-to-ring transferline optics for optimum injection efficiency, SLS-TME-TA-2002-0193, May, 2005.
[3] Zhe Duan, Injector requirements for LE storage ring upgrade projects, this workshop.
[4] G.M. Wang, et al., NSLS-II Booster Extended Integration Test, IPAC2015, TUPHA007.

On-axis injection

Masamitsu Aiba
Paul Scherrer Institut, 5232, Villigen, Switzerland

Abstract—**This report summarizes the author's presentation given at the workshop, 'Beam Tests and commissioning of low emittance storage rings', held at Karlsurhe Institute of Technology on 18th–20th March 2019. Beam injection of light sources and lepton colliders in the context of beam test and commissioning was the scope of the presentation.**

Keywords—**Electron storage ring, injection**

I. Introduction

Top-up injection is essential for light sources and lepton colliders to maximize the output, i.e., photon flux and luminosity, respectively. It was first realized in lepton colliders [1], [2]. The developed technique is often referred to as conventional injection scheme due to the fact that it has become standard for lepton collider and also applied to light sources [3]. However, it has been recognized that the conventional injection scheme is not ideal to realize a highly-performing low-emittance ring. The performance of lepton colliders and light sources is, in general, strongly correlated to the dynamic aperture: the higher performance, the smaller dynamic aperture will be. Since the conventional scheme requires a sufficient dynamic aperture to accept the injected beam the accelerator performance may be limited. Various injection schemes have therefore been developed to primarily overcome the limitation.

II. On-axis injections

The conventional injection scheme is realized with a septum and a series of kickers, which is referred to as kicker bump. The latter forms a closed orbit bump, which brings the stored beam close to the septum blade, and at the same time, an injection beam arrives at the septum. Thus two beams are partially separated with the septum blade in-between, resulting in a betatron oscillation of the injected beam. Afterward the kicker bump is turned off such that the injection beam is brought to the other side of septum blade. The above partial separation is unavoidable in this scheme, and the conventional injection is therefore also called off-axis injection. The dynamic aperture at the location of the septum is required to be sufficiently large for accepting the injection beam partially separated from the stored beam. A natural counter, on-axis injection, has been studied and developed to relax this constraint.

A. Synchrotron Phase Space Injection

Synchrotron phase space injection, a modified conventional injection, was examined at the LEP [4], [5]. The injection beam energy is, in synchrotron phase space injection, shifted slightly, and finite dispersion function is introduced to the ring optics at the location of the septum such that the injection beam is placed onto the corresponding off-energy closed orbit. Such a configuration results in a synchrotron oscillation of injected beam but no betatron oscillation, in other words, it is an on-axis injection. This injection scheme was successful in two aspects: higher injection efficiency was achieved, and adverse radiation doses to the physics detectors during the injection period were lowered. The former is attributed to the fact that (1) the synchrotron oscillation may be more robust than the (large amplitude) betatron oscillation and (2) the injection efficiency may be less sensitive to the injection beam position and angle jitters since the injection beam is placed transversely on axis. The lower radiation dose is then achieved as a consequence of the higher injection efficiency, but it is noted that the design dispersion at the detector is zero so that both stored beam and off-energy injected beam follow the vacuum chamber center. This scheme may be therefore preferable for lepton colliders.

Synchrotron phase space injection requires finite, but small dynamic aperture (ultimately, barely accepting the injection stored beam) over a range of energy deviations, corresponding to the synchrotron oscillation of the injected beam. Therefore, it can overcome the dynamic aperture limitation. However, it is difficult, if not impossible, to introduce a large enough dispersion function into low-emittance multi-bend-achromat lattices of the next generation light source while the collider optics may be more flexible.

It is noted that the so-called multipole-kicker injection [6], [7] can be also on-axis injection in a similar manner, i.e., by introducing finite dispersion at the location of the kicker [8].

B. Swap-out Injection

The dynamic aperture limitation may simply be overcome by swapping the stored beam and the injection beam: the injection beam is prepared with the design charge and injected into the storage ring, and at the same time, the stored beam that is missing a fraction of charge is kicked out from the storage ring. The required dynamic aperture is smallest in this swap-out injection [9], [10]: a similar requirement to the synchrotron phase space injection but off-energy dynamic aperture is not required. Nevertheless, some off-energy dynamic aperture is necessary, not for injection, but rather to ensure a reasonable beam lifetime.

Swapping-out is performed either bunch by bunch or bunch-train by bunch-train. The former requires a short pulse kicker (shorter than twice the bunch spacing) which kicks out only one bunch and inserts the injection bunch. Such a bunch-by-bunch swap-out injection is planned for the upgrade project of APS [11]. The latter may require an accumulator ring to prepare the injection beam and a kicker with flat-top corresponding to the length of the bunch train. Swap-out injection with an accumulator ring is planned, e.g., for the upgrade project of ALS [12].

The stored beam extracted from the storage ring may be treated in various ways, brought to a beam dump, re-injected into the accumulator ring for recycling, etc. In principle, swap-out injection is also applicable to lepton colliders. However, it may not be practical at least for very high energy colliders [13].

C. Longitudinal Injection

Yet another injection scheme, longitudinal injection, has been proposed [14]. The injection beam energy is shifted, and the off-energy injection beam is placed onto the corresponding off-energy closed orbit by a dipole kicker. It is noted that the dispersion function is not necessary in contrast to synchrotron phase space injection. The injection timing is also shifted by a fraction of the rf period, typically a half: the injection beam is inserted between two stored bunches (or two rf buckets). Due to the energy dependence of synchrotron radiation loss, there is a narrow channel of the longitudinal acceptance that extends to the space between rf buckets. An injection beam with adjusted energy and timing, fitting this channel can be trapped into the rf bucket and merged to the stored beam. When the pulse length of the dipole kicker is shorter than the bunch spacing, the injection is fully transparent to the stored beam.

The dynamic aperture requirement is qualitatively the same as that of the synchrotron phase space injection whereas quantitatively the injection beam energy offset (amplitude of injection beam synchrotron oscillation, in other words) may be larger in case of the longitudinal injection.

The longitudinal injection scheme was simulated for the MAX-IV storage ring, equipped with a 100 MHz rf system. It was shown that the injection beam was trapped into the rf bucket and its synchrotron oscillation was damped after a few radiation damping times [14]. The injection efficiency strongly depends on the longitudinal injection beam emittance since the injection beam should fit the narrow channel of the longitudinal acceptance. In the above simulation, 100% injection efficiency was observed for the beams with small longitudinal emittance, generated by a linac injector.

The necessity of small longitudinal emittance can be practically removed by applying rf gymnastics with two rf systems of fundamental and second harmonic frequencies [15], [16]. The second harmonic cavity creates rf buckets between the ones from the fundamental frequency rf. The injection beam with nominal energy can be injected into these newly created empty rf buckets. Afterwards, the phases and voltages of two rf systems are varied to merge the injected bunch into the stored bunch. Such a bunch merging (and conversely splitting) technique is well established in hadron machines, see, e.g., Ref. [17] and references therein. It is noted that the bunch length is significantly varied during the rf gymnastics, which potentially is an issue of instabilities.

Third harmonic cavities are widely used in light sources to lengthen the bunches and thus increasing the instability threshold and/or the beam lifetime. When a higher harmonic cavity, e.g., 2nd harmonic, in addition to 3rd harmonic cavity is employed, the bunch can be further prolonged. The rf bucket is then largely expanded toward the space between bunches. Therefore, a bunch can be injected between two stored bunches and still within the bucket [18]. The necessity of small longitudinal emittance is then removed as in the bunch merging approach, and moreover no rf gymnastic is involved in this case.

One more interesting approach, improving the longitudinal injection, has been proposed for the SOLEIL upgrade [19]. The fraction of bucket area occupied by the stored bunch is rather small. Therefore, the rf bucket shape can be modified by varying the fundamental and 3rd harmonic cavity phases and voltages, keeping the potential of synchrotron oscillation constant locally around the stored beam bunch. The modification of rf bucket is performed so as to quickly damp the injected beam synchrotron oscillation. This may be explained as an analogy to transverse resonance injection where multipole and/or quadrupole magnets are utilized to control the particle trajectory in the transverse phase space. Similarly, the third harmonic cavity together with the fundamental cavity is used here, as a longitudinal nonlinear kicker, to control the particle trajectory in the longitudinal space.

D. Kicker developments

Kicker developments have been intensively conducted for top-up injection as well as for beam injection and extraction in general.

Short pulse kickers are necessary for bunch-by-bunch swap-out injection and longitudinal injections. The pulse length of kicker needs to be on the order of 10 ns or even shorter than 10 ns, depending on the rf frequency. Plenty of research and developments in this field have been performed as can be found in [20]–[23], and more litereature may be found else where.

III. Extraction line for beam tests

It is important to characterize the beam in the low-emittance ring to better understand and control the machine. It is possible to apply destructive measurements in a beam transport line, and such measurements are complementary to the beam measurements in the ring. Colliders are normally equipped with an abort beam line for scheduled/non-scheduled beam dumps, and it can be equipped with beam diagnostics to characterize beams extracted from the ring. On the other hand, this has not been the case for light sources since the beam can be internally dump. The aforementioned swap-out injection, however, requires an extraction beam line to avoid frequent internal beam dumps due to the top-up operation or to re-use the swapped bunches. It may be interesting to characterize the beam extracted from the low-emittance storage ring.

IV. On-axis injection for commissioning

The dynamic aperture of the ring can be significantly deteriorated due to machine imperfections such as misalignment and quadrupole gradient errors. It is recovered through optics and orbit corrections, and beam-based alignments. However, these corrections can be precise only after stable stored beam is established. Hence, at the early stage of commissioning, the dynamic aperture may not be enough for accumulation with off-axis injection. For the commissioning of the next generation light source, especially for the storage ring with off-axis injection, this can be a bottleneck. For instance, the offsets in BPM reading arising from not only alignment errors but also unbalance of electronics can be one or two orders of magnitude larger than the values expected after beam-based alignments. These BPM offsets can be mitigated through either zero calibration in lab prior to the installation or single-pass beam-based alignment as performed in linacs. Apart from these possible efforts, an on-axis injection (without accumulation) could be helpful in the commissioning until precise corrections are applied, given that it is hardly achieved to mitigate all the machine imperfections to negligible level without beam-based corrections. Such a strategy was indeed adopted to the MAX IV commissioning, where a dipole kicker was installed in the beginning and replaced later by a nonlinear kicker. For the collider, this may not be a problem: the beta function at the interection point can be set to a large value to increase the dynamic aperture during the first phase of commissioning, and the beta function at the injection septum/kicker can be increased as high as necessary.

V. Possible on-axis injection at SLS2

The baseline injection scheme of SLS2 is anti-septum injection [24], which is a modified conventional off-axis injection. Although the dynamic aperture requirement is relaxed, an on-axis injection can further relax it. It is therefore under investigation to start with anti-septum off-axis injection and later to switch to an on-axis injection. In this way, the beta function along the straight section can be squeezed as keeping the super-periodicity, resulting in a higher spectral brightness.

VI. Summary

The performance of lepton colliders and light sources has been significantly increased by applying top-up injection. The conventional, off-axis injection scheme, however, requires a sufficient dynamic aperture. This may be a limitation for low-emittance rings. The on-axis injections have been thus studied and developed.

Swap-out injection, one of on-axis injection schemes, necessitates an extraction line. It may be useful to equip diagnostics along the extraction line such that the beam extracted from low-emittance rings can be characterized with destructive measurements.

The accelerator is normally designed such that the dynamic aperture is sufficient after possible corrections. During the early stage of commissioning, however, they are not applied. Thus, for the ring based on off-axis injection, the dynamic aperture may not be sufficient in the beginning. A temporary on-axis injection without beam accumulation may help to speed up the commissioning.

As discussed, the on-axis injection can relax the dynamic aperture requirement. In case of SLS2, this is further beneficial to increase the spectral brightness by squeezing the beta function of straight sections.

Acknowledgment

This project has received funding from the European Union's Horizon 2020 Research and Innovation programme under Grant Agreement No 730871.

References

[1] U. Wienands, "Lepton Collider Operation with Constant Currents", in *Proc. 21st Particle Accelerator Conf. 2005 (PAC'05)*, pp. 149–153.

[2] J. T. Seeman, "Injection Issues of Electron-Positron Storage Rings", in *Proc. of B FACTORIES: The State of the Art in Accelerators, Detectors and Physics*, SLAC-400, pp. 233–241, 1998.

[3] H. Ohkuma, "Top-up Operation in Light Sources", in *Proc. of 11th European Particle Conf. 2008 (EPAC'08)*, pp. 36–40.

[4] S. Myers, "A Possible New Injection and Accumulation Scheme for LEP", LEP Note 334, 1981.

[5] P. Collier, "Synchrotron Phase Space Injection into LEP", in *Proc. of 16th Particle Accelerator Conf. 1995 (PAC'95)*, pp. 551–553.

[6] K. Harada, Y. Kobayashi, T. Miyajima, and S. Nagahashi, "New injection scheme using a pulsed quadrupole magnet in electron storage rings", *Phys. Rev. ST Accel. Beams*, 10, 123501, 2007.

[7] H. Takaki et al., "Beam Injection with a Pulsed Sextupole Magnet in an Electron Storage Ring", *Phys. Rev. ST Accel. Beams*, 13, 020705, 2010.

[8] Á. Saá Hernández, "Longitudinal Top-up Injection for Small Aperture Storage Rings", *Presentation at 4th Low Emittance Ring Workshop*, 2014. https://agenda.infn.it/conferenceDisplay.py?confId=7766

[9] M. Borland, "A super-bright storage ring alternative to an energy recovery linac" *Nucl. Instrum. and Methods in Phys. Research Section A*, Vol. 557, pp. 230–235, 2000.

[10] L. Emery and M. Borland, "Possible Long-Term Improvements to the Advanced Photon Source", in *Proc. of 15th Particle Accelerator Conf. 1993 (PAC'03)*, pp. 256-258.

[11] S. Henderson, "Status of the APS Upgrade Project", in *Proc. of 6th Int. Particle Accelerator Conf. 2015 (IPAC'15)*, pp. 1791–1793.

[12] C. Steier *et al.*, "ALS-U: a Soft X-ray Diffration Limited Light Source", in *Proc. of North American Particle Accelerator Conf. 2016 (NA-PAC'16)*, pp. 263–265.

[13] M. Aiba *et al.*, "Top-up injection schemes for future circular lepton collider", *Nucl. Instrum. and Methods in Phys. Research Section A*, Vol. 880, pp. 98–106, 2018

[14] M. Aiba *et al.*, "Longitudinal Injection Scheme Using Short Pulse Kicker for Small Aperture Electron Storage Rings", *Phys. Rev. ST Accel. Beams*, 18, 020701, 2015.

[15] B. C. Jiang *et al.*, "Using a double-frequency RF system to facilitate on-axis beam accumulation in a storage ring", *Nucl. Instrum. and Methods in Phys. Research Section A*, Volume 814, pp. 1–5, 2016.

[16] G. Xu *et al.*, "On-axis Beam Accumulation Enabled by Phase Adjustment of a Double-Frequency RF System for Diffraction-Limited Storage Rings", in *Proc. of 7th Int. Particle Accelerator Conf. 2016 (IPAC'16)*, pp. 2032–2035, 2016.

[17] R. Garoby, "Bunch Merging and Splitting Techniques in the Injectors for High Energy Hadron Colliders", in *Proc. of 17th Int High Energy Accelerator Conf. 1998 (HEACC'98)*, pp. 172–175.

[18] G. Xu, "Longitudinal Accumulation in Triple RF Systems", *Presentation at Topical Workshop on Injection and Injection System*, 2017 https://indico.cern.ch/event/635514/overview

[19] M.-A. Tordeux, "Longitudinal Injection into Low-Emittance Ring: A Novel Scheme for SOLEIL Upgrade", *Presentation at Topical Workshop on Injection and Injection System*, 2017 https://indico.cern.ch/event/635514/overview

[20] F. Lenkszus *et al.*, "Fast Injection System R&D for the APS Upgrade", in *Proc. of 6th Int. Particle Accelerator Conf. 2015 (IPAC'15)*, pp. 1797–1799.

[21] D. Alesini *et al.*, "Design, Test, and Operation of New Tapered Stripline Injection Kickers for the e^+e^- Collider DAΦNE", *Phys. Rev. ST Accel. Beams*, 13, 111002, 2010.

[22] M. J. Barnes, T. Flowler, G. Ravida and A. Ueda, "Design of the Modulator for the CTF3 Tail Clipper Kicker", *Proceedings of Particle Accelerator Conference, 2007*, pp. 2185–2187 (2007)

[23] T. Naito *et al.*, "Development of a 3 ns rise and fall time strip-line kicker for the International Linear Collider", *Nucl. Instrum. and Methods in Phys. Research Section A*, Vol. 571, pp. 599–607, 2007

[24] C. Gogh and M. Aiba, "Top-Up Injection with Anti-Septum", in *Proc. of 8th Int. Particle Accelerator Conf. 2017 (IPAC'17)*, pp. 774–776.

Injector Requirements for Low Emittance Storage Ring Upgrade Projects

Zhe Duan*
Key Laboratory of Particle Acceleration Physics and Technology,
Institute of High Energy Physics, Chinese Academy of Sciences,
100049 Beijing, China

I. Introduction

The multi-bend achromat (MBA) lattice, will be the basis for next-generation low emittance storage ring-based light sources (LESRs), including many upgrade projects of existing third generation light sources (3GLSs), as well as several ambitious green-field projects [1]. Such designs promise substantial brightness improvements compared to third-generation light sources, while there is likely to be a tradeoff between the optimized brightness, available dynamic aperture for injection and local momentum acceptance related to the beam lifetime. In particular, injectors are required to deliver a full energy electron beam with a sufficient charge and adequate 6D beam dimensions to the storage ring, a proper choice of the injector parameters is one essential design aspect, to enable high efficiency top-up operation of these new facilities.

Most 3GLSs utilize the conventional off-axis injection scheme, which pushes the stored beam towards the injected beam in a local bump with pulsed kicker magnets and capture the injected beam into the acceptance of the storage ring. Injected charge can be accumulated pulse by pulse into the same RF bucket with the help of radiation damping and only a moderate bunch charge is required from the injector. Its requirement on the injection acceptance A is $A \geq 6\sigma_{inj} + 5\sigma_{sto} + t$, where $\sigma_{inj}$and σ_{sto} are the injected beam size and stored beam size at the septum blade, and t is the thickness of the septum blade and some tolerances on orbit errors, which is generally no less than 3$\sim$4 mm. The lattice designs of 3GLSs aim at an injection acceptance at least on the order of 10mm, while the storage ring emittances are in the range of 1$\sim$10 nm, therefore, the tolerance for the injected beam emittance is quite relaxed. Accordingly, a combination of a low energy linac and a full energy booster synchrotron is generally adopted in 3GLSs as a cost effective injector design. The booster emittances at extraction energy range between 10 nm to 150 nm. Low emittance booster designs [2] are enabled by putting the booster into the same tunnel as the storage ring, as well as utilizing combined-function magnet lattices, which promise very clean injection into the storage ring. Generally, a high injection efficiency above 80% is rountinely achieved in the top-up operation of 3GLSs.

In contrast, to address the great challenges to realize a large enough dynamic aperture in LESRs, modification of the existing injector facilities is foreseen, to maintain the conventional injection scheme in some upgrade projects of 3GLSs; besides, novel injection schemes [3] have been proposed with a relaxed requirement on the dynamic aperture, and the injector requirements have to be re-evaluated accordingly. In the following sections the injector requirements for LESRs will be reviewed in terms of transverse emittances, longitudinal dimensions, as well as bunch charge, respectively.

II. Transverse emittances

In the conventional off-axis injection scheme, injection in the horizontal plane is favored since the bump height would otherwise be limited by the small vertical apertures in the insertion devices for vertical injection, therefore a large enough horizontal acceptance is required for a high efficiency injection. However, as shown in Fig. 1, it becomes more challenging to adopt this conventional injection scheme in MBA rings with a larger circumference and/or a more aggressive design packing more dipoles in unit circumference. ALS-U, which looks exceptional in the plot, in fact packs much more dipoles in unit circumference compared to other designs, and the relatively small horizontal acceptance is only acceptable because of the swap-out injection scheme [4] it adopts.

To accomodate a good injection efficiency with a reduced injection acceptance in LESRs, ideas to reduce the septum thickness or inject on-axis have been seriously considered. The requirements on the injection acceptance for different injection schemes could be grouped into two categories, for accumulation schemes, the 6D acceptance must cover the injected beam sizes, the stored beam sizes, as well as some spatial and/or temporal seperations between the injected and stored beams; while for the swap-out scheme, the 6D acceptance only need to cover the injected beam sizes or the stored beam sizes, and thus is less stringent compared to accumulation schemes. Nevertheless, it is favored to adopt a low-emittance injector in any case.

Modification of the existing injector is an attractive option for the upgrade project of 3GLSs. First, lower emittance booster lattice design could be pursued, by using a stronger focusing and removing the achromatic constraints at straight sections; second, a smaller extraction beam emittance could be achieved by repartioning the partition number, via running off-energy at booster extraction energy, or inserting Robinson wigglers into the lattice; third, the extraction beam from

*zhe.duan@ihep.ac.cn

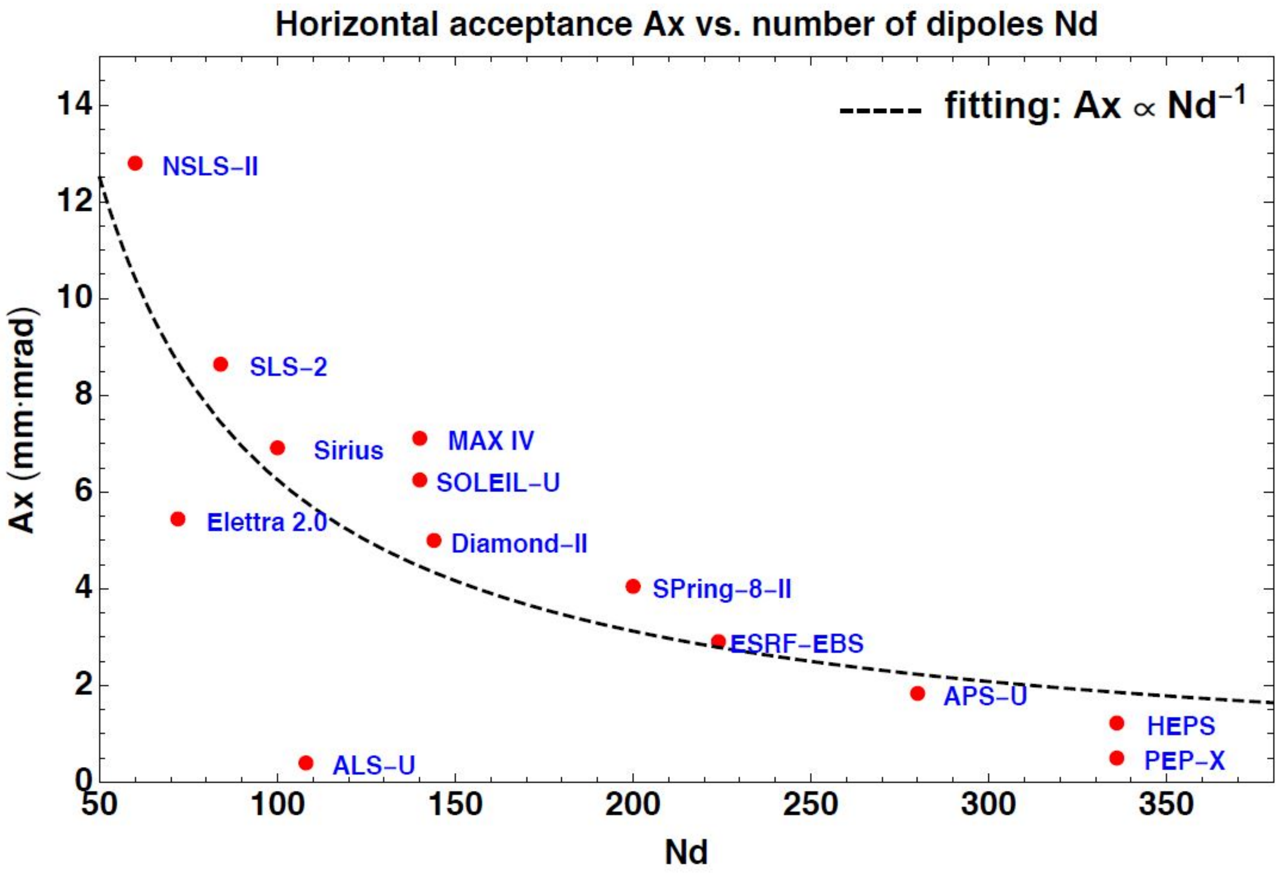

Fig. 1. Horizontal acceptance A_x versus number of dipoles N_d for an incomplete collection of LESRs. The dashed line shows a fitting of $A_x \propto N_d^{-1}$. Here, measurement data are adopted for NSLS-II [5] and MAX IV [6], while simulation results with machine imperfections are adopted for other LESRs [7–17].

booster is by default a flat beam, i.e., the vertical emittance is much smaller than the horizontal emittance, different methods are available to implement emittance exchange in the booster or in the transport line, so as to better fit the injection acceptance of the storage ring. For example, the ESRF booster is modified using a combination of these approaches to fit the injection requirement of the EBS upgrade project [18].

Sometimes modification of the existing injector could not satisfy the injection requirement for a more aggressive ring design, or a new injector is required anyway for a green field project. A full energy linac could be an ideal injector for accumulation schemes. It could provide a sub-nm rms emittance in both transverse planes, and has been the baseline for MAX IV [19], SPring-8-II [14] and HALS [20], where the same linac injector also serves as the driver for a spontaneous radiation source or a free electron laser facility in the same site. However, building a dedicated full energy linac injector could be very costly, especially for high energy LESRs. In contrast, building a low emittance booster is usually more economical. The booster of 3GLSs are generally composed of FODO cells, while the successful operation of 3GLSs gave us confidence to consider using DBA, TBA and even MBA cells in a booster lattice design to reach a nm-level natural emittance, note that the lattice design could be easier since there are no user straight sections. Ultimately, the booster beam emittances should be comparable to the storage ring beam emittances for an ultimate storage ring utilizing the swap-out injection scheme, to minimize the injection transients. Nevertheless, the proper choice of the booster emittance shoud be made following a cost benefit analysis.

III. Longitudinal dimensions

The requirements on the longitudinal dimensions of the injected beam to LESRs, however, are quite dependent on the injection scheme. For accumulation schemes, as it becomes challenging in LESRs to obtain a large dynamic aperture and momentum acceptance at the injection point, a smaller rms energy spread and bunch length are generally favored for a higher injection efficiency into LESRs. In particular, for longitudinal on-axis injection schemes [21], a temporal separation between the injected beam and the stored beam is required, instead of a spatial separation at the injection point. The longitudinal dimensions of the injected beam must be well contained in the RF acceptance of the storage ring, and the transverse beam sizes of the injected beam must be well within the off-momentum dynamic aperture. Therefore, the requirement on a short bunch length and a small energy spread could be quite stringent for a booster injector, and a linac injector is favored in this case.

For swap-out scheme, however, one of the major challenges is to inject a full charge bunch into the storage ring, where the storage ring impedance effects together with the strong lattice non linearity could lead to a transient beam loss [22]. Studies indicated an injected bunch better matched with the stored bunch in the longitudinal phase space is favored for a higher injection efficiency. To this end, the RF phase modulation technique is considered in the booster to shape the bunch longitudinal phase space before extraction to realize a higher injection efficiency [23].

IV. Bunch charge

Accumulation schemes generally requires that each injected bunch only contains a fraction of the stored bunch charge, in contrast, the swap-out injection scheme requires a full charge injector, and it could be difficult for a full energy linac to satisfy the bunch charge requirement. To this end, different ideas have been developed to include an accumulation ring in the injector chain and help deliver full charge bunches.

First, a full energy accumulator ring between the booster and the storage ring is the baseline in ALS-U [24] and also considered in Diamond-II [25]. For these medium energy LESRs, a full energy accumulator ring promises a much reduced emittance compared to the existing booster, and the fixed energy operation is beneficial for accumulation of more bunch charge, the depleted bunches from the storage ring can be recycled in the accumulator ring to further relax the requirement on the booster.

However, a full energy accumulator ring could be expensive for high energy LESRs. Moreover, the major challenge for these high energy LESRs is to deliver tens of bunches with a $\sim$15 nC bunch charge for the timing mode. In the case of APS-U [15], the existing low-energy accumulator ring PAR, is used to capture several linac bunches to form one full charge bunch, and the bunch is then injected into the booster, accelerated to extraction energy and delivered to the storage ring, while the depleted bunch is absorbed by a dedicated beam dump. In contrast, for the green field machine HEPS, the booster is used also as a full energy accumulator ring [26], after bunches are accelerated in the booster to the extraction flat-top energy, the depleted bunches of the storage ring are extracted and merged with the accelerated bunches in the booster, before re-injected into the storage ring. In this way, only a moderate charge (up to 5 nC) is required to be captured and accelerated at the booster injection energy, where instability issues are more of concern compare to the extraction energy.

V. Summary

A low emittance injector is generally favored for LESRs. Different approaches are available and choice should be made based on cost benefit evaluations. Successful commissioning and operation of 3GLSs gave us confidence to commission a low emittance booster in a relatively short time. The requirement on the longitudinal dimensions of the injected beam differ between the accumulation schemes and the swap-out scheme.

Swap-out injection supports a higher brightness lattice design and promises more transparent injection to the users, compared to conventional off-axis injection scheme, but also introduces nontrivial challenges to the injector design and operation. There are on-going work to ensure the delivery of $\sim$15 nC bunch charge with a high efficiency into the storage ring, and a high reliability of the injector system is essential for the robust operation of the swap-out scheme [27].

References

[1] E. Karantzoulis, ibid.
[2] W. Joho, et al., NIM A, 562(2006) 1-11.
[3] M. Aiba, ibid.
[4] L. Emery and M. Borland, Proc. PAC'03, pp 256-258.
[5] F. Willeke et al., Proc. IPAC'15, MOYGB3, pp 11-16.
[6] S. C. Leeman, et al., NIM A 883(2018) 33-47.
[7] SLS-2 Conceptual Design Report, 2017.
[8] Elettra 2.0 Preliminary Conceptual Design Report, 2018.
[9] $https://wiki-sirius.lnls.br/mediawiki/index.php/Machine : Storage_Ring\#Dynamic_and_momentum_aperture$
[10] A. Loulergue, et al., Proc. IPAC'18, THPML034, pp 4726-4729.
[11] A. Alekou, et al., arXiv:1801.02522.
[12] EBS Storage Ring Technical Report, 2018.
[13] Y. Jiao, et al., J. Synchrotron Rad. 25, (2018) 1611-1618.
[14] SPring-8-II Conceptual Design Report, 2014.
[15] Advanced Photon Source Upgrade Project Preliminary Design Report, APSU-2.01-RPT-002, 2017.
[16] C. Sun, et al., Proc. IPAC'17, WEPAB015, pp 2827-2829.
[17] Y. Cai, et al., PRST-AB 15, 054002 (2012).
[18] N. Carmignani, ibid.
[19] The MAX IV Detailed Design Report, 2010.
[20] L. Wang et al., Proc. IPAC'18, THPMK120, pp 4598-4600.
[21] M. Aiba, PRST-AB 18, 020701 (2015).
[22] R. Lindberg, Proc. NAPAC'16, WEPOB08, pp 901-903.
[23] Private communication with Gang Xu and Haisheng Xu.
[24] C. Steier, et al., Proc. IPAC'17, WEPAB103, pp 2821-2823.
[25] I. P. S. Martin and R. Bartolini, J. Phys.: Conf. Ser. 1067, 032005 (2018).
[26] Z. Duan et al., Proc. IPAC'18, THPMF052, pp 4178-4180.
[27] M. Borland, Proc. NAPAC'16, WEPOB02, pp 881-883.

ESRF booster modifications and commissioning

Nicola Carmignani
ESRF, Grenoble, France

I. Introduction

The new storage ring of the ESRF, the Extremely Brilliant Source (EBS), will have a substantial lower dynamic aperture than the present one: about 8 mm instead of 20 mm.

The injection scheme in the new machine will be the same, with a standard 4 kickers bumb in the storage ring.

Simulations have shown that the injection efficiency in the EBS will strongly depend on the emittance of the injected beam (fig. 1).

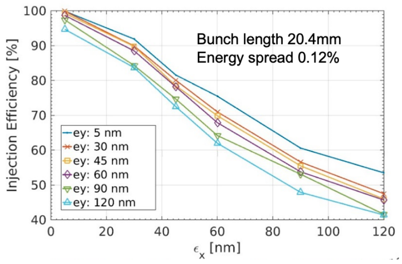

Fig. 1: Injection efficiency vs booster emittance

II. Emittance reduction

We plan to reduce the emittance of the booster in three ways:

- new tune working point;
- off-energy operation;
- full coupling at extraction.

A. New tune working point

Increasing the horizontal tune of the booster by one unit, the horizontal emittance decreases from 120 nm to 100 nm, but the dynamic aperture becomes smaller (fig 2).

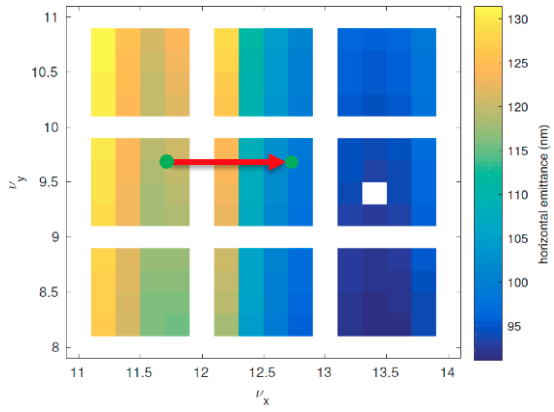

(a) Tune scan booster

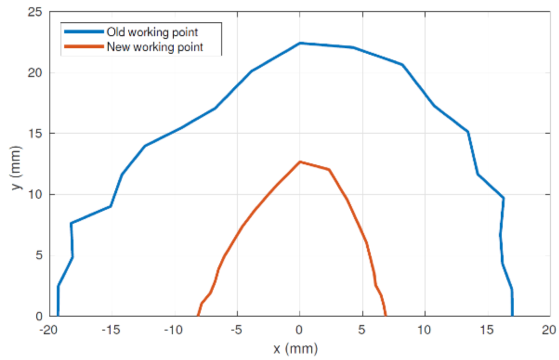

(b) Dynamic aperture for the two working points

Fig. 2: Different working point

B. Off-energy operation

By operating the booster off-energy (δ = - 1.2%, Δ_{RF} = + 40 kHz), horizontal emittance decreases from 100 nm to 63 nm, while bunch length and $\mathcal{J}_x$ increase (fig. 3).

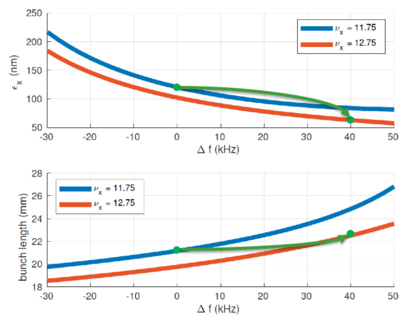

Fig. 3: Emittance and bunch length for different RF frequencies

C. Full coupling at extraction

We will operate the booster crossing the coupling resonance at the extraction time, reducing horizontal emittance (fig. 4).

Because $\mathcal{J}_x$ is not 1, we don't gain a factor 2 in emittance operating the booster on the coupling resonance. The coupled emittance will be 39 nm. The coupled emittance can be computed with formula of eq. (1).

$$\varepsilon_{round} = \frac{\mathcal{J}_x}{\mathcal{J}_x + \mathcal{J}_y} \varepsilon_x \tag{1}$$

Emittance measurements have confirmed the expected reductions.

III. Hardware modifications

The EBS ring will be 40 cm shorter than the old machine. The booster will operate with a 40 kHz frequency mismatch. The EBS and the booster will operate with the same RF

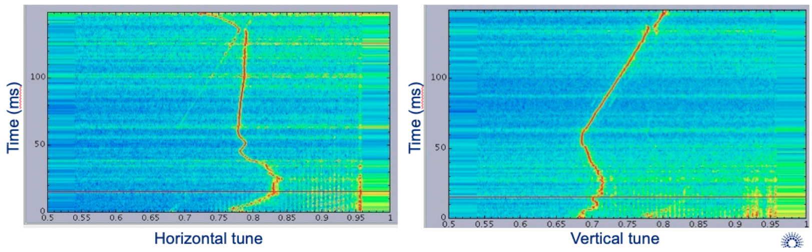

Fig. 4: Horizontal and vertical tune of the booster.

frequency, to allow the synchronization of extraction and injection, so the booster length has to be adjusted.

All the elements of the booster will have to be moved by 17.5 mm to the centre of the ring. The movement is within the adjustment capability of most of the girders of the booster. In some cases, some plates with couples of holes at 17.5 mm distance have been installed between the girders and the magnets (fig. 5).

IV. Injector commissioning

The injector will be commissioned in November 2019. The EBS commissioning will start in December 2nd 2019.

The first turn code, developed for the storage ring, has been successfully tested in the booster during MDT (fig. 6).

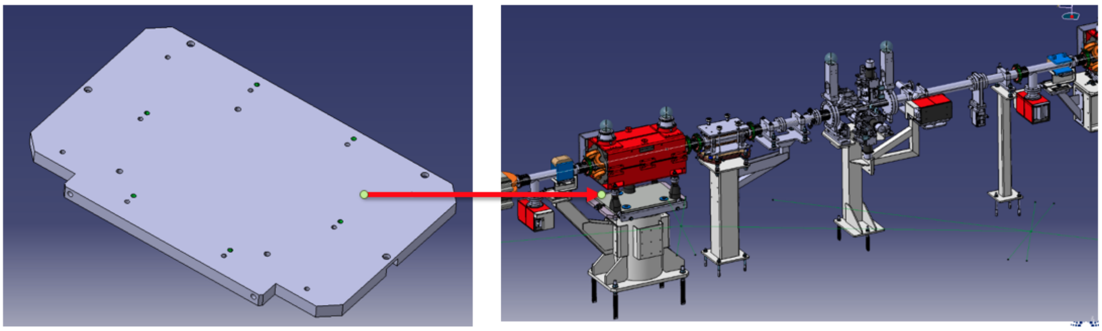

Fig. 5: Plates between girders and quadrupoles installed in the booster.

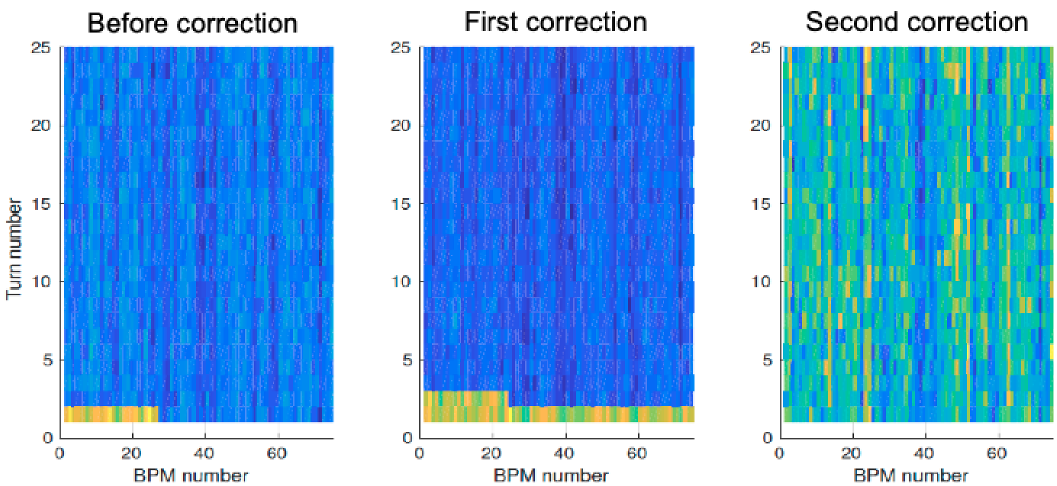

Fig. 6: First turn application working in the booster.

Session 3: Insertion Devices

Summary: Insertion Devices

N. Mezentsev,
Budker Institute of Nuclear Physics, Novosibirsk, Russian Federation
A.I. Wawrzyniak
NSRC Solaris, Krakow, Poland

***Abstract*—Brief summary of reports on session "Insertion devices" of ARIES / ICFA workshop on "Beam tests and commissioning of low-emittance storage rings" is presented.**

***Keywords*—Undulator, cryo-cooled undulator, superconducting undulator, superconducting wiggler**

I. Introduction

During the "Insertion devices" session four talks were presented:

- "MAXIV Undulators Performance" given by Hamed Tarawneh from MAXIV Laboratory, Lund Sweden
- Interaction of in-vacuum undulators with electron beam given by Kai Tian from SLAC
- Supeconducting Wigglers and Undulators given by Nikolay Mezentsev, BINP, Novosibirsk, Russia and Efim Gluskin, APS, USA
- Commissioning experience with commercial S.C. undulators given by Sara Casalbuoni from KIT, Karlsruhe, Germany

II. MAXIV Undulators Performance Given by Hamed Tarawneh from MAXIV Laboratory, Lund Sweden

he operational status of the MAXIV storage rings with various insertion devices (IDs) was presented. At MAXIV only warm IDs are used. For the soft X ray the APPLEII undulators (7) are used whereas for hard X ray range the in vacuum devices (8) are utilized. Currently, there are seven beamlines with IDs available for the users, whereas additional five is under commissioning. In the near future next 3 in vacuum undulators are planned to be installed and commissioned. The IDs at MAXIV are both a commercial and in house developed IDs. The in-vacuum wiggler is built with collaboration with SOLEIL facility.

Usually the performance of the commercial devices need to be checked after manufacture and in many cases they do not meet the specified requirements. For the low emittance storage ring as MAXIV the one of the key parameters is reaching the high beamlines performance therefore building in house IDs is of great importance and interest in order to meet the high requirements.

In order to characterised and improve the magnetic properties of the IDs several methods are used to characterise the magnetic field, namely hall probe, flip coil, stretched wire measurements at MAXIV laboratory. Moreover a new pulsed wire method is being developed allowing for more accurate measurements.

The calculation of the spectra based on the magnetic measurements showing the good correspondence with the measured spectra for MAXIV IDs. During the commissioning the undulators are optimised with respect to the electron distortion. It was presented that there is strong impact on the electron beam orbit from in vacuum devices. The distortion is minimised by installing the corrector magnets and undulators optimisation. The IDs alignment is verified using the undulator harmonics for different displacements and angle of the electron beam. Moreover the photon-beam-based alignment studies are carried on in order to optimise the electron beam inside the undulator. Additionally measurements of the flux versus photon energy with respect to different condition of the electron beam (with/without bunch by bunch feedback, mode zero damper, length of the bunches) allow to properly tune the spectra. There is also need for special features for beamlines which can be achieved by tapering of the undulators.

For the future also cryo-cooled undulators are planned to be developed and installed, which will be dedicated for the hard X –ray beamlines. It is planned also to use 2nd harmonics to cover wider range of the energy.

III. Interaction of In-Vacuum Undulators with Electron Beam Given by Kai Tian from SLAC National Accelerator Laboratory, California, USA

In the second talk the in vacuum undulators interactions with electron beam were presented. The electron beam interacts with the IVU by the short and the long range wake fields. It is of high interest to minimise the interaction between the electron beam and the IVU. For the short range wakefields which corresponds to a single bunch effects the optimisation are done during the design phase of the device by implementing the current sheets, and flexible transitions. This topic has been studied and has good agreement with the theory. Therefore the talk mostly focused on the multi-bunch effects (long range wakefields) which occur due to higher order modes trapped in the IVU.

SPEAR3 is a 3 GeV, 500 mA, third generation light source. The 2-meter-long BL15 insertion device (BL15 ID) in SPEAR3 is the second IVU in the storage ring with an undulator period of 22 mm. During early commissioning of the BL15 ID, we observed that the transverse beam size increased at small, discrete magnet gaps with 500 mA stored beam. Similar problems have been reported and investigated in other facilities as well. Upon further investigation, we discovered that the beam size increase was caused by transverse coupled-bunch instabilities driven by the trapped resonant modes inside the IVU chamber. The geometry of the IVU chamber, with the magnetic structure, resembles many features of a round ridge, which supports lower frequency modes that can be trapped inside the bare vacuum chamber. A transverse mode can be excited by the bunches in the ring. This mode, in turn, if sufficiently strong, can drive the beam unstable. The IVUs are designed for variable gap operations, therefore, the spectrum of the trapped modes shifts in frequency with the changes in the magnet gap of the IVU. The coupling impedance is sufficiently strong that when the mode frequency overlaps the lower vertical betatron sideband of a revolution harmonic vertical instabilities are excited in SPEAR3. Most modern storage rings, including SPEAR3, are equipped with multi-bunch feedback systems, which have been successfully demonstrated to be effective in damping these, and other, transverse coupled-bunch instabilities. However it is preferable to passively eliminate the source of the instability rather than to rely on active damping. The trapped RF modes in the IVU have been studied using high performance simulation codes, Omega3P. Both the electric and magnetic fields of these trapped modes are concentrated at the narrow magnet gap. Damping of both electric and magnetic fields is electromagnetically possible by placing the appropriate absorptive material in or near the gap. While the electric field in the rest of the chamber remain very small, significant magnet fields leak out of the magnet gap and fill the vast space in the chamber. Therefore, if one is limited by practical considerations to placing damping materials only away from the gap, we are limited to absorptive magnetic material. Especially, the magnetic field is enhanced around the bellows of the linked rods. Therefore these modes can be effectively damped by adding magnetic damping materials around these rods. Furthermore, in order to achieve the full spectrum damping to all the ridge-waveguide modes, it is prudent to add the damping materials to all the rods. The damping performance of the ferrite dampers have been studied both in numerical simulations and through RF cold measurements. In the new BL17 ID, the most recently ordered device for SPEAR3 with almost identical design to the BL15 ID, ferrite dampers are successfully incorporated; therefore, this device can serve as the first test-bed for the performance of these dampers. The RF cold test for the BL17 ID equipped with the ferrite dampers agree very well with the numerical simulations. This proves that ferrite dampers are a very effective and simple solution to the problem in SPEAR3 and should also work for other facilities. Besides the ferrite dampers, we have also briefly investigated serval other alternative approaches to damp the trapped modes. Fig. Two examples are a multi-turn loop antenna aiming to couple the mode power out of the chamber and mode curtains for increasing the mode frequencies so that they would not be trapped. However, both options are not as appealing as the ferrite dampers for SPEAR3 and are not well studied. There are some interesting topics worth further efforts, i.e. high fidelity simulations with more accurate models in both time domain and frequency domain; direct measurement of the transverse impedance (Beam based/bench RF) and other effects of these trapped modes. With the concerns of impedances in future LERs, it will be definitely beneficial to address these questions.

IV. SUPECONDUCTING WIGGLERS AND UNDULATORS GIVEN BY NIKOLAY MEZENTSEV FROM BINP, NOVOSIBIRSK, RUSSIA AND EFIM GLUSKIN, APS, USA

In the first part of the report an information on the state of art of manufacture of superconducting multipole wigglers in BINP for various centers of synchrotron radiation is provided. The second part of the report is made on behalf of E.Gluskin about the state of art on production and work of superconducting undulators in APS.

More than two tens of superconducting wigglers and high field shifters were made and installed on various SR sources in the world. The wigglers it is possible to divide into three groups: wigglers with the high magnetic field of 7-7.5 Tesla, with the average field 3-4.3 Tesla and with the field of a 2-2.2 Tesla with the short period.

A high-field superconducting shifter in the location with a small horizontal beta function and zero dispersion would be a virtually point source of high brightness in a wide range of photon energies. Dispersion function, that becomes non-zero in a 3-pole shifter, can be minimized at radiation point using a 5-pole shifter. The installation of two additional correctors on both sides of the shifter makes it possible to create a magnetic distribution in the shifter, at which the radiation point is on axis of the straight section and does not depend on the value of magnetic field in the shifter. In that case radiation from the central, strongest pole passes at zero angles to the straight section. Three of these type shifters with field of 7 Tesla are in permanent use on BESSY (1.7 GeV) and LSU CAMD (1.35 GeV).

Four high field superconducting multipole wigglers with field of 7-7.5 Tesla are successfully working at BESSY (Berlin, Germany), LSU CAMD (USA), Siberia-2 (Moscow, Russia), Delta (Dortmund, Germany). Use of high field multipole wigglers is the adequate decision for SR sources with electron energy of 1.25-1.7 GeV for generation of photons in the field of a hard X-ray.

For synchrotron radiation sources with energy of 3 GeV the most popular are superconducting multipole wigglers with field of 2.5-4 Tesla. Two wigglers with field of 3.5 T and 4.2 T are in operation at Diamond Light Source (3 GeV), 4.2 T the wiggler is in operation at CLS (2.9 GeV, Canada), 4.1 T wiggler is working at LNLS (1.37 GeV, Brazil), 4.2 T wiggler is working on Australian Synchrotron SI source (3 GeV), 2.5 T wiggler is installed on SR KARA source (2.5 GeV, Germany), 3 Tesla wiggler is installed on SR KARA source (2.5 GeV, Germany). and two 3 Tesla wigglers for Moscow SR Center will be installed in the mid of 2019.

Low field (2-2.2T) and short period (3 cm) wigglers were fabricated and installed on ALBA Light Source (3 GeV, Spain) and CLC (2.9 GeV, Canada).

The cryogenic system used for the superconducting wigglers, is based on use of two stage cryocoolers and liquid helium, which temperature reaches 3-3.5K. Cryogenic systems in which the magnets are immersed into liquid helium, and systems in which the magnets are indirect cooled, are developed.

There are three SCUs that have operated at the APS, each for different a period of time. SCU0 operated from January 2013 to August 2016 and was at the APS Sector 6 by SCU18-2 in September of 2016. SCU1, now called SCU18-1, has operated at the APS Sector 1 from January 2015 to the present day. Recently, the HSCU started its first year of operations at the APS Sector 7. Overall, thousands of hours of operational experience with SCUs have been accumulated. The first and most important takeaway from this experience is that the SCUs did not cause even a single beam loss in the storage ring through all these years. Each SCU is equipped with a system that prevents catastrophic and uncontrolled beam motion during a quench. Another important result is that even the total number of quenches for all operational SCUs through all these years was 148, the majority of these events were related to unexpected beam dumps at the storage ring, whereas the total number of self-induced quenches was only ten. To prevent beam dump-related quenches in SCUs by controlling beam loss locations, an abort kicker system triggered by the machine protection system could be used. Such a kicker was installed at the APS in January 2016, and since then the number of beam dump-related quenches drastically decreased. The operational statistics of the APS SCUs are practically the same as for the APS hybrid magnet IDs. The average APS SCU availability is close to 99.57The performance of one of APS's SCUs – SCU1(SCU18-1) – as a radiation source has been studied in details. The absolute flux measurements of monochromatic beam have been performed for undulator radiation harmonics from 1 to 9 and those data were compared with calculated values. The measured flux is $\cong 2/3$ of calculated flux, which is quite reasonable given the nontrivial nature of absolute flux determination. What is more important is that the ratio of flux at high harmonics to flux at first harmonic, at both calculated and measured tuning curves, is quite close. That quite accurately confirms the value of phase errors obtained in the SCU's magnetic measurements. Planar SCUs deliver linearly polarized radiation, and the direction of the polarization vector is perpendicular to the direction of the magnetic field in the SCU. Non-planar SCUs could be built as a pure helical undulator, or by combining two planar SCU magnets in one magnetic structure of an undulator that produces variably polarized radiation. In the last several years significant progress in SCU technology has taken place as well. There were four very important milestones achieved in the process of developing SCU technology at the APS. First of all, it was experimentally demonstrated that SCU magnets could be built to the technical specifications for undulators set by most advanced light sources and FELs, and there is no shimming required to achieve this high level of magnetic performance. Second, the engineering of SCU cryogenic systems matured enough to design and build robust and affordable cryostats. These cryostats, that house SC magnets and a beam vacuum chamber, could operate as a stand-alone system, or become a part of the large cryogenic facility. In either case, their cooling capacity has enough margin to handle heat loads from storage ring- and FEL-based light sources. It was also shown that the beam vacuum chamber is exposed to well-predicted heat loads from e-beam and synchrotron radiation. Third, it was demonstrated that SCUs could be aligned under operational conditions, and the accuracy of such an alignment matches the one of conventional, in-air permanent magnet undulators. Finally, the operational reliability of several SCUs has been confirmed by their practically flawless performance at the APS storage ring. This progress has demonstrated that the magnetic and radiation performance of SCUs matches the performance of the best permanent undulators.

V. COMMISSIONING EXPERIENCE WITH COMMERCIAL S.C. UNDULATORS GIVEN BY SARA CASALBUONI FROM KIT, KARLSRUHE, GERMANY

The parameters and the commissioning steps of the of the commercially available superconducting undulator (SCU20) with the period length of 20 mm and the peak magnetic field of 1.18 T was presented. The SCU20 was developed in collaboration between the Karlsruhe Institute of Technology (KIT) and the company Bilfinger Noell GmbH (Noell). The first commissioning step was to characterise magnetic field of the superconducting coils within use of the CASPERII test stand developed in KIT. The coils configuration in the test stand is close to the final one in the cryostat. This allowed for measurements and the correction of the vertical magnetic field integrals and the roll errors. Next step was to test the device without the electron beam in the final configuration. There was no possibility to characterise the magnetic field in the final cryostat, the methods are under development at KIT. In winter 2017 the SCU20 was installed in KARA storage ring and as it was demonstrated the SCU20 is transparent to the electron beam with values of correctors very close to the ones measured in CASPER II. Moreover the proper correctors settings were obtained very fast (few hours) and tests with all beamlines have shown that the tuning of the SCU20 is well-matched with all beamlines at KIT. The spectra characterisation on NANO beamline is ongoing and so far showing good agreement with the measured one at test stand. This means that the commercially developed superconducting undulator is providing excellent performance and the procedure of commissioning followed at KIT with the CASPER II test stand gives very fast and accurate way to put the device into operation.

Commissioning experience with commercial superconducting undulators

S. Casalbuoni, E. Blomley, N. Glamann, A. Grau, T. Holubek, E. Huttel, D. Saez de Jauregui,
Institute for Beam Physics and Technology, Karlsruhe Institute of Technology, Karlsruhe, Germany
S. Bauer,
Institute for Photon Science and Synchrotron Radiation, Karlsruhe Institute of Technology, Karlsruhe, Germany
C. Boffo , Th. Gerhard, M. Turenne, and W. Walter
Bilfinger Noell GmbH, Würzburg, Germany

***Abstract*—In this contribution the main steps of the commissioning of the first commercially available superconducting undulator (SCU) at the KIT synchrotron are reviewed. A SCU with 20 mm period length (SCU20) has been developed by the Karlsruhe Institute of Technology (KIT) in collaboration with the industrial partner Bilfinger Noell GmbH (Noell).**

***Keywords*—Superconducting undulator, beam heat load, undulator radiation**

I. Introduction

The Karlsruhe Institute of Technology (KIT) and the company Bilfinger Noell GmbH (Noeel) are developing superconducting undulators (SCUs) for the KIT synchrotron and low emittance light sources. The first important milestone reached by the collaboration was the development and successful test with electron beam in the KIT synchrotron of a SCU with 15 mm period length. This device was the first full scale SCU reaching a higher peak field on axis with respect to the competing cryogenic permanent magnet technology with electron beam [1]. In the new SCU with a period length of 20 mm (SCU20) all the lessons learned from the previous device have been applied, with the aim to making it more compact, robust and easier to use [2]. The SCUs developed by the collaboration are based on NbTi wire technology. A big advantage for the users is that our SCUs are conduction cooled, which means that there is no need of liquid helium or nitrogen to operate or cool them to the operating temperature. Both SCU15 and SCU20 have moreover a beam vacuum chamber that can be opened up to 15 mm, which is required at the KIT synchrotron during electron beam injection [2]. The magnet can be powered only when the vacuum gap is closed to 7 mm. The main parameters of SCU20 are listed in Table I.

TABLE I
Main parameters of SCU20 [2].

Period length	20 mm
Maximum peak field on axis	1.18 T
Number of fully wound periods	74.5
Magnetic length	1.554 m
Magnetic gap	8 mm
Vacuum gap closed (open)	7 (15) mm

The SCU20 layout foresees the coils to be able to cope with a beam heat load of 4 W. The end field design to reduce the vertical field integrals below the specified values uses correction coils wound on the same iron yoke as the main coils as well as Helmholtz coils. The horizontal field integrals are corrected with copper coils placed out of the cryostat [3]. In Fig. 1 a picture of SCU20 installed in the KARA (KArlsruhe Research Accelerator) storage ring of the KIT synchrotron is reported.

II. Commissioning

The commissioning of the SCUs happens in three main steps:

- Test of the superconducting coils in the test facility CASPER II (Characterisation Setup for Phase Error Reduction)
- Test of the SCU without electron beam
- Test of the SCU with electron beam after installation in the accelerator

Fig. 1. SCU20 installed in the KIT synchrotron.

The different steps are described below together with few examples of measurements performed.

A. Test of the superconducting coils in the test facility CASPER II

CASPER II, developed at KIT, is a unique horizontal test stand in which conduction cooled coils up to $\sim$ 2 m length can be magnetically characterized [4], [5]. The coils are in a configuration very close to the one in the final cryostat. The superconducting coils are first trained to reach the maximum operating current. Afterwards the coils are left for about 12 hours at maximum current to test their stability [6]. Then the vertical field integrals are minimized to values below the specified ones by means of the correction coils described above. The field integrals are measured with the stretched wire technique. Once the values of the correction coils for different currents of the main coils are established, the local field measurements are performed using a Hall probe placed on a sledge, which is guided along the magnetic axis or parallel to it. This is done to measure the roll off, defined as follows:

$$\text{Roll off} = \frac{B(x = \pm 10\text{ mm}) - B(x = 0\text{ mm})}{B(x = 0\text{ mm})} \qquad (1)$$

The vertical integrated field multipoles have been calculated from the measurements of the first vertical field integral. The measured integrated field multipoles do not affect the dynamic aperture for the optics at 2.5 GeV electron beam energy of the storage ring. The measured roll off induces a negligible dynamic kick [3]. An example of magnetic local field measurement is shown in Fig. 2 for a current in the main coils of 395 A, and with the correction coils set to correct for the vertical field integrals.

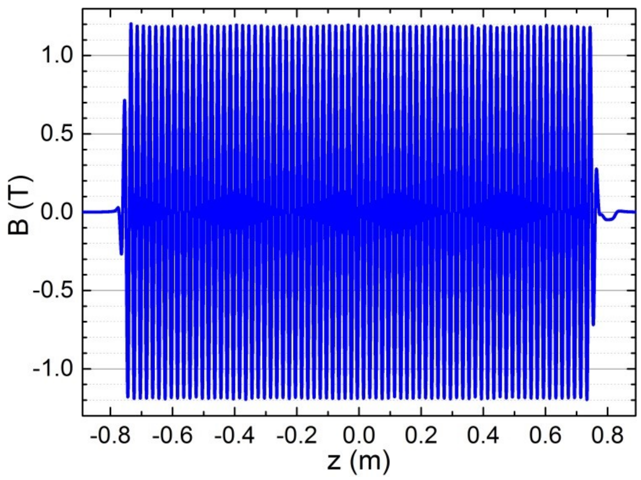

Fig. 2. Magnetic field profile of the SCU20 coils measured at CASPER II with a current in the main coils of 395 A and the correction coils set to current values to minimize the vertical field integrals [2].

From the magnetic field profile it is possible to calculate the flux from a slit with given dimensions and placed at a fixed distance from the undulator. In Fig. 3 it is reported the flux calculated at 10 m from the middle of the undulator through a rectangular slit 50 μm $\times$ 50 μm using the KARA beam parameters for an ideal SCU20, i.e. without mechanical errors and with perfect end fields, for the measured field of the SCU20 coils and an ideal cryogenic permanent magnet undulator (CPMU) with the same parameters as that built at SOLEIL for the same vacuum gap of 7 mm. The comparison of SCU20 with the ideal CPMU18 shows a flux/brilliance at high energies up to five times larger for the SCU20 (Figure 3a). At low photon energies, Figure 3b illustrates that the energy regions allowed with the SCU20 are not reachable with CPMU18 [3].

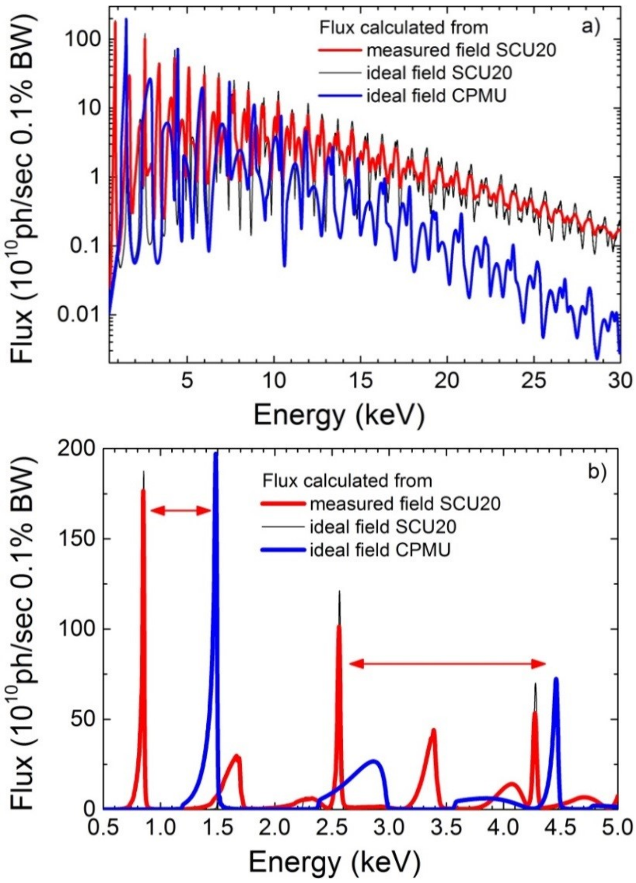

Fig. 3. a) Flux through a slit of 50 m x 50 m placed at 10 m from the source calculated with B2E for the measured magnetic field of the SCU20 at 395 A (red line), as well as for a SCU20 (black line) and a CPMU18 (blue line) with ideal field profile (without mechanical errors and perfect end fields), with 1.5 m and 2 m magnetic length, respectively. b) Zoom of (a) in the low energy range and with a linear scale: the red arrows indicate the extended energy region available with the SCU20 with respect to the CPMU18 [3]. Reproduced under the terms of the Creative Commons Attribution 3.0 license.

B. Test of the SCU without electron beam

Before installation of a SCU in the KARA storage ring several test are performed. First the SCU is cooled down to operating temperature. SCU20 cooldown time is about 5 days. Then the coils need to be trained. In general, since they have a memory effect, few quenches are needed to reach the maximum operating current. In case of SCU20 the coils reached 400 A after the first ramp, so no training was needed. A quench was observed few minutes after that the coils reached the 400 A for the first time. The coils recover the operating temperature after about 15 minutes from the quench, which allows to power them again. An additional test performed before installation in the storage ring is the stability of the magnet, which was tested powering it with maximum current together with the correction coils for about one week. SCU20 successfully withstood the test without quenches. The SCU is then warmed up before installation in the storage ring. Warm up time for SCU20 is about 4 days [7]. It is general practise to measure the local magnetic field as well as the field integral of undulators in their final configuration, which for SCUs translates in measurements in their final cryostat. This has not been performed for SCU20. A measurement system for the final cryostat is under development at KIT. In the next subsection it is however shown that the we can very well rely on the measurements performed at CASPER II, where the coils are tested in a configuration very similar to the one in the final cryostat both from the geometrical and from the cooling point of views.

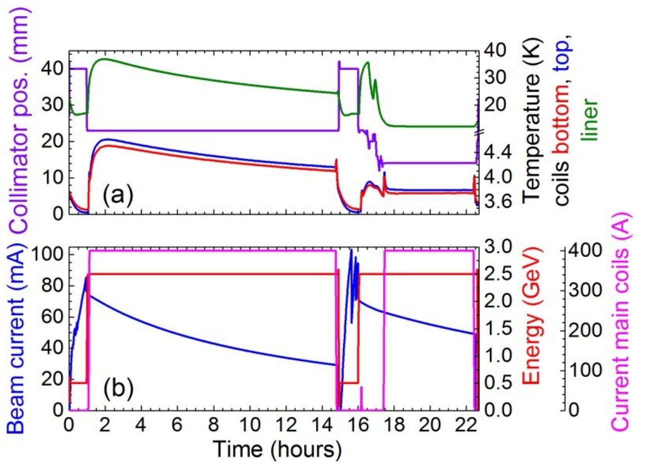

Fig. 4. a) Position of the horizontal collimator (violet line) and the temperature of the top (blue line) and bottom (red line) coils as well as of the liner (green line) as a function of time. b) Beam current (blue line), beam energy (red line), and current in the main coils (magenta line) of the SCU20 as a function of time [7], [8]. Reproduced under the terms of the Creative Commons Attribution 3.0 license.

C. Test of the SCU with electron beam

The installation of SCU20 in the KARA storage ring was performed in the winter shutdown of 2017. The alignment procedure is similar to the one performed with the previous SCU with 15 mm period length and described in Ref. [1]. SCU20 cooled down during the winter holidays and just after three days of machine operation the first X-rays have been observed at the NANO beamline. Since January 2018, SCU20 is operating in the storage ring without quenches [7]. The installation requires the venting of a 5 m long straight section (on a ring of 110.4 m circumference). The beam lifetime was recovered in about 3 weeks of beam operation of the storage ring at 2.5 GeV [7]. SCU20 is transparent to the electron beam with values of correctors very close to the ones measured in CASPER II. This gives confidence in the CASPER II measuring system and in the assembly procedure followed. Adjustment of the currents in the vertical and horizontal correctors was performed in few hours. Experiments involving all beamlines have been performed showing that the tuning of SCU20 is compatible with the operation of all the beamlines of the KIT synchrotron while performing their most sensitive experiments [7]. Furthermore, the robustness of SCU20 has been demonstrated by exposing it to a beam heat load about double of the specified one: 8 W instead of 4 W. This has been made by moving a collimator located between SCU20 and the upstream banding magnet: the beam vacuum chamber and the coils have been exposed to additional synchrotron radiation from the upstream bending magnet, which are otherwise screened by the collimator (see Fig. 4). This experiment shows an excellent thermal decoupling between the beam vacuum chamber and the coils separated only by 0.2 mm per side along 2 m length.

An accurate spectral characterization is ongoing at the NANO beamline. Preliminary measurements of the photon spectrum, reported in Fig. 5, show from the position of the 7^{th} harmonic that the peak field on axis is in very good agreement with the one measured in CASPER II of 1.18 T [7].

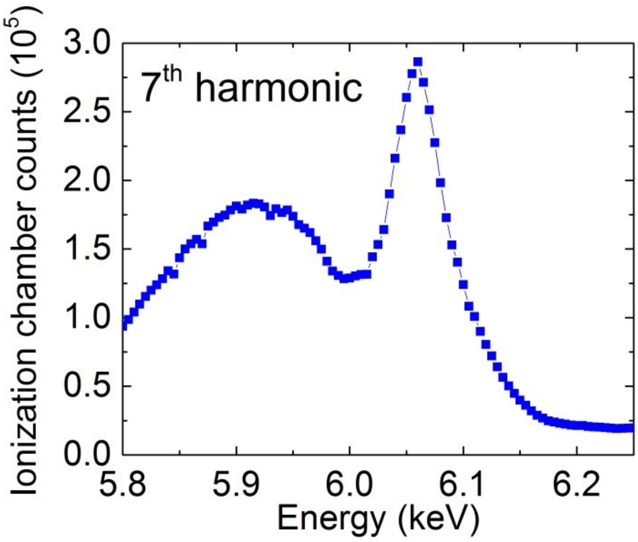

Fig. 5. a) Position of the horizontal collimator (violet line) and the temperature of the top (blue line) and bottom (red line) coils as well as of the liner (green line) as a function of time. b) Beam current (blue line), beam energy (red line), and current in the main coils (magenta line) of the SCU20 as a function of time [7], [8]. Reproduced under the terms of the Creative Commons Attribution 3.0 license.

III. Conclusions

SCU20 is the first commercially available undulator world-wide: a robust device, with reasonable delivery time (approx. 2 years including magnetic field characterization at CASPER II), easy handling during installation and operation and providing superior performance compared to other available technologies [7]. The main steps of its commissioning, being the magnetic field characterization of the superconducting coils, the tests of the assembled SCU20 without and with electron beam, have been described.

IV. Acknowledgments

The authors would like to thank: M. Hagelstein, T. Baumbach, C. Heske, A.-S. Müller, and V. Saile (KIT) for supporting the project, to the IBPT technical group and in particular to Th. Fischböck, M. Süpfle, A. Völker (KIT) for support during installation, to M. Schuh (KIT) and the NANO beamline staff for their help during the SCU20 tests, and to all other beamlines at the KIT synchrotron for their feedback during tuning experiments.

References

[1] S. Casalbuoni, A. Cecilia, S. Gerstl, N. Glamann, A. W. Grau, T. Holubek, C. Meuter, D. Saez de Jauregui, R. Voutta, C. Boffo, Th. Gerhard, M. Turenne, and W. Walter, "Characterization and long term operation of a novel superconducting undulator with 15 mm period length in a synchrotron light source", Phys. Rev. ST Accel. Beams, **19** (2016) 110702; https://doi.org/10.1103/PhysRevAccelBeams.19.110702

[2] S. Casalbuoni, N. Glamann, A. Grau, T. Holubek, D. Saez de Jauregui, S. Bauer, C. Boffo, T. Gerhard, M. Turenne, and W. Walter, "Superconducting Undulators: From Development towards a Commercial Product", Synchrotron Radiation News, **31:3** (2018) 24-28; https://www.tandfonline.com/doi/full/10.1080/08940886.2018.1460171

[3] S. Casalbuoni, N. Glamann, A. Grau, T. Holubek, D. Saez de Jauregui, C. Boffo, T. Gerhard, M. Turenne, and W. Walter, " Field quality of 1.5 m long conduction cooled superconducting undulator, J. Phys.: Conf. Ser. **874** (2017) 012015; https://doi.org/10.1088/1742-6596/874/1/012015

[4] A. Grau, T. Baumbach, S. Casalbuoni, S. Gerstl, N. Glamann, M. Hagelstein, T. Holubek, D. Saez de Jauregui, "Cryogen-free setup for local and integral field magnetic field measurements of superconducting undulator coils", IEEE Trans. Appl. Supercond. **22-3** (2012) 9001504; doi: 10.1109/TASC.2011.2179699

[5] A. Grau, S. Casalbuoni, S. Gerstl, N. Glamann, T. Holubek, D. Saez de Jauregui, C. Boffo, T. Gerhard, M. Turenne, and W. Walter "Characterization of 30-cm-Long Superconducting Undulator Coils With the Magnetic Measurement System CASPER II", IEEE Trans. Appl. Supercond **24-4** (2016) 4100804, https://doi.org/10.1109/TNS.1977.4329085

[6] A. Grau, S. Casalbuoni, N. Glamann, T. Holubek, D. Saez de Jauregui, C. Boffo, T. Gerhard, M. Turenne, and W. Walter "Full-Scale Conduction-Cooled Superconducting Undulator Coils—Training, Stability, and Thermal Behavior", IEEE Trans. Appl. Supercond **28-3** (2018) 4100604; https://doi.org/10.1109/TNS.1977.4329085

[7] S. Casalbuoni, E. Blomley, N. Glamann, A. Grau, T. Holubek, E. Huttel, D. Saez de Jauregui, S. Bauer, C. Boffo, Th. Gerhard, M. Turenne, and W. Walter," Commissioning of a full scale superconducting undulator with 20 mm period length at the storage ring KARA", AIP Conference Proceedings 205 (2019) 030025; https://doi.org/10.1063/1.5084588

[8] S. Casalbuoni, S. Bauer, E. Blomley, N. Glamann, A. Grau, T. Holubek, E. Huttel, D. Saez de Jauregui, C. Boffo, Th. A. Gerhard, M. Turenne, W. Walter," Performance of a Full Scale Superconducting Undulator with 20 mm Period Length at the KIT Synchrotron", Proceedings of IPAC2018, Vancouver, BC, Canada (2018) 4223, THPMF066; doi:10.18429/JACoW-IPAC2018-THPMF066

Session 4: 4. Diagnostics, Controls, Automation, and Feedbacks

Summary: Diagnostics, Controls, Automation and Feedback

I. Agapov, DESY, Hamburg, Germany
U. Iriso, ALBA-CELLS Synchrotron, Cerdanyola del Vallès, Barcelona, Spain
and I. Martin, Diamond Light Source, Oxfordshire UK

I. Session summary

With smaller beam sizes and demanding alignment and stability requirements, the next generation storage rings are considerably more challenging to commission and operate than the previous generation. Progress in diagnostics, feedback systems, controls, and automation is essential for success of these new facilities. In this session, we covered these diverse but interconnected subjects, starting with talks on software tools, simulations, and requirements for facility commissioning, and proceeding to several key issues in feedback and diagnostics.

The APS upgrade project is well under way at ANL. The machine bootstrap was identified as challenging early on and the procedures have been thoroughly simulated largely based on existing software stack used in operation at the present APS, with the conclusion that the tools and approaches are adequate to reach the design goals within a relatively short commissioning time. The results were presented by **Vadim Sajaev (ANL)** in **Automated commissioning plans for the APS upgrade**.

The challenges in machine bootstrapping to be faced by the ALS upgrade project at Berkeley are largely similar, and simulations as well as tests at the existing machine are being performed based on a somewhat different software stack, the MML. The commissioning simulations with the focus on the newly developed tools were shown by **Thorsten Hellert (LBNL)** in **A toolbox for simulated commissioning of light sources.**

Switching the subject to a more specific subsystem discussion, **Alessandro Drago (INFN)** discussed bunch-by-bunch real time feedback both as beam controls and diagnostics tools in **The role of bunch by bunch real time feedbacks in LESR.**

Fast stripline kickers for injection and extraction are indispensable for operation of next generation of storage rings, and progress on the CLIC damping ring kicker was presented by **Ubaldo Iriso (ALBA)** in his talk **Beam Commissioning and Characterization of the CLIC Stripline Kicker at ALBA.**

Two new optical instruments – an electron-optical dissector for longitudinal bunch profile measurement with ps resolution, and a transverse profile measurement based on Avalanche PhotoDoiode linear array, – were presented by **Oleg Meshkov (BINP)** in **New instrumentation for optical beam diagnostics.**

Considerations for first turn diagnostics in low emittance storage rings as well as an overview of the challenges that may be faced when commissioning such facilities were presented and discussed by **Volker Schlott (PSI)** in **Some Considerations on First Turn(s) Dedicated Diagnostics for LE Storage Rings.**

ESRF in Grenoble is expected to start commissioning end of this year, and all subsystems including diagnostics are already at a very advanced stage. Overview of BPM and the innovative BLM system for the ESRF EBS were given by **Laura Torino (ESRF)** in **Diagnostics for first turn commissioning and Beam Loss Detection.**

Miriam Brosi (KIT) in **Studies of longitudinal microbunching instabilities at KARA** presented measurements, comparison with theory, and diagnostics to observe such instabilities when they occur at the KARA ring in the short bunch low-α mode and lead to changes in the bunching structure.

Finally, **Alexey Blednykh (BNL)** (contribution not received) presented the different methods NSLS-II has tried to diagnose the peculiarities of the microwave instability (MWI): using the Synchrotron Light Monitor (SLM), the beam spectra from a stripline, and the radiation spectra from an In-Vacuum Undulator (IVU). The measurements of the energy spread coming from the IVU spectra and the SLM nicely coincide well with the simulation coming from the particle tracking code SPACE. The energy spread growth is not monotonic with the beam current, but rather is characterized by a number of local minima and maxima. However, the measurements from the bunch length using a streak camera needs further investigations because they currently show a disagreement in the order of 15%. Furthermore, they plan to update their longitudinal impedance model by a careful study of the different ceramic chambers at NSLS-II.

Automated Commissioning Plans for the APS Upgrade

V. Sajaev
ANL, Argonne, IL 60439, USA

The Advanced Photon Source (APS) is planning an upgrade to the storage ring that will provide electron beams with extremely low emittance. The new lattice is based on hybrid seven-bend achromat [1] and utilizes reverse bend magnets [2], [3] to achieve natural emittance of 42 pm·rad [4]. APS has a large user community who insist that facility “dark time” (the time when APS is not providing synchrotron light to users) during the upgrade is minimized. To satisfy this requirement, APS is targeting 12 months for removal of old magnets, installation of new ones, and commissioning. Of this 12 month period, only three months are set aside for commissioning of the new multi-bend achromat ring. We see automation as a key to fast commissioning.

To understand how various errors affect the commissioning of the storage ring and what algorithms can be used for error corrections, a simulation of commissioning process was carried out. In this work, we limited ourselves to lattice commissioning, which included everything from the first injection to the lattice correction. The process of ramping beam current, that would require among other things commissioning of bunch lengthening cavity and bunch-by-bunch feedback, was not included.

Lattice commissioning consists of establishing first turn, multi-turn trajectory correction, orbit correction, and beta function and coupling correction. Commissioning is simulated by tracking a bunch of particles with parameters corresponding to the extracted beam from the APS Booster. Early simulations showed that sextupoles should be turned off during first steps of the commissioning to simplify multi-turn trajectory correction.

First, the commissioning program corrects the trajectory of the incoming beam. Simulations show that if the beam can pass through the long narrow vacuum chamber of the septum magnet, it will pass through the first sector as well. Therefore, the Beam Position Monitors (BPM) in the first sector are used to correct trajectory of the incoming beam. Inverse trajectory response matrix is used to determine the incoming beam trajectory, and injection kickers and last correctors in the transfer line are used for correction. Based on the simulations, the expected accuracy of the trajectory correction is 0.5 mm and 0.1 mrad rms. The accuracy is mainly limited by the BPM offset errors. The energy error cannot be determined at this stage yet.

Work supported by the U.S. Department of Energy, Office of Science, Office of Basic Energy Sciences, under Contract No. DE-AC02-06CH11357.

Even after correcting incoming trajectory, the beam will not be able to complete the first turn with 100% certainty, if no further correction is applied. Therefore, the first-turn trajectory correction is required. Due to limited corrector strength and nearly guaranteed beam loss position at the small-gap Insertion Device chambers between the sector arcs, the first-turn trajectory correction is done using sector-by-sector multi-corrector threading: three BPMs on each side of ID straight section are used to calculate position on a virtual BPM in the middle of the straight section, and correctors in the sector upstream of the virtual BPM are utilized to correct the beam position and angle using the ideal trajectory response matrix. Occasionally, the threading fails, then a simplex optimization of transmission is performed in this sector. When threading reaches half turn, the energy error of injected beam is measured using average horizontal BPM error and corrected. The expected accuracy of the relative energy error determination is 10^{-3} rms.

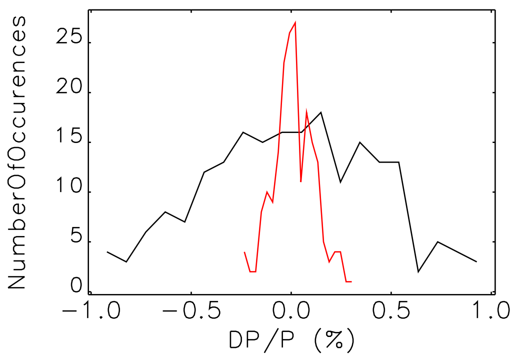

Fig. 1. Injection energy error before and after correction. The achieved energy correction accuracy is 10^{-3} rms.

BPM performance is crucial to the success of the automated commissioning as bad BPMs significantly complicate calculations that rely on small number of BPMs. Wrongly connected or damaged BPM cables will result in large BPM gain, tilt, or offset errors. Even though extensive tests and checks of magnet and BPM connections and polarity will be performed during installation, we cannot guarantee that there will not be any errors. Therefore, in parallel with the sector-by-sector trajectory threading, a crude BPM verification will be done. It will consist of the measurement and fitting of the 4-corrector trajectory response matrix using all BPMs in the sector (4x10 matrix in each plane). This measurement will allow to determine the BPM gain error and tilt with accuracy sufficient to detect BPM connection problems. The main limitation on the accuracy is the injection jitter and BPM noise. If needed, BPM timing scan can also be performed in parallel with sector-by-sector threading. Magnet verification can also be performed in a similar fashion but has not been tested yet.

It was found that after the first-turn threading is complete, the beam barely goes beyond the first turn. At this point, the trajectory at the end of the first turn is set to be equal to the incoming beam trajectory. Ideally, this should result in the closed orbit condition. In reality, the transmission is only improved from one turn to about 5 turns. After that, global trajectory correction is started. The global trajectory correction is run in several loops to minimize corrector strengths.

When transmission reaches 10 turns, rf system set up is performed. Beam energy as a function of turn is measured using average horizontal orbit error and used to set up rf frequency and phase. At the same time, the betatron tune correction is started. The tune is determined from trajectory response: a few-turn trajectory response is analyzed using NAFF for each BPM family on a sector-by-sector basis. The accuracy of the tune determination is limited to about 0.05, but this accuracy is sufficient to keep the tunes away from the integer resonances. Other methods can be also used for tune measurement. RF adjustment and tune correction is run every few iterations of the global trajectory correction.

When global trajectory correction is completed, or when the transmission reaches 20 turns, the orbit correction is started. The beam position is still recorded in turn-by-turn mode, but the multi-turn beam trajectory is averaged on every BPM to produce pseudo-closed orbit. This orbit is corrected using ideal inverse orbit response matrix. At the same time, the sextupole ramp is started. The sextupole ramp, tune correction, and rf system adjustment is run every few iterations of the orbit correction. When the sextupole ramp is complete, the simulations show that the beam will be stored and the median lifetime will be about 15 minutes. This lifetime is enough to perform the beam-based BPM alignment that will result in better orbit correction and will increase the median lifetime to about 30 minutes, at which point the beta function correction can be started.

Automated lattice correction is a routine exercise in present light sources. We will use response matrix fit based correction. The correction will be performed in several iterations. The expected accuracy of beta function correction is 1-2%, with horizontal plane being about a factor of 2 worse than vertical plane. Simulations show that the design low emittance of 42 pm·rad is achieved at this stage, and minimum achievable emittance ratio is about 1%.

I. CONCLUSIONS

Automated commissioning is considered a key to fast lattice commissioning. Automated commissioning simulations are routinely performed for every APS-U lattice candidate and used to evaluate and compare lattice performance. Commissioning simulations are used to test correction algorithms and find which algorithms work best for our lattice. Presently,

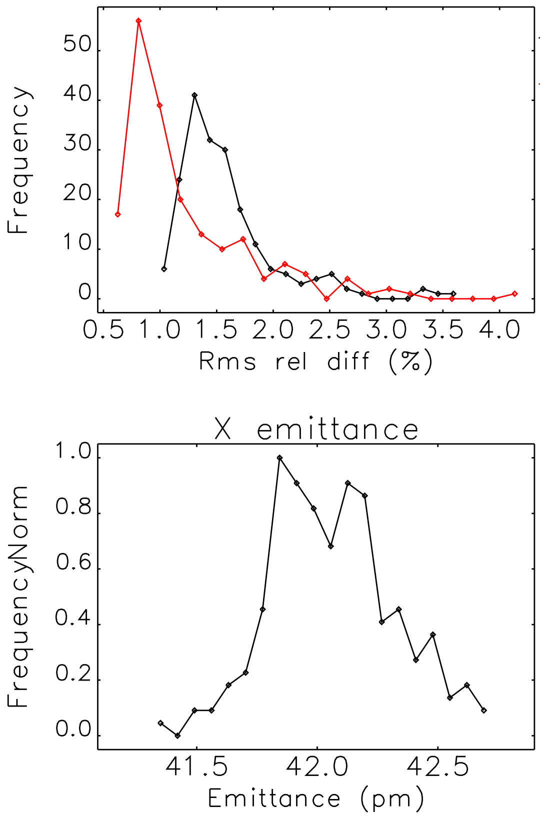

Fig. 2. Final results of the lattice correction. Top: histogram of the expected beta function relative rms error; bottom: expected horizontal emittance.

simulations predict that the closed orbit will be established in about 800 injections. Of those, about 300 injection cycles will be used for trajectory correction, while about 500 injection cycles will be used for BPM verification and tune measurement. Commissioning program testing is ongoing at the existing APS storage ring. It is used to verify algorithms and to ensure that all effects are taken into account.

REFERENCES

[1] L. Farvacque, et. al., "A Low-emittance Lattice for the ESRF," Proc. of IPAC 2013, p. 79 (2013).
[2] J-P. Delahaye and J. P. Potier, "Reverse bending magnets in a combined-function lattice for the CLIC damping ring," Proc. of PAC 1989, p. 1611.
[3] A. Streun, "The anti-bend cell for ultralow emittance storage ring lattices," NIM A, vol. 737, p. 148 (2014).
[4] M. Borland, et. al., "Lower Emittance Lattice for the Advanced Photon Source Upgrade Using Reverse Bending Magnets," Proc. of NAPAC 2016, p. 877 (2016).

A toolbox for simulated commissioning of light sources

Thorsten Hellert
Lawrence Berkeley National Laboratory, USA

Diffraction-limited light sources require a small emittance, which is achieved by much stronger focusing than in third-generation light sources. Very strong focusing elements and a relatively small vacuum chamber make rapid commissioning a significant challenge. Moreover, traditional and somewhat conservative ways to define an error tolerance budget would lead to impractical engineering constraints. To this end, we present the development of an AT [1] based toolkit, which allows for realistic commissioning simulations of light sources by taking into account a multitude of error sources as well as diligently treating beam diagnostic limitations. Realistic simulations of the operation of a complex machine like an accelerator not only require a good model of the beam dynamics, but also have to acknowledge the fact that only incomplete information about the actual machine state is available during operation, due to the many unknowns in the machine geometry, the magnetic fields and the beam-diagnostic systems. The presented toolbox addresses this issue by making clear distinctions between machine parameters that are accessible during operation and the parameters that go into the beam dynamics simulation of the machine, e.g. by implementing a transfer-function, relating magnet setpoints to the actually realized magnetic fields, as systematically shown in Fig. 1. Once the toolbox is initialized, elements like magnets, BPMs or cavities may be registered with corresponding uncertainties of e.g. BPM offsets. A separate function applies all errors randomly based on the registered uncertainties. The implemented error model includes, among others, static and shot-to-shot injection errors, calibration errors, offsets and rolls of all magnets, diagnostic errors such as BPM offsets and noise, RF frequency, voltage and phase errors, circumference error and the possibility to load and include multipole-error tables. The magnet-support model allows for the registration of girders, plinths and sections, each with individual offset and roll uncertainties. Diagnostic functionalities include the calculation of BPM readings based on the current tracking mode (turn-by-turn/orbit), the turn-by-turn beam transmission, the response matrix ('measurement' and model based on current setpoints), the dynamic and momentum aperture and the beam life time. We have successfully established correction chains for the ALS-U accumulator and storage ring as well as for the transfer lines between the two. The correction steps include an iterative trajectory and orbit correction, static injection error correction, RF phase and frequency correction, 2-turn BBA, trajectory based coarse optics correction and an interface to AT LOCO. The toolbox including various examples and an online manual will be published at IPAC2019 [2].

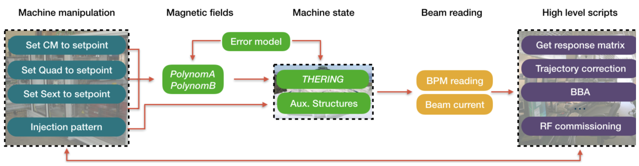

Fig. 1. Schematic drawing of the workflow for the simulated commissioning toolbox. Accessible setpoints are deliberately separated from magnetic fields. The input for high-level scripts are only BPM readings as well as magnet setpoints. Changing the machine state is only possible by changing e.g. a setpoint of a quadrupole magnet or the injection pattern.

References

[1] Andrei Terebilo. Accelerator toolbox for MATLAB. In Workshop on Performance Issues at Synchrotron Light Sources Berkeley, California, October 2-4, 2000, 2001.

[2] Thorsten Hellert et al, An accelerator toolbox (AT) utility for simulating the commissioning of storage-ring light sources. IPAC 2019, Melbourne, Australia (to be published)

The role of bunch by bunch real time feedbacks in LESR

Alessandro Drago
INFN-LNF, Istituto Nazionale di Fisica Nucleare, Lab.Nazionali di Frascati, Frascati, Italy

I. Introduction

The commissioning of a low emittance storage ring can be carried out in part by traditional instrumentations and methods and in part by more specific techniques. Having in mind this consideration, the bunch-by-bunch feedback is not only a control system but also a diagnostic device that can work both as a programmable bunch-by-bunch acquisition system and as a flexible generator of custom excitations. During the commissioning the feedback can help to evaluate many characteristics and behaviours of the beam: first turns orbit, set up of the injection kickers, betatron tunes and tune spread, dynamic aperture, grow rate instabilities versus high beam currents. Even if, during the regular runs, the feedback systems could be completely turned off, still, in the test and commissioning phase, the feedback can play an important role to achieve the foreseen beam behaviour.

II. Drawbacks

Being an active system the feedback excites the beam by producing some undesired noise both of internal (inside the system) and external (from the pickups) origin. In a low emittance beam this is a truly harmful effect that has to be limited as more as possible. If the beam has the usual "ribbon" shape, the vertical dimension of the beam is the most suffering and it is possible to see some vertical enlargements at the SLM. If the storage ring works as collider the enlargement effect given by the feedback noise can be further amplified by the kick from the other beam (observed at DAFNE and KEK). Nevertheless, feedbacks are useful! Indeed, in the modern feedback design, all the systems work bunch-by-bunch and, as consequence, they are able to monitor the diagnostic behaviour for each bunch. And moreover when a new run starts, the vacuum state is usually poor and the feedback system is helpful to increase the beam current and to bring the vacuum to the expected value.

III. Feedback for low emittance beams

After the year 2009, at LNF, the proposal of a low emittance e+/e- collider was considered (the SuperB project) to continue and to replace the lepton collider activity of DAFNE. Even if the project was finally abandoned, the DAFNE feedbacks were improved to accomplish the goal to be compatible with a low emittance storage ring. Two modifications were implemented: a) the systems were upgraded from 8 bit A-to-D conversion to 12 bits to decrease the quantization noise; b) a new low noise analog front end was designed. The basic R&D ideas to adapt the DAFNE transverse bunch-by-bunch feedback systems for low emittance beams were the followings: 1) less noise in the loop: by implementing a low noise analog front-end and A/D & D/A conversion at 12/16/20 bits; 2) more sensitivity: implementation as in the previous point; 3) larger dynamic range: possible by using A/D & D/A conversion at 12/16/20 bits; 4) better use of power signals by designing new kickers; 5) better beam diagnostics; 6) adaptive control strategy. Looking to these points we can observe that some of them are strongly correlated, in particular for the first 4 items. Considering the digital conversion and processing, a fundamental key-point to eliminate or to attenuate strongly the noise inside the feedback loop is the quantization noise. The question is: in the analog to digital conversion how many bits are the right choice? This is also related to the dynamic range of the feedback loop that is basically given by three active blocks: front-end, digital processing unit (included A to D and D to A converter), and back-end with power amplifiers. Evaluating in LNF laboratory, for the power amplifiers (commercial devices) that we use at DAFNE, a dynamic range of about 90-95 dB has been measured. Of course, in the loop, the block with the lowest dynamic range plays as bottleneck, and typically this is the digital block that include A to D conversion, individual FIR filters for each bunch signal and D to A conversion. Possible options in the choice of the best number of bits to have both low quantization noise and large dynamic range are: 8 bits = 48 dB dynamic range (used in the past at DAFNE for transverse feedback), 12 bits = 72 dB (used at DAFNE after the upgrade of the transverse feedback), 16 bits = 96 dB, 20 bits = 120 dB. Considering the power amplifier dynamic range, the best choice would be a conversion by 16 bits. This, for many reasons, both technological and related to the compatibility with previous feedback system versions, was not possible for DAFNE. Indeed, the R&D efforts have been stopped after the upgrade to 12 bits (that however are much better than 8 bits). Twelve bits do not seem sufficient for ultralow emittance beams but for the DAFNE emittance they are enough. Going to discuss the point 5), the bunch by bunch diagnostics is an interesting field where to focus the R&D efforts for the circular accelerator especially for the low emittance rings. Modern feedback systems, processing bunch-by-bunch signals, allow such diagnostics during the beam regular runs even without stopping the normal activities. The most frequently used measurements in the storage ring DAFNE are: beam transverse fractional tunes (in real time), bunch-by-bunch transverse fractional tunes and tune spreads (off line), coherent instability growth rates (off line). A further partial list of other diagnostic features is as in the following: first turns orbit (observing the passage of the bunch through the horizontal and vertical pickups) can be monitored with potential indication of characteristics of the bad orbit; the number of turns before a loss of beam can be monitored; correct set up of the injection kickers can be studied: the excess of power and bad timing is easily monitored by looking to the motion of the adjacent bunches in the feedback plot of beam motion; dynamic aperture can be evaluated: the excitation made by the feedback in vertical and horizontal can be very useful to kick the beam and the feedback can record the oscillation data.

IV. Conclusion

Even if transverse feedback are active instruments and can apply undesired noise to the low emittance beams, they are extremely useful device to make fast and efficient commissioning of storage rings.

Beam Commissioning and Characterization of the CLIC Stripline Kicker at ALBA

Ubaldo Iriso,
ALBA-CELLS Synchrotron, Cerdanyola del Vallès, Barcelona, Spain

The prototype of the extraction kicker of the CLIC Damping Ring has been tested at ALBA. This kicker must provide very stable kicks to guarantee a constant luminosity in a bunch-by-bunch collision rate. Probably, the most challenging requirements are the flat top reproducibility ($1e^{-4}$), and the field homogeneity ($< 2e^{-4}$) inside a stable region of ± 1 mm. With the current technology at 3rd generation of storage rings, the measurement of these parameters are a challenge on itself. The installation of this stripline at ALBA produced big outgassing rates, and the most likely cause was the presence of high mass ions (A=52 and 80) desorbed after the synchrotron radiation hitted the MACOR rings which were use to hold the stripline electrodes. After the removal of these rings, the pressure improved but the stripline still could not be left in the storage ring during users operation, and it was installed in/out for specific tests. The kick angle was characterized using a HV DC kick of 10 kV, and the installation of extra BPMs around the stripline. By properly calibrating the two BPMs up and downstream the stripline in their non-linear region (± 1 mm), the BPMs offsets, gains and x/y coupling were found, and the local kick angle (544 $\pm$ 0.2) urad was measured with the required precision. As for the longitudinal field homogeneity, the pulse width was varied between 160 and 700 ns and its stability was inferred by scanning a single bunch along the flattop and measuring the global orbit distortion in the 120 BPMs. The HV kick was performed using ad-hoc electronics which also allowed to trim the decay voltage amplitude to produce more stable kicks. The electronics worked as expected, and considering the decoherence effects, the measured kick homogeinity was only 0.04%. Although this is an astonishing precision, it is slightly larger than the required precision 0.01%. Finally, it was presented the impedance characterization of the CLIC stripline by differential TMCI measurements (global difference before and after the stripline installation) and local impedance measurements using the local bump method. Both results agreed with the expectations.

New instrumentation for optical beam diagnostics

S. Andreev, A. Smirnov, N. Vorobiev, A. Zarovsky, A. Komelkov,
Prokhorov General Physics Institute of the Russian Academy of Sciences, GPI RAS
V. Borin, G. Kurkin, O. Meshkov[3] , V. Kaminskiy , D. Shwartz, M. Timoshenko, and V. Dorokhov
Budker Institute of Nuclear Physics, BINP SB RAS

***Abstract*—Two new optical detectors are presented. The first device is the new version of the electron-optical dissector, which is designed for synchrotron radiation sources and electron-positron colliders. At such a facilities, it is necessary to record simultaneously the temporal profiles of electron and positron bunches filling from two to several hundreds neighboring separatrices of an accelerator ring. In order to obtain the crossed-sweep mode, high-frequency (HF) sinusoidal voltages with multiple frequencies are fed to two pairs of deflecting plates of the tube, located perpendicular to each other. This shift of pulses will allow separate acquisition of the bunch profiles from neighboring separatrices of an accelerator, which are superimposed on each other in the absence of the crossed sweep. The second device is based on the Avalanche PhotoDiode linear array and can be applied for study of transverse beam profile with turn-to turn temporal resolution.**

***Keywords*—Electron-optical dissector, picosecond, APD array**

I. Introduction

The beam diagnostics is crucially important for proper operation of the cyclic accelerator and Synchrotron Radiation sources among them. The regular measurements and control of the beam transverse and longitudinal dimensions are necessary during daily performance of the installations. We present two new optical devices for measurements of longitudinal and transverse beam dimensions and spectra of oscillations.

II. The features of the detectors.

The electron-optical dissector, described in this article, combines an image converter tube PIF-01/S1(S20) [1] and an Electron Multiplier Tube (EMT). A sweeping voltage applied to the deflecting plates of the tube oscillates with a high harmonic of an accelerator beam revolution frequency ν_{RF} The exit of the streak tube is equipped with a narrow slit and electron image of longitudinal beam profile is slowly scanned across the slit. The electrons passing through the slit are amplified by EMT [2], [3]. A typical slow scanning time is about 20 ms now. Thus, the acquired beam longitudinal profile is averaged over many thousands beam turns. Dissector is able to acquire the turn-to turn longitudinal dynamics of the beam if the slow sweep is switched off, and the device operates in a phase slit mode [4]. The spectrum of the longitudinal beam oscillations appeared due to beam-beam effects on the VEPP-2000 electron-positron collider [6] is presented in Fig. 1, left. The second new optical detector was applied in these experiments as well. This device is based on 16–pixels avalanche photodiodes AA16-0.13-9 APD linear array and has an ability to record up to 4 millions of the turn-to turn transverse beam profiles. An example of the acquired dipole and quadrupole radial beam oscillations caused by beam-beam effects is presented in the Fig. 1, right.

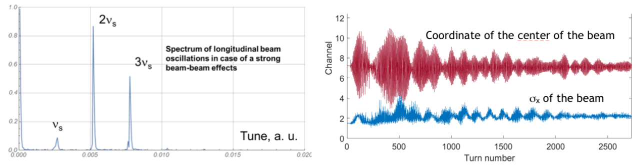

Fig. 1. Left: spectrum of longitudinal beam oscillations in case of strong beam-beam effects acquired on VEPP-2000 electron-positron collider with electron-optical dissector. Right: dipole and quadrupole radial beam oscillations caused by beam-beam effects and recorded by AA16-0.13-9 APD linear array.

The obtained value of 1.7 ps of the dissector temporal resolution [5] satisfies demands of beam longitudinal profile measurements on the most of circular accelerators. Now the main challenge for us is to provide the measurements of the length of the selected bunch in the multi-bunched beam. As a first attempt, we have tried to solve this problem using the features of the design of the PIF-01 streak tube. The tube has second deflecting plates, which can be applied for dual sweep mode of the dissector performance. It allows us to separate the signals from the multi-bunch beam on the "odd" and "even". The proof-of-concept experiment was successful [5].

III. Acknowledgments

The reported research was partially funded by Russian Foundation for Basic Research and the government of the region of the Russian Federation, grant № 18-42-543004

References

[1] V. P. Degtyareva, Yu V. Kulikov, M. A. Monastyrski, et. ai. "The New Streak Image Tube PIF-01", Proc. SPIE 0491, 16-th Intl. Congress on High Speed Photography and Photonics, (1 February 1985); doi:10.1117/12.967917.
[2] E. I. Zinin et al., Nucl. Instrum. Methods Phys. Res. 208, 439 (1983).
[3] E. I. Zinin and O. I. Meshkov, "Optical dissector for longitudinal beam profile measurements," JINST 10, 10024 (2015). doi 10.1088/1748-0221/10/10/P10024
[4] D. Malyutin et al., "Injection and Bunch Length Studies at the BESSY II Storage Ring", Proceedings of the 6th Int. Beam Instrumentation Conf. (IBIC'17), Grand Rapids, Michigan, USA, August 2017, TUPCC06.

3) also with Novosibirsk State University, Novosibirsk, Russia

[5] S. Andreev, V. Dorokhov, Ya. Getmanov, A. Komelkov, D. Malutin, A. Matveenko, O. Meshkov, M. Ries, A. Smirnov, N. Vorobiev, A. Zarovsky, G. Kurkin, "Picosecond dissector with crossed sweep and optimization of picosecond dissector parameters," Proc. SPIE 11051, 32nd International Congress on High-Speed Imaging and Photonics, 110510M (28 January 2019); doi: 10.1117/12.2524826

[6] P. Shatunov et al., Status and perspectives of the VEPP-2000, Phys.Part.Nucl.Lett. 13, no.7, pp. 995-1001, 2016.

Some Considerations on First Turn(s) Dedicated Diagnostics for LE Storage Rings

Volker Schlott,
Paul Scherrer Institut, Villigen, Switzerland

I. MOTIVATION

The small vacuum chamber dimensions of diffraction-limited light sources lead to strongly reduced dynamic apertures, particularly when alignment errors of components (e.g. specified: $< 30\ \mu$m (2σ); initially $\sim 50\ \mu$m (2σ)) and initial resolution limitations of measurement systems (e.g. 100 μm of mechanical and electrical offsets of BPMs) are taken in consideration. In addition comparably large emittances from the injector chain as well as drifts and jitter of injection elements aggravate the situation and tighten the demands on first turn diagnostics.

II. MEASUREMENT OF INJECTOR PERFORMANCE AND PREPARATION OF DIAGNOSTICS SYSTEMS

While performance specifications for injector diagnostics in (present) 3rd generation light sources were quite relaxed, precise orbit control possibly orbit feedbacks as well as measurement and (online) monitoring of injector performance (e.g. charge stability, emittances, angular and position stability of extracted beams as well as monitoring of losses in transfer lines) will be of high importance for efficient and reliable storage ring injection and top-up operation. In addition, more attention, diligence and tight quality control might be required for the preparation of diagnostics systems prior to beam commissioning. In this sense, unwanted error sources such as defective feedthroughs and wrong cabling should be avoided and pre-beam (in lab) calibration of e.g. BPM electronics as well as SW-tools, which allow in-situ integrity checks, should be prepared to ease and support beam commissioning. However, initial BPM readings may still provide only a limited accuracy of a few hundred microns due to initial alignment errors, displacements of feedthroughs in the pick-ups, differences in cable attenuation and limitations of pre-beam (in-lab) calibration.

III. THE WORKING HORSE: BEAM POSITION MONITORS

The BPM sum signal from all four buttons ($I_A + I_B + I_C + I_D$) provides a relative current / transmission measurement at the BPM locations around the storage ring. With a first-turn / tur-by-turn measurement mode, the BPMs can be used to optimize injection parameters and to thread the beam around the ring. Once a first turn is obtained, most of the injection schemes for light source upgrade projects require a sufficiently accurate position measurement to perform a first orbit correction, which is mandatory to allow the accumulation of beam in the storage ring. In this way, unhealthy BPM readings should be automatically detected (e.g. through automated integrity checks) and large offsets, which may lead to false position readings due to non-linearity in the pick-up, should be corrected (e.g. by polynomial fitting). Once beam-based-calibration of BPM systems can be done with stored beam, storage ring commissioning and operation can fully rely on this key diagnostics system. A list of first turn / turn-by-turn BPM specifications is given below and a comprehensive overview of state-of-the-art BPM systems (including new developments using pilot tone calibration) can be found under: https://indico.cern.ch/event/743699/

TABLE I
FIRST TURN / TURN-BY-TURN BPM SPECIFICATIONS.

operation mode:	first turn/turn-by-turn
	(e.g. SLS 2.0: 500 kHz BW)
beam current (charge):	10 mA (10 pC) 1 mA (1 nC)
position noise:	$< 50\ \mu m$ $1\ \mu m$ (rms)
position drift:	not important for first turns
data buffer depth:	> 8000 turns (x, y and intensity)
linearity correction:	for large beam offsets (e.g. polyn. correction)
alignment tolerance:	20 / 5 μm (rms) to adjacent sextupole
pre-calibration:	QC procedures for feedthroughs and pick-ups
	possibly test bench measurements
	lab calibration for electronics /
	/ in-situ w. pilot tone
	(typically hundreds / best case tens of μm)
validity checks:	with automated SW-tools
	or BPM expert modes

IV. THE LIFE INSURANCES: BEAM LOSS AND SCREEN MONITORS

Monitoring of beam losses may reveal locations of aperture restrictions in the extraction / injection areas and around the storage ring and can be used to identify malfunctioning (failure, jitter or excessive drift) of components. The monitoring and comparison of loss pattern during early system / machine commissioning and later on during user operation provides additional and redundant information to the first turn current and transmission measurements from BPMs. BLMs are typically more sensitive than BPMs and can also be used to integrate loss rates over longer time periods, which may trigger interlock systems (e.g. machine protection) when exceeding pre-defined threshold values. Along transfer lines and extraction / injection points, long Cerenkov fibers can be pulled along the beam pipe, providing a spatial loss resolution of < 0.5 m. A number of fast (turn-by-turn) loss monitors consisting of scintillators in combination with photo-multiplier tubes (e.g. 4 to 6 per sector) can provide an overall loss pattern along the storage ring. Commercial solutions are available, allowing synchronized turn-by-turn readings and integration into safety systems. A set of screen monitors (one at the septum and one further downstream in the injection straight) might be helpful for visualizing the injected and possibly first turn(s) beam in case of emergency. However, due to impedance reasons, screen monitors are not popular and thus not widely used in storage rings. With the improved first turn capabilities and high reliability of BPM systems, screen monitors may become completely obsolete in storage rings.

V. From First Turns to User Operation

The use of synchrotron radiation in the visible, UV and X-ray regime provides non-invasively information on the time structure (e.g. filling pattern monitors (using visible SR on fast diodes or streak cameras) or profile / emittance of the beam (using visible, UV or X-ray radiation) as interference, π-polarization or pinhole monitors. Such monitors may also help as first turn diagnostics during commissioning but will be more important and even mandatory to establish the nominal operating conditions and to control and maintain (e.g. top-up) user operation. In the same way, absolutely calibrated charge (in transfer lines) and current (in the storage ring) monitors provide information about transmission / injection efficiency as well as storage ring current and high precision lifetime measurements. A comprehensive overview on state-of-the-art profile / emittance monitors for low emittance storage rings and DL light source upgrade projects was presented at an ARIES WS at ALBA, Barcelona (2018) and can be found under https://indico.cells.es/indico/event/128/overview

VI. Some Considerations on on-axis longitudinal Injection

For some light source upgrade projects (e.g. ALS-U, APS-U or PETRA IV), on-axis (and swap out) injection is the only way to fill and operate their storage rings. One proposal for (longitudinal) on-axis injection requires the bunch from the booster at a slightly higher energy than the beam in the storage ring and injects without an injection bump off-phase into the RF bucket of the storage ring such that the injected beam damps longitudinally (instead of usually transversally) into the RF bucket due to radiation damping. With typical RF frequencies of 100 500 MHz and corresponding bucket separations of only a few nanoseconds, very fast kicker magnets are required for such injection schemes. Current and charge monitors can be used to monitor the net injection efficiency but provide only integral information on the beam transfer and transmission. A dual-sweep streak camera or dissector (in conjunction with a visible light synchrotron radiation monitor) may be used to observe the longitudinal dynamics of this injection process. Such beam tests have recently been made at SOLEIL. Optional a longitudinal multi-bunch feedback system may be used for measuring this kind of injection process but it requires a sufficient dynamic range to measure the injected signal, which may only be in the order of 10% of the stored beam signal.

Diagnostics for First Turn Commissioning and Beam Loss Detection

L. Torino
European Synchrotron Radiation Facility, Grenoble, France

Abstract—**The preparation and the tests of the diagnostics subsystems necessary for the commissioning of the Extremely Brilliant Source (EBS) are on going at the European Synchrotron Radiation Facility (ESRF) [1]. In particular the Beam Position Monitor (BPM) and the Beam Loss Detector (BLD) systems are of great interest for the commissioning of the first turn. Both systems are distributed to cover all the machine, and can be synchronized to measure the beam circulation on a single turn scale or smaller. The BPM and the BLD systems have been upgraded and tested as much as possible on the old ESRF machine to gain experience and know-how for the future commissioning.**

I. The BPM System

The BPM system for EBS is composed by a total of 320 BPM blocks, 10 BPM blocks per cell. The readout electronics comprehend 192 Libera Brilliance (6 per cell) and 120 Libera Sparks (4 per cell). Both the electronics produces data-streams, and buffers with identically synchronized sampling-rates. The complete system, and the related software have been installed and tested on the old ESRF machine. Scripts for the synchronization and to switch the system in turn by turn mode has also been developed [2]. A big preparation work has been carried out on the BPMs block, and it is still on going. The Lambertson method has been used in order to check the correct behaviour of each block, and to estimate the offset and the tilt produced by misalignment of the single buttons. The output of the measurement provides the sensitivity of individual buttons and allows to compute a correction factor to be applied to the signal. The same technique also allows to identify badly positioned buttons, or short-circuits created by external contamination. This last problem has been solved by applying high voltage to burn the contamination [3]. Another problem to be addressed for new machines is that the reduction of the vacuum chamber size leads to very compact BPM blocks and to a consequent reduction of the linear region for the application of the standard Difference over Sum (DoS) formula to measure the beam position. Studies on this topics has been carried out using the BPMLab software [4]. The solution will be the use of 2D polynomial instead of the DoS formula to compute the beam position. Before the long shutdown, dedicated machine time has been used to perform a re-commissioning of the old ESRF storage ring. The BPM system has been used to acquire synchronized turn by turn data. The sum of the signal from each button of the block provides a direct information about the longitudinal position at which the beam has been lost. The horizontal and vertical positions obtained using polynomial correction are instead used to feed the simulation which automatically set the steerers to achieve the first turn. An example of these results is shown in Fig. 1.

II. The BLD System

Diagnostics redundancy is necessary at all accelerators phase, and specially during commis- sioning. It is extremely useful to have another distributed and synchronized system to follow the beam during the first turns. The BLD system has been developed and commissioned on the old ESRF machine, to be used also with this aid. Even if it is not capable of measuring the transverse position of the beam, it has a very high sensitivity which allow to measure where the beam is lost even in case of low current [5]. The EBS BLD system is composed by 128 scintillator-photomultiplier detectors (4 per cell), and 32 Libera-BLM electronics (1 per cell). Each Libera-BLM powers, controls, and reads-out four detectors. The possibility of triggering the device, and selecting the output impedance 50 Ohm, together with a 8 ns temporal resolution allows to perform Turn by Turn, and almost bunch by bunch measurements. The same electronics also provides the possibility to switch to not-synchronous slow data acquisition by setting the impedance to 1 MOhm. This configuration will be used during standard operation. Before the installation in the old machine, a procedure has been developed to measure the detector sensitivity using a radioactive source. In this way inter-calibrated loss measurements are obtained. The BLD system has also been tested during the commissioning like machine dedicated time. Results obtained for losses measurement when the beam is circulating for less than one turn and for stored beam are presented in Fig. 2.

III. Conclusions

The preparation and the tests performed on the old ESRF machine of the two main systems that will be used for the EBS commissioning has been presented. The BPM and BLD systems will be soon installed and tested, and will be strongly used for first turn commissioning.

References

[1] "ESRF Upgrade Programme Phase II (2015-2022) - Technical Design Study", http://www.esrf.fr/Apache_files/Upgrade/ESRForange-book.pdfs
[2] K. B. Scheidt "Complete Test Results of New BPM Electronics for the ESRF New LE- Ring". IBIC2018, TUPB02.
[3] B. Roche "Characterisation of ESRF-EBS BPM blocks ". Presentation at DEELS2018.
[4] BPMLab, https://intranet.cells.es/Divisions/Accelerators/RF_Diagnostics/Diagnostics/OrbitPosition/Tools/bpmlab
[5] L. Torino, K. B. Scheidt "New Beam Loss Detector System for EBS-ESRF". IBIC2018, WEOB01.

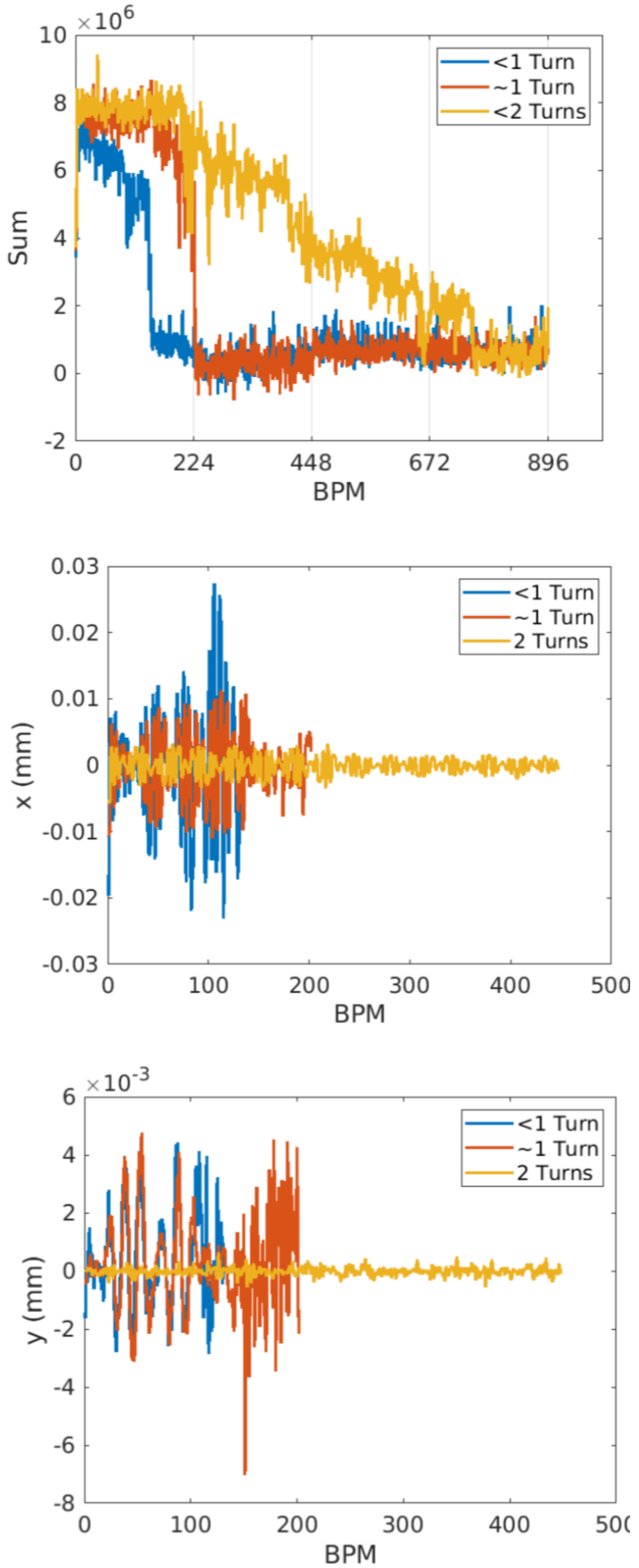

Fig. 1. Sum, horizontal and vertical position obtained during a commissioning-like machine dedicated time. One turn corresponds to 224 BPMs. In blue the beam was circulating for less then one, turn, in orange one turn, and in yellow roughly two turns.

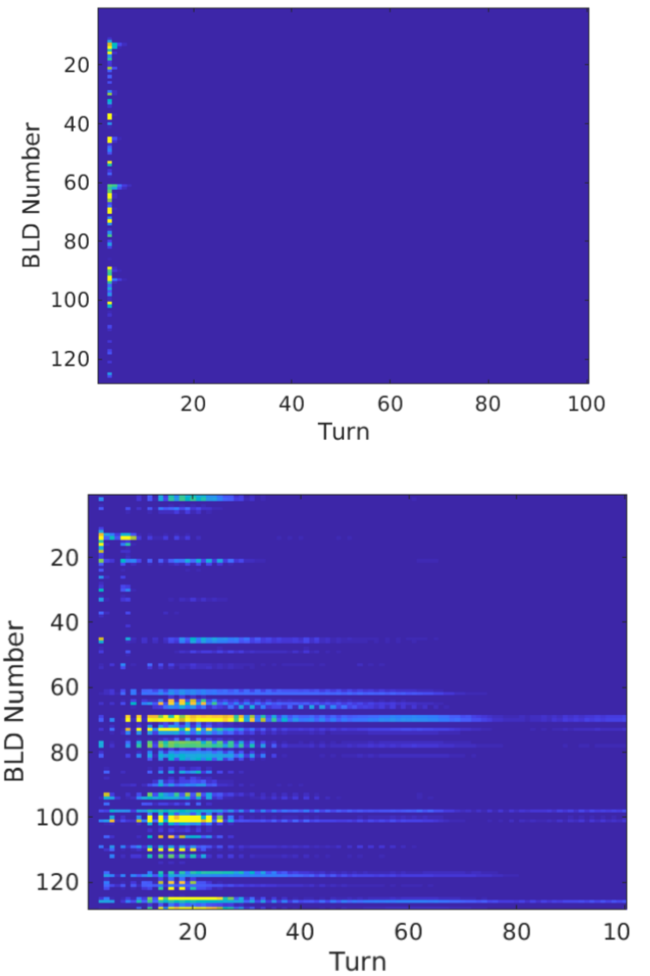

Fig. 2. Losses measured by the 128 BLDs over 100 turns, for the beam circulating for less then one turn and for stored beam.

Studies of the Longitudinal Microbunching Instability at KARA

Miriam Brosi, Edmund Blomley, Tobias Boltz, Erik Bründermann, Michele Caselle, Stefan Funkner, Benjamin Kehrer, Michael J. Nasse, Gudrun Niehues, Meghana Patil, Lorenzo Rota*, Patrick Schreiber, Marcel Schuh, Johannes L. Steinmann, Marc Weber and Anke-Susanne Müller ,
Karlsruhe Institute of Technology, Karlsruhe, Germany

The KIT storage ring KARA (Karlsruhe Research Accelerator) provides a short-bunch operation mode with a reduced momentum compaction factor to achieve bunch lengths in the order of picoseconds [1], [2]. For bunches this short the microbunching instability can occur. It is a longitudinal instability which is driven by the self-interaction of a bunch with its own coherent synchrotron radiation (CSR). The shorter the bunch the higher the frequencies up to which CSR is emitted and the stronger the effect of the microbunching instability. The behavior of the bunch under the influence of the instability changes depending on different parameters such as bunch current, momentum compaction factor, and RF voltage [3], [4].

To simulate the influence of the instability on the bunch, Inovesa [5], [6], a Vlasov-Fokker-Planck solver, was developed at KIT. For each time step, the simulation calculates the wake potential from the CSR impedance and the longitudinal bunch profile. The resulting kick is applied to the charge distribution in phase space. From the experimental side, a direct measurement of the longitudinal phase space distribution is not possible. Therefore, derived bunch parameters are measured. This includes the longitudinal bunch profile, the energy spread, and the emitted CSR.

At KARA, dedicated diagnostic with turn-by-turn / bunch-by-bunch resolution is used [7]. The high repetition rate of 2.7 MHz for turn-by-turn (500 MHz for bunch-by-bunch) measurements combined with a long-term observation puts stringent requirements on the used diagnostics. Additionally, high temporal resolution in the sub-ps range is necessary to resolve the substructures forming on the longitudinal bunch profile.

For the emitted CSR in the THz range, this is achieved by the combination of fast room-temperature Schottky barrier diode detectors [8], [9], sensitive from 50 GHz up to 1 THz (analog bandwidth > 4 GHz), with the KArlsruhe Pulse Taking and Ultra-fast Readout Electronics (KAPTURE) [10], [11]. The newest version, KAPTURE 2 [12], consists of eight readout channels, each with a 18 GHz track-and-hold unit and a 12-bit 1 GHz ADC. Each channel has an individual delay unit with 3 ps step size allowing a local sampling rate of up to 330 GS/s after the signal is split into the different channels. By measuring all bunches simultaneously KAPTURE allows using the snapshot measurement method [4], which drastically speeds up measurements of bunch current dependent effects. This was for example used to scan the threshold current of the instability for different machine parameters [4], [13].

The longitudinal bunch profile is measured with an electro-optical near-field setup [14], [15]. In combination with a fast spectrometer, turn-by-turn single shot bunch profiles can be measured. This is achieved with a grating and the line array detector KALYPSO [16], [17]. KALYPSO III is under development and will provide up to 10 Mfps with 512 pixels. Also the sensors can be customized by choosing a different array size, channel pitch, and anti-reflective coating [18].

Additionally, KALYPSO is now tested as a detector for measuring the horizontal bunch size [19]. This is of interest as it is related to the energy spread of the bunch via the dispersion, the emittance, and the beta function [20].

KAPTURE and KALYPSO allow for on-turn synchronous observation of the CSR emission (THz), the longitudinal bunch profile and the horizontal bunch size / energy spread [7], [19]. In the measurements, the effect of the microbunching instability is visible in the longitudinal as well as the horizontal plane. The synchronized measurements show that the onset of the increase in emitted THz power coincides with the development of substructures on the longitudinal bunch profile. Also a sawtooth pattern can be seen in the bunch length as well as in the horizontal bunch size over time with the same repetition rate as the THz outbursts.

These diagnostic methods permit deeper insight into the nature of the microbunching instability. Even beyond that, the increased repetition rates and synchronization of complementary diagnostics promise to shed new light on the beam dynamics of short electron bunches at storage rings.

Now at SLAC National Accelerator Laboratory, Menlo Park, CA, United States.

References

[1] Müller, A.-S. et al.: Far Infrared Coherent Synchrotron Edge Radiation at ANKA. In: *Proceedings of 2005 Particle Accelerator Conference*, 2005.

[2] Klein, M. et al.: Modeling the Low-Alpha-Mode at ANKA with the Accelerator Toolbox. In: *Proceedings of IPAC*, 2011.

[3] Bane, K. L. F. ; Cai, Y. ; Stupakov, G.: Threshold studies of the microwave instability in electron storage rings. In: *Phys. Rev. ST Accel. Beams* 13 (2010), Oct, 104402. http://dx.doi.org/10.1103/PhysRevSTAB.13.104402.

[4] Brosi, Miriam et al.: Fast mapping of terahertz bursting thresholds and characteristics at synchrotron light sources. In: *Phys. Rev. Accel. Beams* 19 (2016), Nov, 110701. http://dx.doi.org/10.1103/PhysRevAccelBeams.19.110701.

[5] SCHÖNFELDT, Patrik et al.: Parallelized Vlasov-Fokker-Planck solver for desktop personal computers. In: *Phys. Rev. Accel. Beams* 20 (2017), Mar, 030704. http://dx.doi.org/10.1103/PhysRevAccelBeams.20.030704.

[6] SCHÖNFELDT, Patrik et al.: Inovesa/Inovesa: Gamma Two. (2018), Jul. http://dx.doi.org/10.5281/zenodo.1321580.

[7] KEHRER, Benjamin et al.: Synchronous detection of longitudinal and transverse bunch signals at a storage ring. In: *Phys. Rev. Accel. Beams* 21 (2018), Oct, 102803. http://dx.doi.org/10.1103/PhysRevAccelBeams.21.102803.

[8] http://www.acst.de/

[9] http://vadiodes.com/

[10] CASELLE, M. et al.: An ultra-fast data acquisition system for coherent synchrotron radiation with terahertz detectors. In: *Journal of Instrumentation* 9 (2014), Nr. 01, C01024. http://dx.doi.org/10.1088/1748-0221/9/01/C01024.

[11] CASELLE, M. et al.: Commissioning of an Ultra-fast Data Acquisition System for Coherent Synchrotron Radiation Detection. In: *Proceedings of 2014 International Particle Accelerator Conference*, 2014, S. 3497. http://accelconf.web.cern.ch/accelconf/IPAC2014/papers/thpme113.pdf.

[12] CASELLE, M. et al.: KAPTURE-2. A picosecond sampling system for individual THz pulses with high repetition rate. In: *Journal of Instrumentation* 12 (2017), Nr. 01, C01040. http://stacks.iop.org/1748-0221/12/i=01/a=C01040

[13] BROSI, Miriam et al.: Systematic studies of the microbunching instability at very low bunch charges. In: *Phys. Rev. Accel. Beams* 22 (2019), Feb, 020701. http://dx.doi.org/10.1103/PhysRevAccelBeams.22.020701.

[14] HILLER, N. et al.: A setup for single shot electro optical bunch length measurements at the ANKA storage ring. In: *Proceedings of IPAC*, 2011.

[15] FUNKNER, Stefan et al.: High throughput data streaming of individual longitudinal electron bunch profiles. In: *Phys. Rev. Accel. Beams* 22 (2019), Feb, 022801. http://dx.doi.org/10.1103/PhysRevAccelBeams.22.022801.

[16] ROTA, Lorenzo et al.: KALYPSO: A Mfps Linear Array Detector for Visible to NIR Radiation. In: *Proceedings of the 5th Int. Beam Instrumentation Conf., IBIC2016, Barcelona, Spain* (2017). http://dx.doi.org/10.18429/jacow-ibic2016-wepg46.

[17] ROTA, L. et al.: KALYPSO: Linear array detector for high-repetition rate and real-time beam diagnostics. In: *Nuclear Instruments and Methods in Physics Research Section A: Accelerators, Spectrometers, Detectors and Associated Equipment* (2018), oct. http://dx.doi.org/10.1016/j.nima.2018.10.093.

[18] CASELLE, M. et al.: Single-Shot Longitudinal Beam Profile and Terahertz Diagnostics at MHz - Towards GHz-Rates with High-Throughput Electronics. In: *Proc. of International Beam Instrumentation Conference (IBIC'17), Grand Rapids, MI, USA, 20-24 August 2017*. Geneva, Switzerland : JACoW, Mar. 2018 (International Beam Instrumentation Conference 6). https://doi.org/10.18429/JACoW-IBIC2017-TU2AB3.

[19] STEINMANN, Johannes L. et al.: Turn-by-Turn Measurements for Systematic Investigations of the Micro-Bunching Instability. In: *Proc. of 60th ICFA Advanced Beam Dynamics Workshop on Future Light Sources (FLS2018), Shanghai, China, 5-9 March, 2018* (2018), March, Nr. 60. http://dx.doi.org/https://doi.org/10.18429/JACoW-FLS2018-TUP2WD03.

[20] KEHRER, Benjamin et al.: Time-Resolved Energy Spread Studies at the ANKA Storage Ring. In: *Proc. of International Particle Accelerator Conference (IPAC'17), Copenhagen, Denmark, 14-19 May, 2017*. Geneva, Switzerland : JACoW, May 2017 (International Particle Accelerator Conference 8). https://doi.org/10.18429/JACoW-IPAC2017-MOOCB1.

Session 5: High Current Effects

Summary: High Current Effects

Ryutaro Nagaoka, Louis Emery

***Abstract*—a review is made of the three contributions in the high current effects session of the workshop. Treated topics concern numerical evaluation of wake fields and impedances, comparison of calculated impedance with those obtained with beam-based measurement, and the use of obtained impedance models to simulate beam instability. They include attempts to explain the origins of discrepancy between the calculated and measured impedance, a consistent good reproduction of measured collective effects with the obtained impedance model, as well as elaboration in instability simulations by including single particle nonlinear dynamics and local position dependence of the ring physical aperture and optics.**

***Keywords*—storage ring, synchrotron light source, electron beam dynamics, wake fields, impedance, collective effects, beam instability, simulations**

I. Introduction

IN view of their increasing importance in modern and next generation low-emittance rings, a session on high current effects was organized in the workshop “Beam tests and commissioning of low-emittance storage rings”. The above appears to be a clear trend at least for two following reasons: First is that the intensity of the stored beam is always counted as the key performance raising parameter, where the latter is usually the brightness or luminosity, which scales at least linearly with the former. Second is the fact that reduced chamber aperture is required for the strong focusing of the low-emittance optics which in turn increases the machine impedance, as well as to the resultant reduced natural bunch length enhancing the beam interaction with high frequency impedance. Indeed, the next generation low-emittance rings generally require more stringent control of the machine impedance and collective effects driven by the former.

There were three contributions in the session, which shall be described synthetically hereafter.

II. Comparison of Impedance Beam-Based Measurements and Simulations

The first of the three contributions of the session was presented by Victor Smaluk from NSLS-II, addressing the interesting question of how various impedances measured in different machines are related with each other and in particular compare with model predictions [1]. The study focused on single bunch effects, by looking at physical quantities such as the longitudinal and transverse effective impedances, the energy loss factor, and the transverse kick factor, which depend on the convolution of the impedance with the bunch power spectrum. The physical observables are the bunch lengthening, synchronous phase shift, coherent betatron tune shifts, chromatic head-tail damping, as well as orbit distortions due to transverse impedance. Impedance models are obtained either by numerical computing them with 3D EM-solvers, or using analytical models such as a broad-band resonator and a pure inductance. For example in the NSLS-II case, simple models work well enough if the bunch is longer than 10-15 ps RMS. Fifteen storage rings in which the measurement of current-dependent bunch lengthening and coherent betatron frequency shift was performed were followed to analyze their measured data. The bunch lengthening was fitted with the modified Zotter equation (inductive model), which is consistent with the Haissinski equation (broad-band resonator model). The coherent betatron frequency shift was fitted with the linear formula valid for small frequency shifts. The results are shown in Fig. 1.

The impedances obtained from the beam-based measurements above were then compared with their respectively published impedance budgets. In the best cases, the impedance budgets are found to agree with the measurements to within 20-30%, while in other cases, the discrepancy can exceed 100%. For old machines, it may be argued that possible reasons for the discrepancy include limited analytical formulae, insufficient computing power for simulations, inadequateness in simulation codes as well as loose tolerances. On the other hand, for many new machines the impedance budget is calculated by element-wise computing of the wake potentials using 3D simulation codes.

Here V. Smaluk investigated the following three possibilities for the discrepancy using the simple pillbox cavity model and the code `ECHO` [2] for numerical calculation: 1) Interference of wake fields excited by a beam in adjacent components of the vacuum chamber; 2) Effect of the mesh size set for the simulation codes; 3) Inadequately wide band of the calculated impedance, if the bunch length used in the numerical computation is not short enough.

It was found that, at least for this simple pillbox cavity model, the wake field interference can result in a more than 100% error; the effect of the mesh size does not exceed 5%, if it is smaller than 1/5 of the r.m.s. bunch length; a shorter model bunch can change the longitudinal loss factor and the transverse kick factor by 4-6%; the longitudinal effective impedance is more sensitive: up to 15%. Following the above findings, an experimental cross-check is proposed, namely measuring local impedance of one of high-impedance sections and comparing it with the impedance computed for the whole section and versus a sum of element-by-element computations.

A point that attracted audience’s attention through V. Smaluk’s talk was the rather large discrepancy which may result

This work was supported by ARIES, which is funded from the EU’s Horizon 2020 Research and Innovation programme under Grant Agreement No 730871.

R. Nagaoka is at Synchrotron SOLEIL, Gif-sur-Yvette, France (email: nagaoka@synchrotron-soleil.fr). L. Emery is at the Advanced Photon Source at Argonne National Laboratory, Argonne, IL 60439, USA (e-mail: lemery@anl.gov).

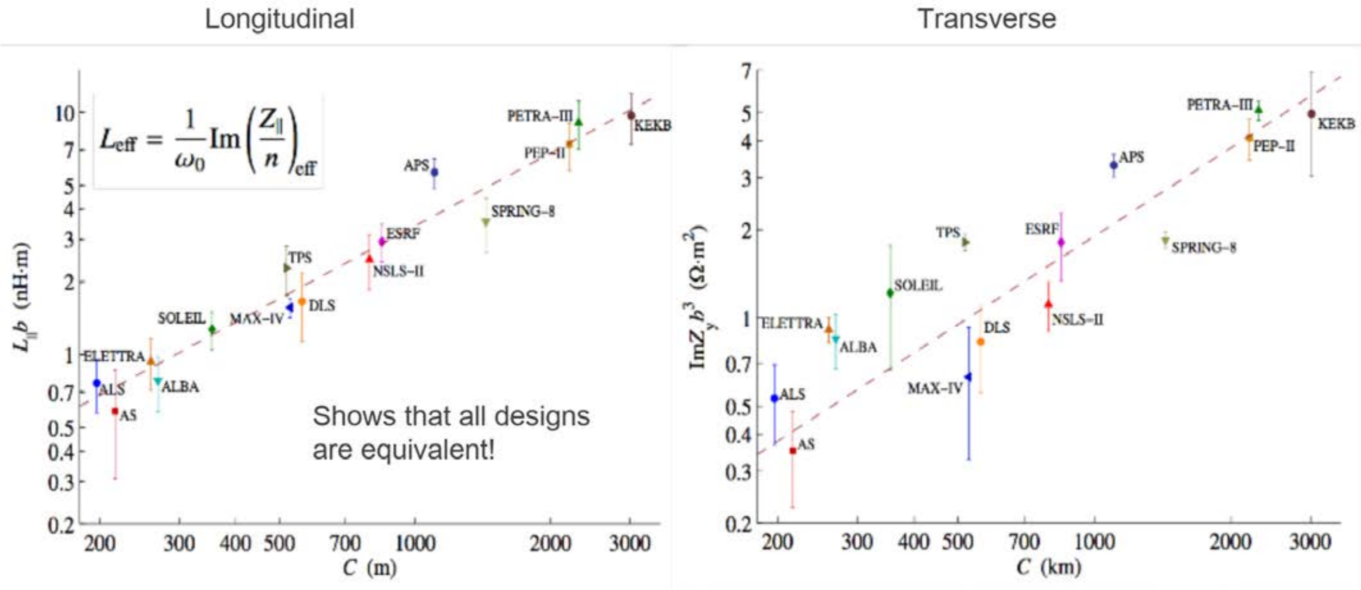

Fig.1. Fit of the beam-based data measured in fifteen different storage rings using the same model to compare the resultant impedances. Left: Extracted effective inductance from bunch lengthening. Right: Extracted effective vertical impedance from coherent betatron tune shift

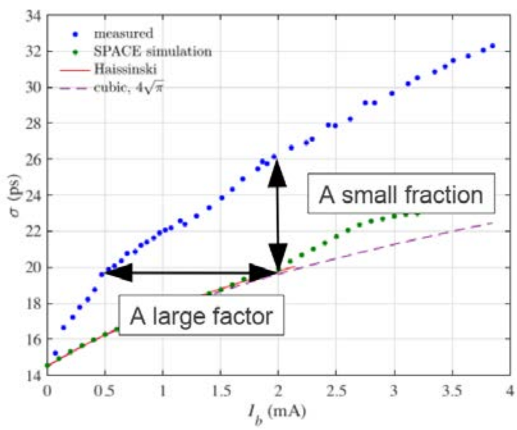

Fig.2. Typical discrepancy between the measurement and prediction over the impedance extracted from the bunch length measurement, discussed after the presentation of V. Smaluk

(exceeding 100%) on the impedance between the measured and expected, depending actually upon rather limited differences (typically 20-30%) in the measurement. An example of such situation is shown for the extraction of longitudinal impedance from the bunch lengthening measurement (Fig. 2). Since the impedance in this case is fitted from the slope of the bunch length versus current, a small systematic error in the measurement could have a non-negligible impact. Such aspect must not be overlooked when searching for possible sources of error.

III. Experimental Verification of Impedance Modelling for Next-Generation Light Sources

The second contribution was given by Ryan Lindberg from APS, presenting the impedance model constructed for the current APS storage ring, along with a series of comparisons made on the physical observables computed using the former with the experimentally measured data, with the goal of getting useful indications and guidelines for the future upgrade of their machine to an ultra-low emittance ring, where the importance of properly controlling the collective effects is expected to be furthermore enhanced. Studies focused on single-bunch collective effects, and hence on the modeling of short-range wakefields and impedances. The steps developed at APS to this end are as follows: 1) Identify relevant geometric and resistive wall sources of impedance. 2) Compute the resistive wall impedance using analytic formulas. 3) Calculate each element's geometric impedance with the numerical code `GdfidL` [3]. 4) Model point-particle Green function by the wakefield of a σ_b = 1-mm bunch. 5) Weight transverse dipole and quadrupole wakefields by local beta function and sum. 6) Take FFT of "summed wakefield" in each plane to get the "summed impedance". 7) Track particles in `elegant` [4].

The longitudinal impedance constructed according to the described steps was shown in the frequency range up to 100 GHz, along with the information of vacuum components giving major contributions on the imaginary part, which were BPMs, bellows, flange gaps and transitions to and from narrow gap ID sections. In constructing the impedance model, it was noticed in particular that to predict correctly the microwave instability requires fully resolving the first resonator-like peak, which for the APS was found to occur near $f \approx 20$ GHz. Another noteworthy point reported was that in doing the beam instability simulations, the wakefields (or impedance) as computed were used, without trying to enforce causality or doing any deconvolution. There it is believed that for the relatively long bunches in the APS storage rings it is better to use a frequency filtered result that discards high frequency contributions presumed to be irrelevant, than to try and reconstruct the high-frequency components. The simulation results obtained according to the described procedure were shown in comparison with those measured, for bunch lengthening and energy spread widening versus single bunch current, and transverse single bunch current limit versus chromaticity, where excellent agreement is found for all three quantities (Figs. 3).

On the basis of the obtained impedance model that very well reproduces the current-dependent single bunch effects

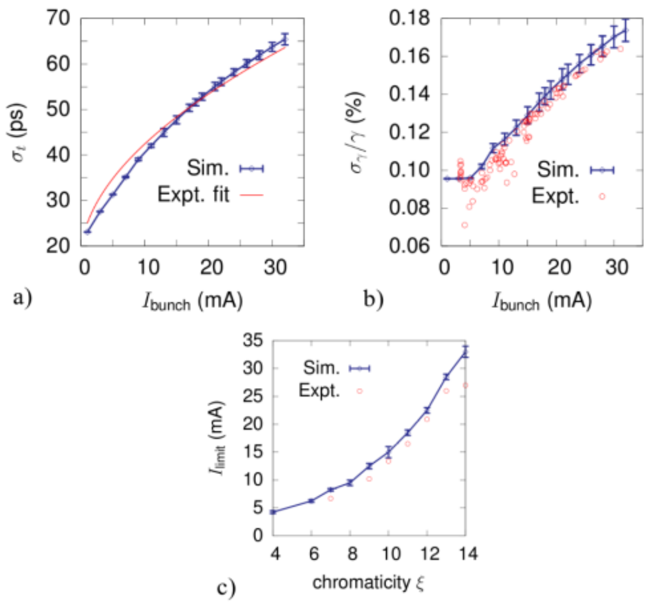

Fig.3. Comparison of measured and simulated collective effects at the APS. a) plots the bunch lengthening with single bunch current, while b) plot the energy spread. c) plots the single bunch current limit as a function of chromaticity

as shown in Fig. 3, several interesting and furthermore elaborated studies were presented. One was the verification of the relative contributions of different parts of the ring to the total machine impedance. Since the constructed model indicated roughly 30% contributions respectively from narrow gap ID sections and transitions around the former, one can change the total effective transverse impedance by varying the beta functions in a controlled manner. The single bunch accumulation limit was then followed experimentally as a function of the impedance variation and compared with the expectation (Fig. 4).

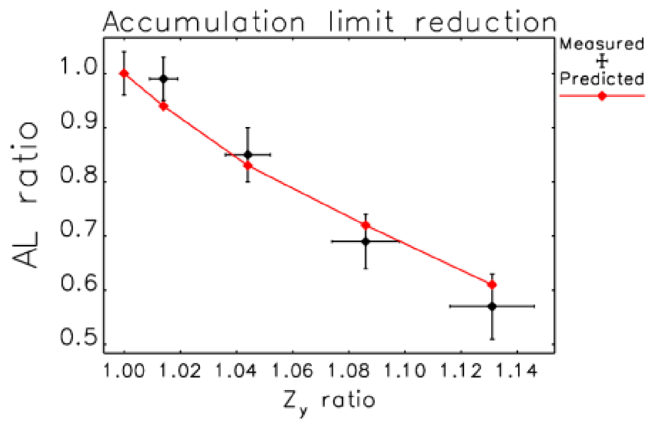

Fig.4. Measured and simulated variation in the accumulation limit as a function of the vertical impedance

Another study explored the impact of transverse wakes on the injection saturation by following the fraction of surviving particles as a function of the transverse oscillation (kick) amplitude. Simulation of the injection process with the element-by-element single particle tracking integrating the position-dependent transverse wake-induced kicks managed to reproduce well the measured trend that the beam survival rate decreases more gradually with increasing kicks as the beam intensity increases.

A detailed analysis was made on an ID transition which was specially designed to have 30% smaller impedance than the existing ones, which however turned out to be 20% larger on the contrary when installed and measured experimentally with the orbit bump method. Upon a closer look, a welding bead of ~0.8 mm in average height was found on the border of the transition to the ID section. Numerical simulations with `GdfidL` along with studies with analytical impedance model were made, finding good agreement with the measured impedance kick.

IV. CHARGE LIMIT SIMULATON OF THE HEPS ACCELERATORS

The third contribution was given by Haisheng Xu from IHEP, who presented the key collective effect issues studied for the storage and the booster rings of the ongoing project HEPS. The project is building a large scale (6 GeV, 1360.4 m) ultra-low emittance (34 pm) light source ring in Beijing [5]. The major challenges for collective effects come from the fact that two beam filling modes are envisaged for the storage ring, where one which is the high brightness mode (200 mA, 680 bunches) and the other the high-bunch-charge mode (200 mA, 63 bunches), which are to be delivered with swap-out injection. Namely, to meet the latter condition as much as 14.4 nC of charge must be ramped in the booster and injected in a single shot in the storage ring. To carry out simulations of beam instability, impedance models were constructed for the storage ring and the booster, evaluating respectively 15 and 6 key vacuum components.

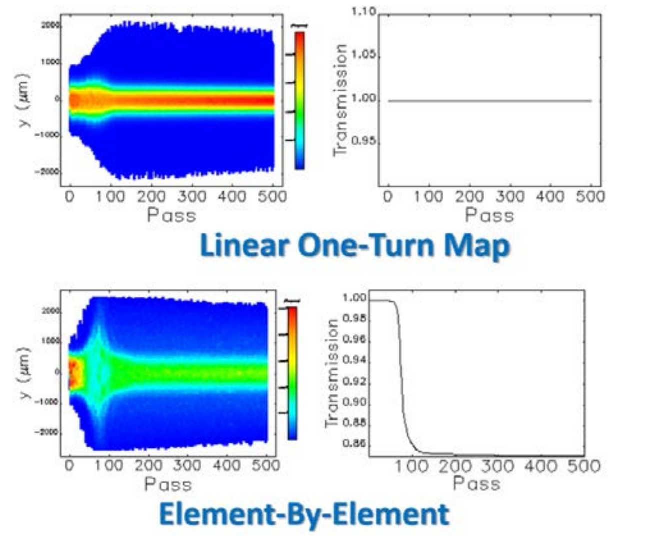

Fig.5. Comparison of two methods of tracking simulating injection of a high charge bunch (15 nC, initial vertical offset of 300 microns), showing the importance of element-by-element tracking

For the storage ring, two instabilities have been looked at in detail: The transverse single bunch and the fast beam-ion. To cope with the reduction and the spread of the synchrotron frequency induced by harmonic cavities which are foreseen, simulations were done with `elegant` [4]. Simulations show that even though positive chromaticity helps stabilizing the beam, the beam blows up in the time scale of ~100 turns as the bunch charge is increased to 40 nC range, requiring element-by-element tracking to be performed instead of the usual one-turn mapping, with proper local physical aperture information along the ring to be accurate (Figs. 5). Optimization of injection efficiency with transverse bunch-by-bunch feedback included in the simulation is underway.

Due to the small transverse beam size and high beam intensity, beam ion instability is considered important for HEPS. The instability growth time is estimated both analytically and numerically with the weak-strong model. The results show that when the amplitude is small compared to the beam size, the exponential growth time is of several milliseconds. However, for large oscillation amplitudes, growth rate reduces rapidly and the oscillation amplitude increases quasi linearly with a growth time of tens of milliseconds. The growth rate finally gets saturated when it is comparable with the radiation or transverse feedback damping rate. Reasonably good agreement is found between analytical estimation and numerical simulations. Analytical estimates show emittance growth even at low beam current. Since growth rates are faster than radiation damping, efficient transverse feedback system is required in order to keep the beam quality.

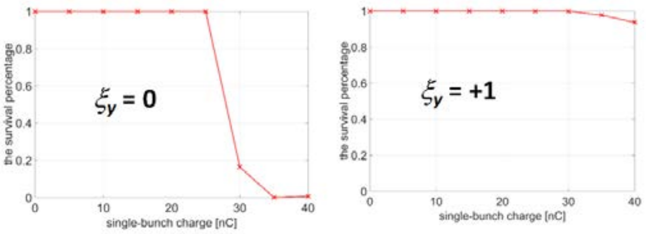

Figs.6. Comparison of beam surviving rate in the booster as a function of bunch intensity between the vertical chromaticity of zero and one

Even though the "high energy accumulation" scheme was proposed to relax the requirement of single-bunch charge at low energy [5], the HEPS booster is still required to ramp about 5 nC in a single bunch, which is quite challenging. Transverse single-bunch instability in the booster needs therefore be studied in detail. Tracking simulations at both zero and +1 chromaticity considering the energy ramping and using one-turn map with nonlinear terms show that the particle loss seems more serious when the chromaticity is zero (Figs. 6). It was also noticed that the transverse beam size may increase at relatively low energy, which then gets damped as the energy ramps. As in the case of storage ring, the above suggests the need of introducing physical aperture of the vacuum chambers in the simulation to be more accurate, which is planned in the next step.

CONCLUSION

The three contributions we had in the high current effects session of the workshop all presented valuable elements that help improve our understanding of impedance and collective effects, and show the necessity of certain elaborations in instability simulations in correctly understanding the encountered physical phenomena, in particular the importance of taking into account the interplay between single particle and coherent beam dynamics. Above all, the works shown in the three contributions commonly suggest the increasing importance of collective effects and of mastering them in the next generation ultra-low emittance storage rings, whose performance is further pushed to the limit.

ACKNOWLEDGEMENTS

We thank the three contributors for having provided us with materials that helped make this summary.

REFERENCES

[1] V. Smaluk, "Impedance computations and beam-based measurements: A problem of discrepancy", Nuclear Inst. and Methods in Physics Research, **A888** (2018) 22–30.

[2] I. Zagorodnov, "Computation of electromagnetic fields generated by relativistic beams in complicated structures", proceedings of NAPAC2016, Chicago, 2016, pp. 642-646.

[3] W. Bruns. "The GdfidL Electromagnetic Field simulator", http://www.gdfidl.de.

[4] M. Borland. "`elegant`: A flexible SDDS-compliant code for accelerator simulation", ANL/APS LS-287, Advanced Photon Source (2000).

[5] Y. Jiao et al., "The HEPS Project", Journal of Synchrotron Radiation 25 (6), pp. 1611-1618, 2018.

Experimental verification of impedance modeling for next-generation light sources

Ryan Lindberg

***Abstract*—Predicting the impedance of next-generation storage rings is a challenging but important part of their design. We discuss impedance modelling that has been done for the APS, and present a number of experiments that have been done to try and validate the resulting predictions. These results have guided our present approach to impedance modeling as we look towards the next-generation APS Upgrade.**

***Keywords*—Storage rings, impedance, collective effects**

I. Introduction

UNDERSTANDING and predicting collective effects in next-generation storage rings is an important but challenging problem. In order to gain confidence in extrapolating to the future, we need to show that we can explain collective effects observed in present machines. A critical part of this is developing an impedance model of the storage ring that we can then verify with experiments. This can then be used to inform what are the relevant sources of impedance, and guide future design.

This paper begins with a discussion of the Advanced Photon Source (APS) impedance model, and how we use it to predict a variety of collective effects at the APS. We then describe several comparisons of the model predictions to measurements made at APS, focusing on a few measurements made recently of transverse collective effects. Finally, we conclude.

II. Impedance model of the APS

We will focus on single-bunch collective effects, and therefore on the modeling of short-range wakefields and impedances. The APS impedance model was developed using the following steps:

1) Identify relevant geometric and resistive wall sources of impedance.
2) Compute the resistive wall impedance using analytic formulas.
3) Calculate each element's geometric impedance with the numerical code `GdfidL` [1].
4) Model point-particle Green function by the wakefield of a $\sigma_b = 1$-mm bunch.
5) Weight transverse dipole/quadrupole wakefield by local beta function and sum.
6) Take FFT of "summed wakefield" in each plane to get the "summed impedance".
7) Track particles in `elegant` [2]

This work was supported by the U.S. Dept. of Energy Office of Sciences under Contract No. DE-AC02-06CH11357.

R. Lindberg is at the Advanced Photon Source at Argonne National Laboratory, Argonne, IL 60439, USA (e-mail: lindberg@anl.gov).

This procedure was initially developed at the APS by Y.-C. Chae. The computed longitudinal impedance for the APS is shown in Fig. 1.

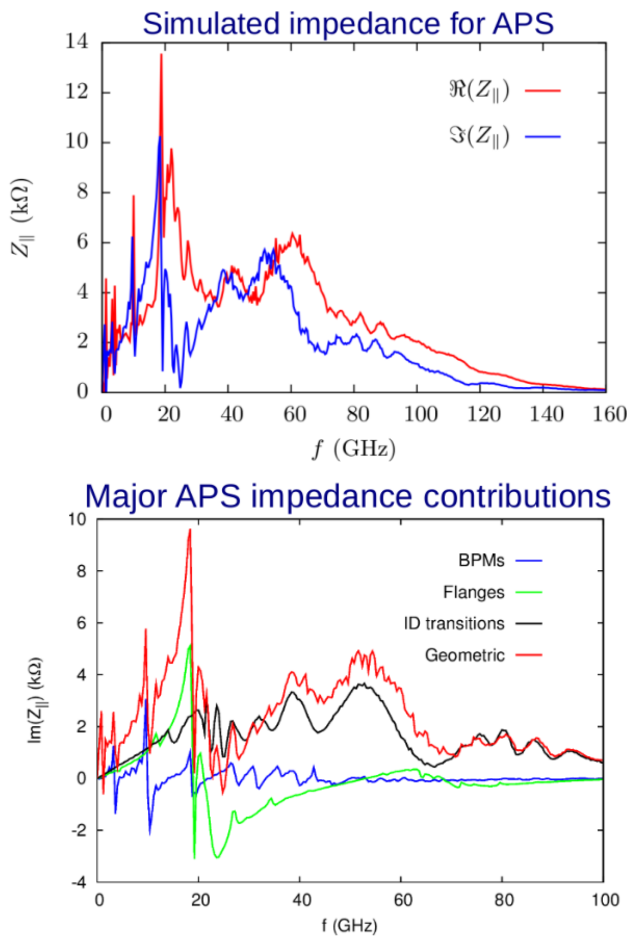

Fig. 1. Longitudinal impedance model of the APS. Top plots the total imepdance, while the bottom splits $\Im(Z_\parallel)$ into its primary components.

A few additional comments on the procedure are warranted. The first step is the most critical, but also the only one that has no definitive procedure, since discriminating what is relevant is a bit of an art. We have found that it is critical to include components that are repeated throughout the ring, such as BPMs, bellows, flange gaps, and ID transitions, are accounted for, and also to account for all other components that has significant geometric discontinuities. In addition, it is a challenge to insure that what is being modeled accurately represents what is in the ring. We believe that most discrepancies between collective predictions and measurements are due to those two factors, since if we accurately model all relevant sources of impedance the predictions should be good ones.

Once the impedance sources have been identified, we compute the geometric impedance using `GdfidL`, although any such similar code may also be used. The important constraint here is that one must resolve the impedance out to a sufficiently high frequency by using a sufficiently short bunch length σ_b in the code. In particular, we have found that correctly predicting the microwave instability requires fully resolving the first resonator-like peak, which for the APS is seen to occur near $f \approx 20$ GHz. Since the simulated impedance is ideally equal to the point-particle Green function filtered by the Gaussian $e^{-\sigma_b^2\omega^2/2}$, this implies that we should require $\sigma_b \ll 2.5$ mm.

Finally comes the particle tracking. For this purpose we use `elegant`, although there are several other suitable alternatives. An important point to be made here is that we typically apply the wakefield (or impedance) once per turn, and include all the other relevant physics including rf acceleration, nonlinear tune-shift with amplitude, linear and non-linear chromaticity, and synchrotron radiation. In addition, we use the wakefield (or impedance) as computed, without trying to enforce causality or doing any deconvolution. Rather, we believe that for the relatively long bunches in storage rings it is better to use a frequency filtered result that discards high-frequency contributions presumed to be irrelevant, than would be to try and reconstruct the high-frequency components.

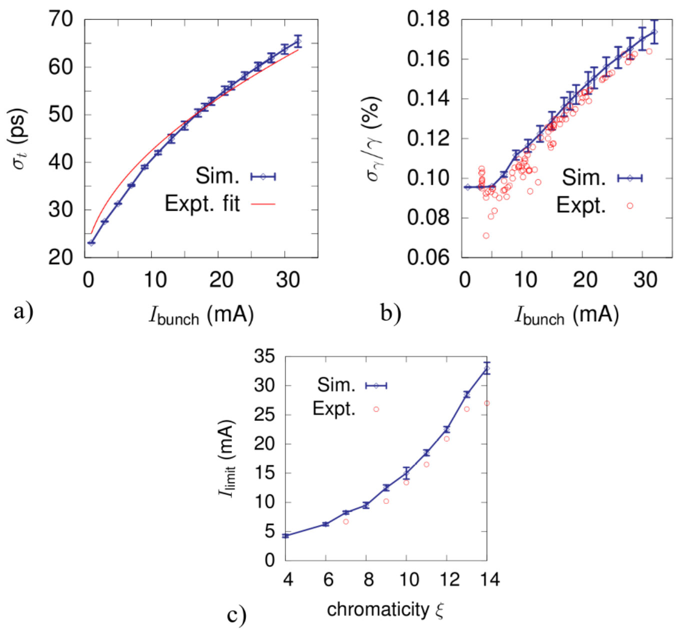

Fig. 2. Comparison of measured and simulated collective effects at the APS. a) plots the bunch lengthening with single bunch current, while b) plot the energy spread. c) plots the single bunch current limit as a function of chromaticity.

We show some comparisons of simulation predictions that use the methods just described to experiemnts at the APS in Fig. 2. Panels (a) and (b) show longitudinal collective effects. Panel a) shows quite good agreement in the predicted and measured bunch lengthening with charge, while b) shows that the simulations predict both the the onset of the microwave instability at $\sim$ 7 mA, and the subsequent energy spread growth at higher charge. Finally, Fig. 2(c) compared the single bunch stability limit as a function of the chromaticity.

In the next section we discuss some more detailed measurements and modeling that have been made regarding transverse collective effects at the APS.

III. Verifying transverse collective effects

Modeling transverse collective effects correctly first requires one to correctly model bunch lengthening and energy spread increase due to the longitudinal impedance, since the transverse kick is the convolution of current profile and dipole wakefield. In addition, one must compute the impedance with a sufficiently narrow bunch length σ_b to resolve both the current shape and the chromatic frequency shift $\omega_\xi = \xi\omega_0/\alpha_c$; for the APS this condition is less stringent than the $\sigma_b = 1$ mm required to accurately predict the microwave instability. Next, one must include both dipolar and quadrupolar wakefields, where the dipolar wakefield applies a kick that is proportional to the displacement of the source particle, while the quadrupolar wakefield gives a kick that is proportional to the test particle. Finally, one must use a sufficient number of particles/current bin and have a sufficiently accurate model of the ring. At the APS we typically use 200,000 particles for simulation, and employ a linear ring model when making stability calculations, while we have found that element-by-element tracking may be required to simulate transient effects such as those that occur at injection. Once we have the impedance model, we can make tests that go beyond the stability analysis of Fig. 2(c).

One such test that was made at the APS and reported in [3] relied on the fact that the total vertical impedance can be varied by changing the linear optics since $Z_y \sim \beta_y Z_D$. Indeed, if one can increase β_y where the impedance is large while reducing in where Z_D is small then one can potentially increase the total impedance while maintaining the linear tune. We can understand how this was done at the APS if we recognize that for normal operation the APS vertical impedance has three approximately contributions: one-third each from the ID straights, the transitions to and from the IDs, and from the rest of the ring. Hence, the vertical impedance can be increased by up to $\sim 13\%$ if we increase $\langle\beta_y\rangle$ in the straight section by 1.75 while decreasing $\langle\beta_y\rangle$ in the rest of the ring by ~ 0.65, all while maintaining the vertical tune since the ID lengths are relatively short.

The resulting variation in the accumulation limit is shown in Fig 3. We see that the measured accumulation limit is nearly halved when the impedance increases to 1.13 of its nominal value, which agrees well with predictions. The simulation results depend fairly strongly on the precise injection con-ditions; in particular, it was found that agreement relied upon matching the small vertical motion due to coupling observed in the experiement, which was done in the simulations using an initial 0.3 mm offset.

Another study that was recently completed investigated the role of collective effects on the dynamic acceptance [10].

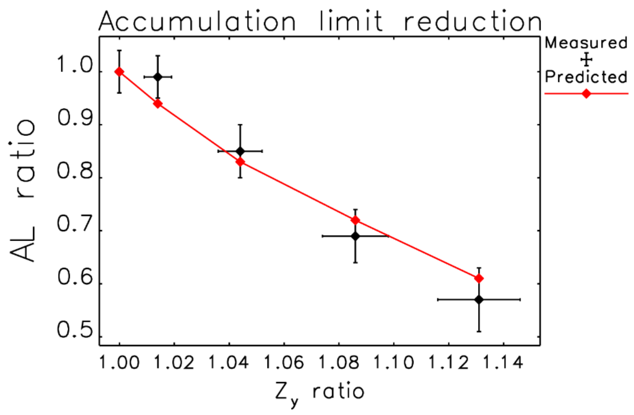

Fig. 3. Measured and simulated variation in the accumulation limit as a function of the vertical imepdance.

While the dynamic acceptance is typically considered from a single-particle perspective, transverse wakefields during traditional accumulation can reduce the acceptance. This happens when the oscillating beam drives wakefields that lead to emittance growth, so that the acceptance becomes "fuzzier" as the stored charge increases. Figure 4(a) shows measurement results that illustrate this effect, in which the fraction of the surviving charge is plotted as a function of the kick amplitude. At low charge the acceptance drops quite sharply to zero around 0.47 mrad, while showing a more gentle variation as the charge increases.

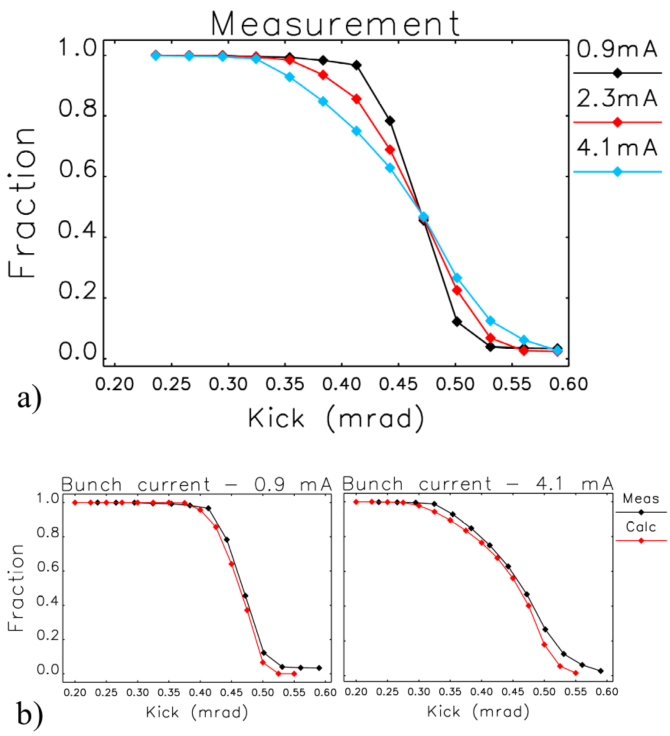

Fig. 4. a) Fraction of surviving particles as a function of the kick amplitude for three different currents. b) Comparison of simulation and measurement for the dynamic acceptance at 0.9 mA (left) and 4.1 mA (right).

Comparisons to tracking simulations are shown for the lowest (0.9 mA) and highest (4.1 mA) cases in Fig. 4(b), where we see rather good agreement. The simulations use the fully calibrated APS model with element-by-element tracking and 40 impedance elements/turn. We found the last part to be necessary since most of the particle loss occurs in the first 20 turns, in which case the dynamics occurs over too short a time-scale to be accurately modeled by a single impedance element applied once per turn.

The fact that the dynamic acceptance depends upon the charge can be important for next-generation light sources that rely on traditional accumulation. This is particularly true for ultra-low emittance rings with strong nonlinearities and/or if the ring plans to employ more "exotic" insertion devices with narrow horizontal gaps, since these cases often have little margin for emittance growth.

IV. IMPEDANCE COST OF IMPERFECT ID TRANSITIONS

Transitions to and from the narrow gap insertion devices (IDs) typically constitute a significant contribution of the transverse impedance of storage ring light sources. As mentioned previously, at the APS approximately one-third of the vertical impedance is due to the transitions to and from the ID straights, where the vertical aperture reduces from the nominal 42 mm to a minimum gap between 5 and 8 mm depending upon the ID in question, and back to the nominal chamber. Since the transitions are such a significant source of impedance, Y.-C. Chae designed a new ID transition design by numerically optimizing a two-taper scheme as depicted in Fig. 5. Note that the taper angle is larger at larger aperture, and that the impedance reduction associated with the transition in Fig. 5 also been theoretically explained by Stupakov [4].

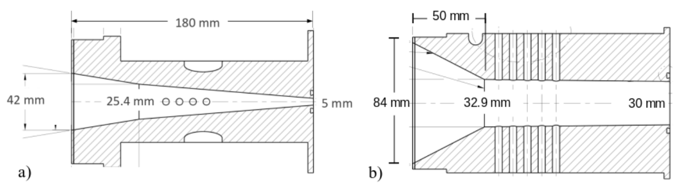

Fig. 5. Geometry of the optimized transition. a) shows side view of the transition, while b) shows a top view.

The optimized ID transition was installed in the APS storage ring and its impedance was measured by the local bump method [5], [6], with the expectation that the measured vertical kick factor would be reduced by $\sim 30\%$. Unfortunately, it was observed that the "optimized" kick factor was about 20% larger than that of the usual transition. Additionally, the aperture as measured by the electron beam was 1 to 2 mm smaller than expected. For this reason, the chamber was replaced.

After the optimized ID chamber was removed, subsequent measurements revealed an unusually large weld bead at the narrow gap where the transition joined the ID straight section. This weld bead was measured to have an average height $\sim$ 0.8 mm, which both explains the measured reduction in the aperture and will also result in an additional source for wakefields. But could these weld beads be the culprit for the measured increase in impedance? To help answer this question, we used `GdfidL` to compute the kick factor of the new transition including obstacles (weld beads) of varying heights. The results are plotted in Fig. 6(a), where we see that small obstacles whose height is ~ 0.6 mm eliminates any impedance advantage of the optimized transition. Furthermore, we expect that the measured 0.8 mm weld beads will actually increase impedance. For comparison, Fig. 6(a) also includes the theory of small obstacles from Refs. [7]–[9]; while we expect the predicted quadratic increase of the kick factor on height, the quantitative agreement is somewhat surprising since the theory is idealized.

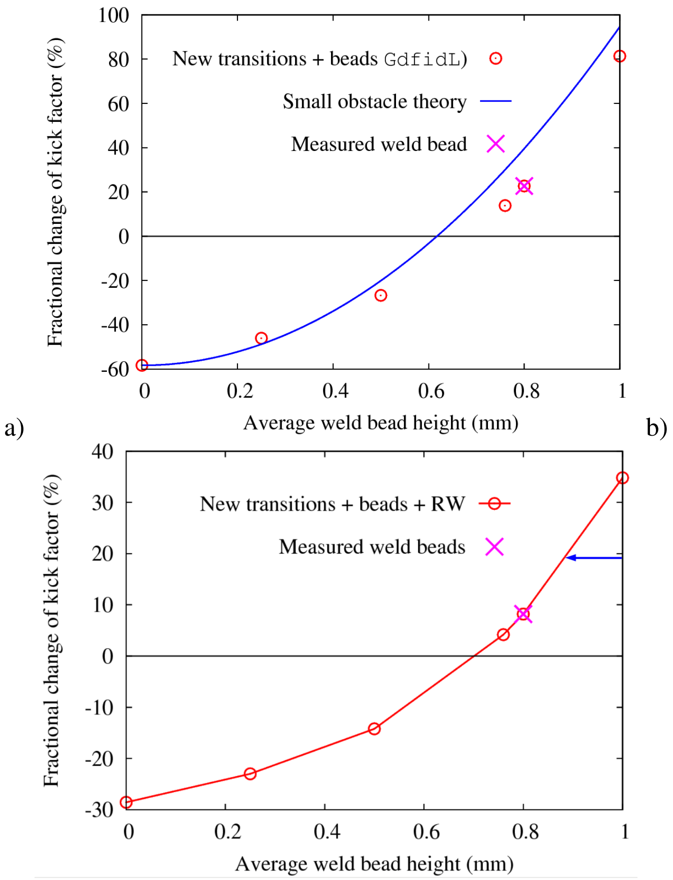

Fig. 6. a) Simulated change in the kick factor of the optimized transitions from that of the original as a function of the weld bead height. The solid blue line is from the theory of small obstacles. b) Simulated change in the kick factor of the optimized ID including the resistive wall as a function of the weld beam height. The beam-based measurement is indicated by the blue arrow.

The simulation results in Fig. 6(a) are for the transition alone, but comparisons to the experiment must also include the contribution due to the resistive wall of the 5 m long ID chamber. We plot the total change in the kick factor as a function of the obstacle height in Fig. 6(b), with the in red and the measurement labeled by the blue arrow. Figure 6(b) shows that the best estimate of the measured weld bead height eliminates nearly all the discrepancy between the ideal optimal and the measurement, but a small difference remains. Regardless, these results show how significant imperfections and unintentional obstacles can be, particularly when they occur at narrow apertures. Indeed, for this reason the transitions to and from the IDs in the APS-U are being designed to be cut directly from the extrusion using a a mill or plunge EDM, thereby ensuring a smooth surface at the small gap.

V. Conclusions

Collective effects will ultimately limit the performance of a storage ring, and it is therefore important to understand and be able to predict the ring impedance during the design process of any next-generation, low-emittance light source. In this paper we have outlined how the present APS has developed such an impedance model, and indicated a number of experiments that have been done to validate the model. In particular, we have showed how collective effects may limit injection efficiency during traditional accumulation, and have pointed out the importance of proper design and manufacture of vacuum components that have small apertures. We are in the process of leveraging these experiences as we design and prepare to build the ultra-low emittance APS Upgrade.

Acknowledgment

The authors would like to acknowledge useful discussions with Michael Borland, Louis Emery, and Vadim Sajaev from the APS, Alexei Blednykh at NSLS-II, and Yong-Chul Chae who is now at DESY.

References

[1] W. Bruns. The `GdfidL` Electromagnetic Field simulator. `http://www.gdfidl.de`.

[2] M. Borland. "`elegant`: A flexible SDDS-compliant code for accelerator simulation", ANL/APS LS-287, Advanced Photon Source (2000).

[3] V. Sajaev, M. Borland, Y.-C. Chae, and L. Emery"Experimental verification of single-bunch accumulation limit dependance on impedance at the APS", in Proc. of the 2013 NA-PAC, Pasadena, CA, pp. 405.

[4] G. Stupakov, private communication and "Low frequency impedance of tapered transitions with arbitrary cross sections", *Phys. Rev. ST-Accel. Beams* 10, 094401 (2007).

[5] V. Kiselev and V. Smalyuk, "Experimental study of impedances and instabilities at the VEPP-4M storage ring", in Proc. of the 1999 DIPAC, Chester, UK, 1999, pp. 1005.

[6] Emery, G. Decker and J. Galayda, "Local bump method for measurement of transverse impedance of narrow-gap ID chambers in storage rings", in Proc. of the 2001 PAC, Chicago, USA, 2001, pp. 1823.

[7] S.S. Kurennoy, "Beam coupling impedances of obstacles protruding into a beam pipe", *Phys. Rev. E* 55, 3529 (1997)

[8] S.S. Kurennoy and R.L. Gluckstern, "Impedances of azimuthally symmetric irises and cavities with semielliptical profile in a beam pipe", *Phys. Rev. E* 55, 3529 (1997).

[9] G.V. Stupakov, "Impedance of small obstacles and rough surfaces", *Phys. Rev. ST-Accel. Beams* 1, 064401 (1998)

[10] V. Sajaev, R. Lindberg, M. Borland, and S. Shin, "Simulations and measurements of the impact of collective effects on dynamic aperture", *Phys. Rev. Accel. Beams* 22, 032802 (2019).

Charge Limit Simulations of the HEPS Accelerators

Haisheng Xu, Na Wang
Institute of High Energy Physics, Chinese Academy of Sciences, Beijing, China

Abstract—**High Energy Photon Source (HEPS) is a 6 GeV ultra-low emittance ring based synchrotron light source to be built in Beijing, China. The beam emittance is pushed down to about 34 pm in the baseline design of the HEPS storage ring. To estimate the performance of the machine, we carried out systematic studies to understand the charge limit determined by the collective effects. Here, we first briefly present our studies of transverse single-bunch instability and the preliminary estimate of the fast beam-ion instability in the HEPS storage ring. Then, we also discuss a bit about the studies of transverse single-bunch instability in the HEPS booster with the consideration of energy ramping process at different chromaticities.**

Keywords—**Ultra-low emittance ring, Impedance, Collective Instabilities**

I. Introduction

High Energy Photon Source (HEPS) is a greenfield machine designed by IHEP, CAS, China. The accelerator part of HEPS consists of a 500 MeV LINAC, a booster to ramp the beam energy from 500 MeV to 6 GeV, and a 6 GeV ultra-low emittance storage ring. The storage ring of HEPS is based on modified hybrid seven-bend achromat (7BA) concept, with implementation of longitudinal gradient bends, transverse gradient bends, and anti-bends. The natural emittance the baseline design is about 34.2 pm. The circumference of the ring is 1360.4 m. Two operating modes, high-brightness mode (200 mA, 680 bunches) and high-bunch-charge mode (200 mA, 63 bunches), are presently proposed. More detailed information of the lattice can be found in [1].

We believe that the beam loss is the first thing to worry about in the studies of the collective effects. Therefore, we would like to focus on the effects due to high charge, which may cause beam loss, in this presentation.

The main body of the presentation is divided into two main parts. Firstly, we present the studies of the transverse single-bunch instability and the preliminary estimates of the fast beam-ion instability for the HEPS storage ring. In the second part, we discuss the study of transverse single-bunch instability in the HEPS booster with the consideration of energy ramping process.

To carry out the studies of the impedance induced collective instabilities, we first create the impedance model for the HEPS storage ring and the booster, respectively. For the HEPS storage ring, 15 contributions are included in the present impedance model. The total impedance spectrum has been used in the calculations of the collective instabilities in the HEPS storage ring. In the tracking process, the beam-impedance interactions are computed in frequency domain. The impedance model for the HEPS booster is still very preliminary including only 6 key contributions. However, we believe that it's a good starting point for the study of collective instabilities in the booster. Update of the impedance models for both HEPS storage ring and the booster is still on-going since the more detailed engineering design of the components is still on-going.

The work was supported by National Natural Science Foundation of China (No. 11775239 and No. 11805217), NKPSTRD (2016YFA0402001), and Key Research Program of Frontier Sciences CAS (QYZDJ-SSW-SLH001). The author H. S. Xu would like to thank the '100 Talents Program of Chinese Academy of Sciences' for the support.

H. S. Xu and N. Wang are with Key Laboratory of Particle Acceleration Physics and Technology, Institute of High Energy Physics, Chinese Academy of Sciences, Beijing, China. (e-mails: xuhs@ihep.ac.cn, wangn@ihep.ac.cn).

II. Instabilities in HEPS Storage Ring

In this part, we basically focus on two topics. First one is the study of transverse single-bunch instability. The second one is the very preliminary estimate of the fast beam-ion instability.

A. Transverse Single-Bunch Instability

Transverse single-bunch instability may cause serious particle loss if it happens. Usually, finite nonzero chromaticity is implemented to stabilize the beam in the real operation of the machines. In our case, the third harmonic cavity is proposed to provide bunch lengthening. However, the decrease of synchrotron oscillation frequency as well as the increase of synchrotron oscillation frequency spread make the analytic estimation of threshold current with harmonic cavity quite difficult. We therefore carry out tracking simulations by `elegant` code [2] and its parallel version [3]. The tracking results show that the +5 chromaticity is sufficient to stabilize the beam even at 30 nC/bunch. The result corresponding to 40 nC/bunch shows significant growth of beam size in short time (in about 100 turns, while the synchrotron radiation damping time corresponds to about 3000 turns) after injection, which motivates us to pay more attention to the transient process right after injection.

In the above mentioned tracking simulations, one-turn map is used for tracking particles. However, we realize that this tracking technique may not be sufficient if we would like to include the more realistic physical apertures along the ring. Therefore, we carry out element-by-element tracking and compare the results obtained by one-turn map tracking and element-by-element tracking. The comparison shows that the element-by-element tracking provides more details, for instance, the particles loss due to the more realistic physical aperture along the whole ring. We noticed that the similar results was reported by APS-U some time ago.

We also include the transverse bunch-by-bunch feedback system in our tracking simulations. The preliminary simulations show that the feedback helps stabilize the beam at relatively high charge. We believe that we should keep optimizing the injection efficiency including feedback system at high charge in the future.

B. Fast Beam-Ion Instability

Due to the small transverse beam size and high beam intensity, beam ion instability is one of the potential issues for HEPS. The growth time of the instability at the design beam intensity is estimated by both analytical theories and numerical simulations based on the weak-strong model.

The results show that when the amplitude is small compared to the beam size, the oscillation amplitude of the beam increases exponentially with a growth time of several milliseconds. However, for large beam oscillation amplitude, the instability growth rate reduces rapidly and the oscillation will increase almost linearly with a growth time of tens of milliseconds. The growth rate will finally g et s aturate when it is comparable with the synchrotron radiation damping or transverse feedback damping. Reasonably good agreements have been reached between analytical estimation and numerical simulations.

Meanwhile, analytical estimations have been carried out by assuming different beam currents and different vacuum pressures, which gives us an important reference for the initial beam commissioning. The results show that emittance growths are foreseen at even low beam current. Since the growth rates are faster than the synchrotron radiation damping, efficient transverse feedback system is required in order to keep the beam quality.

III. Instabilities in HEPS Booster

The swap-out injection scheme is chosen for the HEPS storage ring, meaning that a full-charge bunch needs to be injected into the HEPS strage ring. For instance, the single-bunch charge needs to be about 14.4 nC in the HEPS storage ring in the high-bunch-charge mode (200 mA, 63 bunches), which implies that the booster needs to provide such a high charge bunch to the storage ring. This requirement is very challenging for the HEPS booster. Therefore, the "high-energy accumulation" scheme has been proposed to relax the requirement of single-bunch charge at the low energy of the HEPS booster. However, the HEPS booster is still required to have the capability to ramp about 5 nC in a single bunch, which is also quite challenging. This is the main motivation for us to study transverse single-bunch instability in the booster in a more systematic manner.

We present here the tracking simulations at both zero chromaticity and the +1 chromaticity considering the energy ramping. One-turn map with nonlinear terms is used for tracking. Simulations show that the particle loss seems more serious when the chromaticity is zero. another phenomenon is that the transverse beam size may increase at relatively low energy and then be damped as the energy ramps. This phenomenon reminds us that we may have to include the physical aperture of the vacuum chambers more carefully. Otherwise, the particles with large amplitude may get lost. In the next step, we plan to try element-by-element tracking with more realistic physical aperture along the whole booster ring.

IV. Summary and Outlook

Transverse single-bunch instability in the HEPS storage ring has been studied under the condition with (+5,+5) chromaticity and with third harmonic cavity. The threshold current is high enough. However, the beam blow-up right after injection needs careful study.

Preliminary study of the transient effect after injection in the HEPS storage ring shows that this effect strongly limits the single-bunch charge. Further systematic studies are needed.

The proposal of high-charge operation in the HEPS storage ring and the idea of implementing swap-out injection scheme introduces difficulty to the charge limit in the booster.

Systematic studies of the transient effects after injection are needed.

Acknowledgment

The authors would like to thank the colleagues in the Accelerator Physics Group of IHEP for the fruitful discussions.

The simulations were mainly carried out on the cluster operated by the IHEP computing center. The authors would like to thank the staff in the IHEP computing center for their kind support.

References

[1] Y. Jiao, etc., "The HEPS Project", *Journal of Synchrotron Radiation* 25 (6), 1611-1618, 2018.

[2] *elegant: A Flexible SDDS-Compliant Code for Accelerator Simulation*, M. Borland, Advanced Photon Source LS-287, Septumber 2000.

[3] *Pelegant: A Parallel Accelerator Simulation Code for Electron Generation and Tracking* Y. Wang and M. Borland, in the Proceedings of the 12th Advanced Accelerator Concepts Workshop, AIP Conf. Proc. 877, 241 (2006).

Session 6: Low Emittance

Summary: Low Emittance

Les Dallin
Canadian Light Source, Saskatoon, Canada
and Akira Mochihashi
Karlsruhe Institute of Technology

Introduction to Reports by
K. Ohmi
SuperKEKB Low Emittance Tuning
T. K. Charles
Low Emittance Tuning for FCC-ee
A. Papash
Dynamic Aperture in Low Emittance Storage Ring

I. Introduction

THE development of low emittance lattices has resulted in much improved performance in recent years. Light source storage rings are reaching emittances that put the source size comparable to the photon source size in the IDs used to produce synchrotron radiation. These emittances are achieved in using multi-bend achromats (MBAs) with many bend magnets interspersed with focussing elements. The resulting low dispersion in the bends produces the low emittance but at the same time requires strong sextupole (and possibly higher order) magnets to correct the large chromaticities produced by the 1st order optics. To improve luminosity colliders require both low emittance and strong focusing at the interaction region. The very large variations in β-functions to produce the focusing (e.g., β_y's from 1.7 mm to 6960 m in the FCC-ee) also require strong sextupoles to control the chromaticity.

The strong sextupoles in turn act to reduce the dynamic aperture (DA) and the momentum aperture (MA) of these rings. Care must be taken to apply the chromatic correction with possibly many families of sextupoles that also cancel geometric effects introduced by the chromatic sextupoles. To optimize the DA and MA computer codes are used to minimize the resonant driving terms (RDTs) produced by the higher order elements. This can be done by trial-and-error, by simultaneously solving the equations of motion for all the terms and/or by using multi-objective generic algorithms (MOGA): an iterative process.

Once a low emittance lattice with good DA and MA is produced, the lattice must be evaluated against the effects of possible misalignments of the magnets and the higher order multipoles in these magnets. Alignment schemes can be optimized by possibly using girders upon which individual elements can be extremely well aligned. Different schemes are then evaluated by observing the reduction of DA and MA using randomly generated misalignments. To reduce the effects of these errors local and global orbit correction schemes are required. For very large machines with tight tolerances, the initial orbit correction may have to be done section by section until a closed orbit is established and the global correction applied. As discussed in the FCC-ee project, it may also be necessary to start with the sextupoles turned off and slowly bring them up to the design value as the correction scheme is developed.

Initial commissioning of low emittance lattice can proceed similar to the process used to define the alignment scheme. The first turn around the lattice can be done in sections until the orbit is corrected, a closed orbit is established and global orbit correction is applied. This possibly may be done first with the sextupoles turned off. Once the beam is stored the emittance and the machine parameters can be adjusted to achieve the desired tune, machine functions, emittance, etc. For colliders the beam must be steered and properly focused at the interaction regions to optimize the luminosity.

II. SuperKEKB Low Emittance Tuning

SuperKEKB is an asymmetric (e^+, e^-) collider whose circumference is 3016 m and with beam energies of 4 GeV for the positrons and 7 GeV for the electrons. The SuperKEKB is composed of two rings; the low energy ring (LER) for the positrons and the high energy ring (HER) for the electrons, and the beam-beam collision has been designed to have large Piwinski angle of 26. The x-y coupling is one of the key parameters for the SuperKEKB to realize better performance, especially for the luminosity. There are two components of the x-y coupling which mainly determine the luminosity: the global and the local x-y coupling. The global coupling determines vertical emittance and the local coupling at interaction point (IP) determines emittance growth due to the beam-beam interactions. In SuperKEKB, the correction of the global coupling has been carried out by measuring the change in the horizontal and vertical closed orbits by using 6 steering magnets. By using this method with the correction by skew quadrupoles, the vertical emittances of 23 pm and 9 pm have been achieved at LER and HER while the horizontal emittances are 3 nm and 5 nm, respectively. In SuperKEKB, they have found out a discrepancy between the estimated luminosity from the measured beam size at an arc section and the measured luminosity. The discrepancy has come from the local x-y coupling at IP because the local coupling at IP affects the beam-beam performance and enhances the emittance growth accordingly. The source of the local coupling can be explained by the skew rotation of the quadrupole magnets for the final focusing at IP. By exciting the corrector coils with the skew quadrupole field, the local x-y coupling has been corrected and the luminosity performance has been improved twice. However, the luminosity performance is still not sufficient for their target, and an effect of non-linear aberrations at IP is supposed to be the most probable reason for such degradation of the luminosity. Computer simulations based on the weak-strong model have been performed and the possibility that decreases in the luminosity by the non-linear aberrations at IP has been discussed so far. They plan to perform the correction against the non-linear aberrations in Phase-III commissioning which starts from March 2019.

III. LOW EMITTANCE TUNING FOR FCC-EE

The e+/e- collider of the Future Circular Collider (FCC) is a ~100 km circumference ring operating at four energies from 45.6 GeV to 182.2 GeV. A correction scheme for the high energy operation has been developed for a machine with misalignments and field errors. The correction scheme involved "Dispersion Free Steering (DFS), coupling correction through consideration of the Resonant Driving Terms (RDTs) and beta-beat correction via a response matrix Singular Value Decomposition (SVD) approach". The correction progressed using an iterative process starting with the sextupoles turned off and then turning them on in small steps. Orbit correction, coupling correction, tune matching, beta-beat correction and dispersion correction were applied at each step. "For misalignments of 100 μm in x and y and a roll angle error of 100 μrad of all magnet types, and with relative BPM errors of 20 μm and 1000 μrad, the final vertical emittance achieved was 0.202 pm rad, and a coupling ratio of $\varepsilon_y / \varepsilon_x = 0.01$ %."

IV. DYNAMIC APERTURE IN LOW EMITTANCE STORAGE RING

Nonlinearities arising from the chromatic perturbations and sextupoles in circular accelerators limit the stable area of beam oscillations in light sources and lead to the reduction of the beam lifetime. The dynamic aperture problem is one of the most challenging research topics for accelerator physicists. New generation diffraction limited light sources designed for ultimate small beam emittance are based on the multi-bend achromat lattice with strong focusing. High chromaticity accompanied by small dispersion (to ensure ultra-low beam emittance) requires strong sextupoles. As a consequence, the particles might fall into unstable phase space even at small deviations of the reference orbit. Analytically, the horizontal dynamic aperture (DA) under the effect of a single sextupole magnet is inversely proportional to the integrated sextupole field and to the power of -3/2 of the betatron function at the sextupole. By considering a chromatic sextupole that is located at non-zero dispersion section, the horizontal DA is written by an approximate scaling law that shows that the DA is proportional to the dispersion function and inversely proportional to the chromaticity. To expand the DA under the non-linear effect such as from the sextupoles, a countermeasure considering the non-linear resonance can be applied. For example, to minimize the amplitude dependent tune shift which comes from the resonance driving term, the beam position should be corrected to be at the central position of the sextupole magnetic field. From this point of view, the beam position monitors should be located at each sextupole magnet as close as possible. The betatron phase advance between two adjacent sextupoles should be optimized to cancel out the non-linear aberrations. It should be possible to achieve an ultra-low emittance storage ring with tolerable and realistic dynamic aperture if we can fully consider and take care of these non-linear beam dynamics issues.

Low emittance and luminosity tuning in SuperKEKB

K. Ohmi
KEK, Tsukuba, Japan

***Abstract*— x-y coupling correction is very important for not only light source but also e+e- colliders. Global x-y coupling determines vertical emittance. Local x-y coupling at IP determines beam-beam performance. We discuss global and local x-y coupling in SuperKEKB. To improve luminosity performance further, correction of nonlinear coupling and chromatic coupling should be touched.**

***Keywords*—e⁺e⁻ collider, large crossing angle, low beta, low emittance.**

I. Introduction

SuperKEKB, which is a B meson factory, is an asymmetric $e^+ e^-$ collider with the energy of 4(e^+) and 7(e^-) GeV. SuperKEKB consists of two storage rings of the low energy (LER, e^+) and high energy ring (HER, e^-) with the circumference 3016m. The beam-beam collision is adopted large Piwinski angle scheme in which Piwinski angle is $\phi_c\sigma_z/\sigma_x$=26 at the design, where ϕ_c, σ_z and σ_x are the half crossing angle, bunch length and horizontal beam size at the interaction point (IP), respectively. The design beam current is 3.6 and 2.6 A for LER and HER, with the bunch repetition of 4ns. The both rings are regarded as very high current 3rd generation light source in the point of view of the design parameters. The design parameters and those in Phase II commissioning (2018) are summarized in Table 1.

x-y coupling is one of key parameters, which determines the luminosity performance in colliders. Global x-y coupling determines vertical emittance. Local x-y coupling at IP determines emittance growth due to the beam-beam interactions. Higher order nonlinear aberrations

II. Global xy coupling and emittance

2.1 Characterization of x-y coupling

Particles in the storage rings oscillate with the betatron/synchrotron frequencies (tunes). The three tunes ν_x, ν_y and ν_s are not eigen-frequency of horizontal, vertical and longitudinal oscillations. We focus horizontal and vertical betatron motion $\boldsymbol{x}^t=(x,x',y,y')$. The 4x4 revolution matrix (M(s)) is diagonalized into two 2x2 submatrices (U(s)) by following R and B matrices,

$$\boldsymbol{x}(s+C)=M(s)\boldsymbol{x}(s) \qquad \boldsymbol{X}(s+C)=U\boldsymbol{X}(s)$$

$$\boldsymbol{x}=RB\boldsymbol{X}$$

$$U=\begin{pmatrix}U_X & 0\\ 0 & U_Y\end{pmatrix} \qquad U_X=\begin{pmatrix}\cos\mu_X & \sin\mu_X\\ -\sin\mu_X & \cos\mu_X\end{pmatrix}$$
$$M(s)=R(s)B(s)UB^{-1}(s)R^{-1}(s) \tag{1}$$

B characterizes elliptical motion of each degree of freedom in the phase space.

$$B=\begin{pmatrix}B_X & 0\\ 0 & B_Y\end{pmatrix} \qquad B_X=\begin{pmatrix}\sqrt{\beta_X} & 0\\ -\alpha_X/\sqrt{\beta_X} & 1/\sqrt{\beta_X}\end{pmatrix}$$

R which characterizes x-y coupling is parametrized as

$$R(s)=\begin{pmatrix}r_0 & 0 & r_4 & -r_2\\ 0 & r_0 & -r_3 & r_1\\ -r_1 & -r_2 & r_0 & 0\\ -r_3 & -r_4 & 0 & r_0\end{pmatrix} \quad r_0=\sqrt{1-r_1r_4+r_2r_3}$$

Beam envelope matrix is expressed by

$$\langle\boldsymbol{x}(s)\boldsymbol{x}^t(s)\rangle=R(s)B(s)\langle\boldsymbol{X}\boldsymbol{X}^t\rangle B^t(s)R^t(s). \tag{2}$$

The beam envelope matrix in the normal mode is represented by emittances,

$$\langle\boldsymbol{X}(s)\boldsymbol{X}^t(s)\rangle=\begin{pmatrix}\varepsilon_X & 0 & 0 & 0\\ 0 & \varepsilon_X & 0 & 0\\ 0 & 0 & \varepsilon_Y & 0\\ 0 & 0 & 0 & \varepsilon_Y\end{pmatrix}. \tag{3}$$

Tune ($\mu_{XY}=2\pi\nu_{XY}$) and emittance ($\varepsilon_X=\langle|X|^2\rangle$, $\varepsilon_Y=\langle|Y|^2\rangle$) are defined in the normal coordinates (X,Y), but not in physical coordinates (x,y).

Vertical emittance is expressed by dispersion in the normal coordinate [1].

$$\varepsilon_Y\propto\oint\frac{\gamma_Y\eta_Y^2+2\alpha_Y\eta_Y\eta_Y'+\beta_Y\eta_Y'^2}{\rho^3}ds$$

To reduce the vertical emittance, x-y coupling in bending magnets should be suppressed.

2.2 Global x-y coupling correction and measurement of emittances in SuperKEKB

In SuperKEKB, x-y coupling correction has been performed by the orbit response method [2]. 6 independent closed orbit are measured by exciting 6 steering magnets in horizontal. Skew magnets are excited so as to suppress orbit leakages into vertical.

Figure 1 and 2 shows vertical orbit leakage for 6 horizontal orbit in HER and LER.

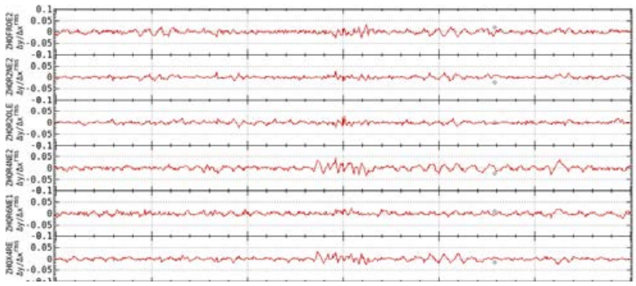

Figure 1: Vertical orbit leakage for 6 horizontal closed orbit in HER.

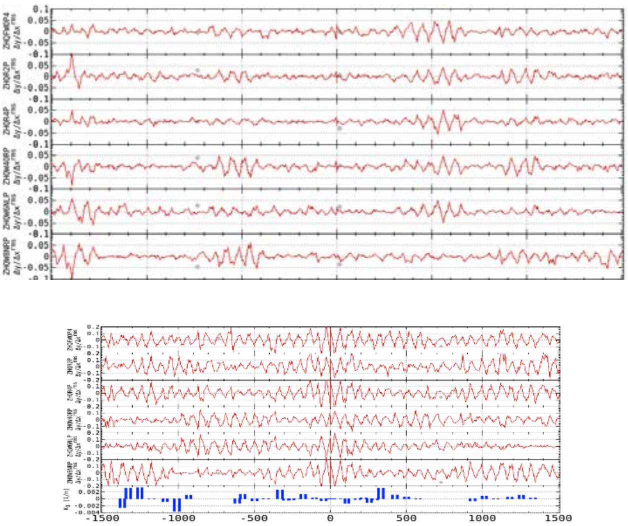

Figure 2: Vertical orbit leakage Δy/Δx for 6 horizontal closed orbit in LER. Top and bottom pictures are after and before x-y coupling correction.

Beam size is measured by X-ray monitors [3]. Vertical emittance ε_y=23 pm and 9pm were achieved for LER and HER, respectively, where horizontal emittance is ex=3nm and 5nm.

III. Local x-y coupling at IP

For e^+e^- colliders, x-y coupling at IP has a special meaning as follows.

3.1 Beam size at IP

Vertical beam size at IP is given using Eq. (3) as

$$\sigma_y^2(s) \approx \sigma_Y^2 + \sigma_X^2\left[\frac{{r_2}^2}{\beta_x^2} + {r_1}^2\right] + \left(\eta_y\sigma_\delta\right)^2 \tag{4}$$

where σ_X and σ_Y are the beam size in the normal coordinate

$$\sigma_Y^2(s) = \beta_Y(s)\varepsilon_Y \qquad \sigma_x^2(s) \approx \sigma_X^2(s) = \beta_X(s)\varepsilon_X$$

The local beam size is determined by the emittance of Y mode and leakage from X mode represented by R. The vertical beam size is defined by distribution projected into y plan. Luminosity is determined by convolution of the projected vertical beam size,

$$L = \frac{1}{4\pi}\frac{N_+N_-}{\sigma_x\sigma_y}n_bf_{rev}$$

$$\sigma_{x/y} = \sqrt{\left(\sigma_{x/y,+}^2 + \sigma_{x/y,-}^2\right)/2}$$

Figure 3 shows overlap of colliding beam distributions for finite $R_{1,2}$ or η_y of electron beam (blue). R_1 is tilt of real x-y plane, while R_2 and η_y are tilt of x'-y and y-δ(=Δp/p) plane, respectively.

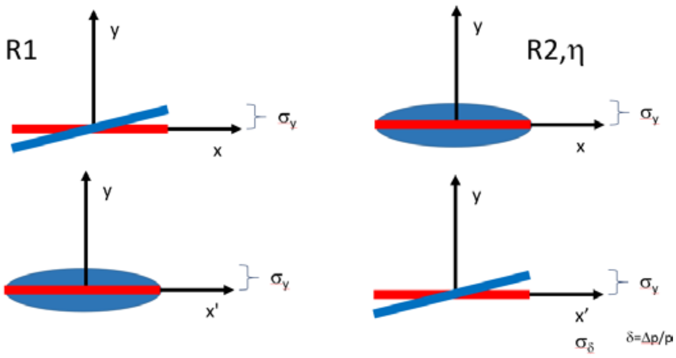

Figure 3: Schematic view of overlap of colliding beam distributions for finite $R_{1,2}$ or η_y.

Specific luminosity is index to inform the beam size at IP.

$$L_{sp} \equiv \frac{L}{n_bI_+I_-} = \frac{1}{4\pi e^2}\frac{1}{\sigma_x\sigma_yf_{rev}}$$

The beam size is measured at X-ray monitors installed at arc section. At very low current, in which beam-beam effect should be negligible, the beam size is the same as that in single beam operation without collision. In early stage of Phase-II commissioning (June, 2018), luminosity at very low bunch current (0.01mA/bunch, while the design 1.4mA/bunch) was lower than the geometrical value using the measured beam size (X-ray monitor) translated to IP.

The discrepancy of luminosity was caused by x-y coupling at IP. The luminosity coincided with that given by the beam size R_2=7mm at the very low current. X-y coupling at IP affects beam-beam performance also in high current. Emittance growth due to the beam-beam effect was enhanced by the x-y coupling.

The source of R_2 at IP can be explained by skew rotation of the final quadrupoles. Transformation with R_2 is expressed by

$$\mathcal{M}_{in/out} = \exp(\pm{:}R_2p_x^*p_y^*{:}) = \exp(\pm{:}R_2xy{:}) \tag{5}$$

Transformation containing beam-beam interaction is expressed by

$$\mathcal{M}_{out}\mathcal{M}_{bb}\mathcal{M}_{in}\,,$$

where $\mathcal{M}_{bb}$ is transfer map of the beam-beam interaction. The transfer map expressed by p_x^* and p_y^* is translated to $x/(\beta_x\beta_x^*)^{1/2}$ and $y/(\beta_y\beta_y^*)^{1/2}$ at the final quadrupole location, respectively, where $\beta_y\beta_y^*=1\text{m}^2$. It is most plausible that R_2 is induced by skew rotation of the final quadrupoles. Corrector coil with skew quadrupole field are excited to correct R_2.

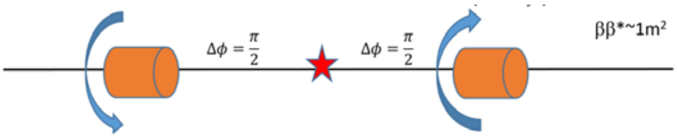

Figure 4: Schematic view of IR, IP and final quadrupole with skew rotation.

After the correction of R_2, luminosity performance in SuperKEKB was improved twice. However the luminosity performance was not sufficient for our target. Figure 5 shows specific luminosity and beam-beam tune shift estimated by luminosity after the R_2 correction. The specific luminosity decreases to $15\text{x}10^{30}$ $\text{cm}^{-2}\text{s}^{-1}/\text{mA}^2$ at $I_+I_-=0.4\text{mA}^2$. The beam-beam tune shift was 0.02, where we take lower number in the $e^{+/-}$ tune shifts, because stronger beam (e^-) experiences smaller tune shift of weaker beam with emittance growth.

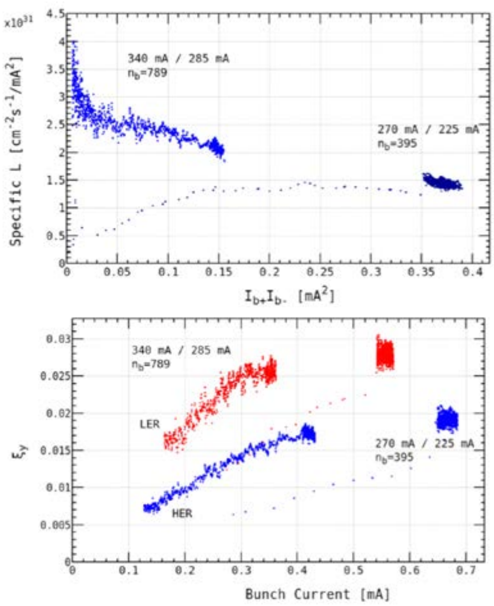

Figure 5: Achieved specific luminosity and beam-beam tune shift in Phase II commissioning.

IV. NONLINEAR ABERRATIONS AT IP

Beam-beam simulation based on the weak-strong model was executed to simulate effects of aberrations at IP. Electron beam is assumed to be strong beam with fixed Gaussian distribution, as shown in Fig.5. Positron (weak) beam is represented by macro-particles. Aberrations are introduced to positron ring (LER). Strengths of aberrations are decided so that the specific luminosity at $I_+I_-=0.4\text{mA}^2$ is $15\text{x}10^{30}$ $\text{cm}^{-2}\text{s}^{-1}/\text{mA}^2$. Figure 6 shows specific luminosity as function of bunch current product for several nonlinear aberrations.

The aberration is expressed for example as

$$\mathcal{M}_{in/out} = \exp\left(\pm{:}\,c p_x^{*2} p_y^*{:}\right) \qquad c = 8\text{ m}$$

The strengths of other aberrations are written in the figure. We understand that aberration of $cp_x^{*2}p_y^*$ term causes similar behaviour on the specific luminosity with the measurement in Fig. 5.

Figure 7 shows specific luminosity as function of bunch current product for chromatic coupling $R_i'=dR_i/d\delta$ at IP. The strengths of the chromatic coupling are normalized the same way as the nonlinear aberration. The chromatic coupling is measured by turn-by-turn monitors located near IP. R_3' and R_4' were measured to be 300m^{-1} and 20, respectively. R_1' and R_2' were hard to measure, because y at IP is very small number which is summation of y's with opposite sign at final quadrupoles. While R_3' and R_4' are given by p_y, which is large number. R_1' =12 and R_2'=3 are possible sources of the luminosity degradation at high current.

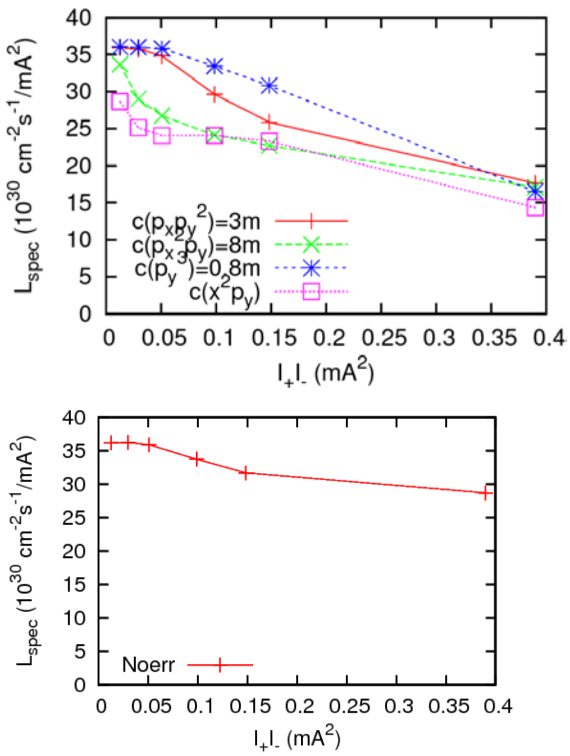

Figure 6: Specific luminosity as function of bunch current product for several nonlinear aberrations at IP. Bottom picture depicts specific luminosity without aberrations as a reference.

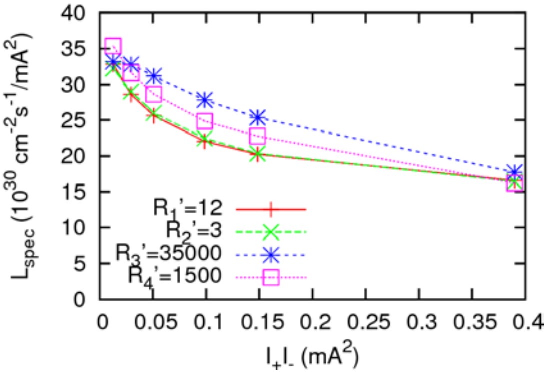

Figure 7: Specific luminosity as function of bunch current product for chromatic coupling at IP.

TABLE I
PARAMETERS FOR SUPERKEKB

Parameter		Design		Phase II	
		LER	HER	LER	HER
Bunch population	$N_{+/-}$ (10^{10})	9	6.5	4.8	4.0
Emittance	$\varepsilon_{x/y}$ (nm/pm)	3.2/8.64	4.6/13	2.1/2.1	4.6/30
Synchrotron tune	ν_s	0.0247	0.028	200/3	100/3
Beta function at IP	$\beta_{x/y}$ (mm)	32/0.27	25/0.3	0.022	0.026
Hor. Beam-beam tune shift	$\Delta\nu_{x/}$	0.0028	0.0012	0.0073	0.0025
Ver. Beam-beam tune shift	$\Delta\nu_{y/}$	0.088	0.081	0.075	0.077
Beam-beam parameter	ξ_L	0.088	0.081	0.03	0.02
Piwinski angle	$\sigma_z\theta_c/\sigma_x^*$	24.7	19.4	12.1	11.6

CONCLUSION

SuperKEKB Phase II commissioning was done March to July, 2018. Beam-beam performance was improved by correction of final quadrupole skew rotation. However the specific luminosity is limited to 15x10^{30} m^{-2}s^{-1}/mA^2 at I_+I_-=0.4mA^2. The beam-beam tune shift estimated by the luminosity is limited 0.02. Nonlinear aberration $\exp(:8p_x^{*2}p_y^*)$, chromatic coupling R$_1$' =12 ($\exp(:12x^*p_y^*\delta)$) or R$_2$'=3 m ($\exp(:12p_x^*p_y^*\delta)$ are possible candidates to recover the luminosity. We are challenging the corrections of IP aberrations in Phase-III commissioning start from March 2019. Our goal is L_{sp}=220x10^{30} cm^{-2}s^{-1}/mA^2 at I_+I_- =1.5mA^2..

ACKNOWLEDGEMENTS

The authors thank members of commissioning team of SuperKEKB.

.

REFERENCES

[1] K. Ohmi, K. Hirata, K. Oide, Phys. Rev. E49, (1994).
[2] A. Morita et al., Phys. Rev. ST-AB10, 072801 (2007).
[3] E. Mulyani, J. Flanagan, H. Ikeda, H. Fukuma, M. Tobiyama, proceedings of IPAC18, THPML074.
[4] K. Ohmi et al., Proceedings of eeFACT18 (IHEP, Beijing), TUOBB01 (2018).

Emittance Tuning for FCC-ee

T.K. Charles, European Organization for Nuclear Research (CERN), Geneva, Switzerland
School of Physics, University of Melbourne, 3010, Victoria, Australia
B. Holzer, European Organization for Nuclear Research (CERN), Geneva, Switzerland
K. Oide, European Organization for Nuclear Research (CERN), Geneva, Switzerland
KEK, Oho, Tsukuba, Ibaraki 305-0801, Japan
F. Zimmermann, European Organization for Nuclear Research (CERN), Geneva, Switzerland

***Abstract*—The 100 km Future Circular Collider e+/e- collider (FCC-ee) requires luminosities in the order of 10^{35} cm^{-2} s^{-1} and very low emittances of 0.27 nm rad for the horizontal plane and 1 pm rad in the vertical. In order to reach these requirements, extreme focusing of the beam is needed in the interaction regions, with a vertical beta function of 0.8 mm at the IP. These challenges make the FCC-ee design particularly susceptible to misalignment and field errors. This proceeding summarizes the optics and orbit correction methods that were employed in order to control the coupling and vertical dispersion, in order to minimize the vertical emittance. Thousands of misalignment and error seeds were introduced in MADx simulations and a comprehensive correction strategy, which includes macros based upon Dispersion Free Steering (DFS), linear coupling correction based on Resonant Driving Terms (RDTs) and Singular Value Decomposition (SVD), was implemented.**

***Keywords*—emittance tuning, optics correction, colliders, Future Circular Collider**

I. Introduction

THE e+/e- collider of the Future Circular Collider (FCC) will have four energies of operation ranging from the Z-pole (45.6 GeV) to the ttbar production threshold (182.5 GeV) [1]. A summary of some key parameters can be found in Table 1 with the details outlines in the recently published Conceptual Design Report [2].

Table I
Baseline beam parameters of the four operational energies for FCCee [2].

Parameters	Z	W	H	ttbar
Beam Energy [GeV]	45.6	80	120	182.5
ε_x [nm rad]	0.27	0.28	0.63	1.46
ε_y [pm rad]	1.0	1.7	1.3	2.9
Beam current [mA]	1390	147	29	5.4
β_x* [m]	0.15	0.2	0.3	1
β_y* [mm]	0.8	1	1	1.6
Luminosity [10^{34} cm^{-2} s^{-1}]	>200	>25	>7	>1.4

In order to reach these high luminosities (Table 1), strong focusing is required in the interaction region. For the 182.5 GeV ttbar operation, a vertical beta function of 1.7 mm is required. Within the final focus region, a maximum beta function in the horizontal and vertical planes are, $\beta_{x,\,max}$ = 1625.1 m and $\beta_{y,\,max}$ = 6958.6 m (see Fig. 1). The large beta values near the IP and the strong sextupoles required for chromaticity correction, make this machine very sensitive to magnet misalignments and field errors.

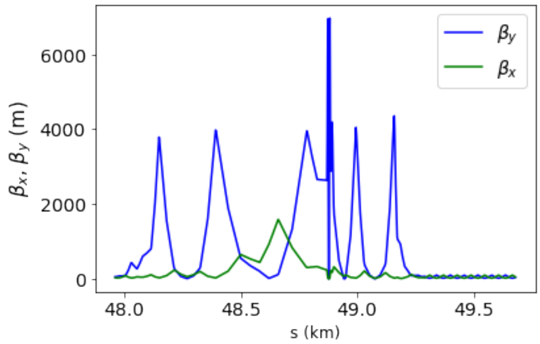

Fig. 1. Beta functions near one of the IPs for the 182.5 GeV lattice, showing the maximum values of the beta functions, $\beta_{x,\,max}$ = 1625.1 m and $\beta_{y,\,max}$ = 6958.6 m.

II. Correction Methods

Reducing the *x-y* coupling and residual vertical dispersion over the ring is critical to minimizing the vertical emittance and reaching high luminosity. To do this, a number of correction methods are utilised, that are based upon Dispersion Free Steering (DFS), coupling correction through consideration of the Resonant Driving Terms (RDTs) and beta-beat correction via a response matrix Singular Value Decomposition (SVD) approach.

To perform the correction, corrector magnets and Beam Position Monitors (BPMs) are installed at every quadrupole magnet around the 100 km ring, tallying 1598 in the horizontal plane and 1596 in the vertical plane. One skew quadrupole and one trim quadrupole are installed at every sextupole magnet for coupling correction and beta beat correction.

Coupling between the horizontal and vertical planes need to be limited to below 0.1 %, not only in order to ensure the equilibrium vertical emittance is small, but also in order to reduced beam-beam blow up thought to be enlarged when the coupling ratio is greater than 0.1 % [3]. The coupling can be quantified with the two RDTs, f_{1001} and f_{1010}.

A response matrix, **M** of the RDTs and vertical dispersion, D_y, can be calculated as a response to a skew quadrupole field, $\vec{J}$. The system, which can be inverted via SVD, is [4]:

$$\begin{pmatrix} \vec{f}_{1001} \\ \vec{f}_{1010} \\ D_y \end{pmatrix} = -\mathbf{M}\,\vec{J} \tag{1}$$

where $\vec{f}_{1001}$ and $\vec{f}_{1010}$ are the complex coupling RDTs computed at the BPM locations.

A correction strategy was devised and implemented in order to minimize the final vertical emittance. The first step of this strategy is to set all of the sextupole strengths to zero. This is because the initial magnet misalignment, roll angles and field errors are likely to direct the beam off centre through the sextupole magnets, which has the same effect as a skew quadrupole would in its place. This results in a vertical displacement of the closed orbit with respect to the sextupole's magnetic center, and can generate vertical emittance growth through the introduction of vertical dispersion. Therefore the correction strategy begins with turning the sextupoles off.

After an initial close orbit correction, and a series of coupling, beta beat corrections and tune matching, the sextupoles are set to 10 % of their design value. The correction algorithm continues, increasing the sextupole strength by 10 % at a time. Once at 100 % of the sextpuole's design value, additional coupling and dispersion correction are employed to ensure low vertical emittance can be achieved.

All of the corrections were applied in MADx [5], which called macros written in python. The beam energy was set to 1 GeV, the RF turned off, and energy loss from synchrotron radiation was not included to begin with. This allows for faster computation and is considered valid for a fully tapered machine [6]. At the final stage of the simulations, synchrotron radiation is turned on for the emittance calculation, which is based upon the Chao formalism for equilibrium emittance [7].

A. *Correction Strategy*

The following correction strategy was implemented. Throughout the correction algorithm the tunes, orbit and maximum value of the beta functions, are constantly monitored and when these parameters are too high or low the required correction scheme is called.

1) Introduce BPMs and corrector magnets at every quadrupole, and introduce skew and trim quadrupoles at every sextupole. Misalignment and roll errors are then applied to magnets around the ring, distributed via a Gaussian distribution truncated at 2.5 sigma. Several simulations with different random seeds were used.
2) Sextupole magnets were turned off, and an orbit correction performed with MICADO in MADX.
3) Coupling correction was performed, followed by rematching of the tune, followed by beat-beat correction.
4) DFS (D_y correction) was then performed followed by coupling correction (which is needed due to the change in the corrector strengths brought about by DFS). These two correction techniques were performed one after another for a set number of iterations.
5) Sextupole magnets are then set to 10% of their design strength. And the following corrections applied:
    a) orbit correction
    b) coupling correction
    c) tune matching
    d) beta beat correction
    e) coupling and vertical dispersion correction
    f) increase sextupole strengths by 10 % , and repeat Step 5 until 100 % of design sextupole strength is reached.
6) If necessary, the final correction of coupling and beat-beat correction was applied to ensure low vertical emittance.

III. Corrected Lattices

In this section we compare the results for three situations – the errors introduced by Tables 2, 3, and 4. For all cases the horizontal and vertical misalignments and roll angles for arc quads, sextupoles and dipoles was 100 µm and µrad. All misalignment and roll errors were applied to magnets around the ring, distributed via a Gaussian distribution truncated at 2.5 sigma.

Table 2

Misalignment and roll errors introduced into the lattice before correction applied. The results are summarized in Fig.1.

Magnet element	σ_x (µm)	σ_y (µm)	σ_θ (µrad)
Arc quadrupoles	100	100	100
IP quadrupoles	50	50	50
Sextupoles	100	100	100
Dipoles	100	100	100

After applying the correction scheme outlined in the previous section, the final emittances can be reduced to an acceptable level. Figure 1 shows the distribution of horizontal and vertical emittances for 500 random seeds, when the IP quadrulpoles had an rms offset in *x* and *y* of 50 µm and rms roll angle of 50 µrad (see Table 2). The mean final vertical emittance achieved was 0.102 pm rad, and the mean final horizontal emittance was 2.49 nm rad. The ratio of the emittances (or the coupling ratio), $\varepsilon_y/\varepsilon_x$ = 0.004 %.

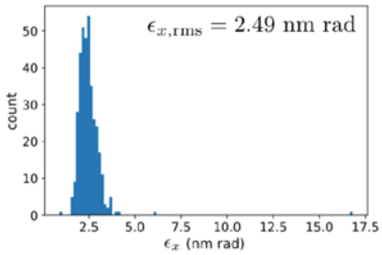

(a)

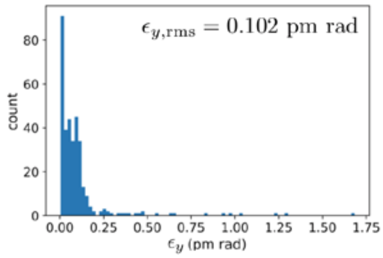

(b)

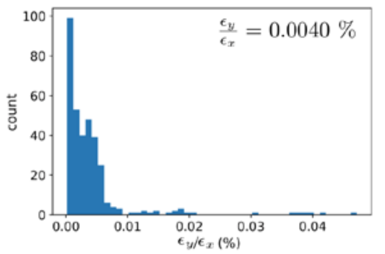

(c)

Fig. 2. Distribution of (a) horizontal emittance, (b) vertical emittance, and (c) coupling ratio of the corrected lattices. The errors that were introduced are summarized in Table 2, IP quadrupoles misaligned with $\sigma_x = \sigma_y = 50$ µm and $\sigma_\theta = 50$ µrad.

Figure 2 shows the distribution of horizontal and vertical emittances, when the IP quadrulpoles tolerance was relaxed to 100 µm and 100 µrad (see Table 3). In this scenario, the mean final vertical emittance achieved was 0.202 pm rad, and the mean final horizontal emittance was 2.47 nm rad. The ratio of the emittances (or the coupling ratio), $\varepsilon_y / \varepsilon_x = 0.005$ %.

TABLE 2
MISALIGNMENT AND ROLL ERRORS INTRODUCED INTO THE LATTICE BEFORE CORRECTION APPLIED. THE RESULTS ARE SUMMARIZED IN FIG.2.

Magnet element	σ_x (µm)	σ_y (µm)	σ_θ (µrad)
Arc quadrupoles	100	100	100
IP quadrupoles	100	100	100
Sextupoles	100	100	100
Dipoles	100	100	100

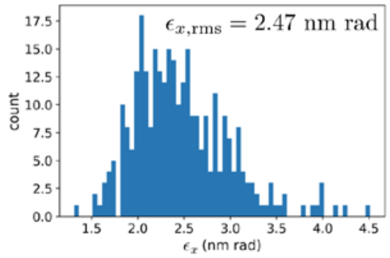

(a)

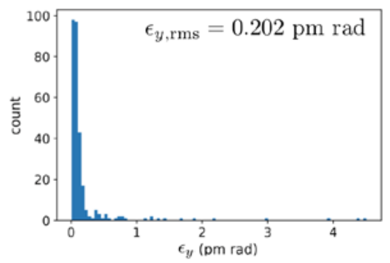

(b)

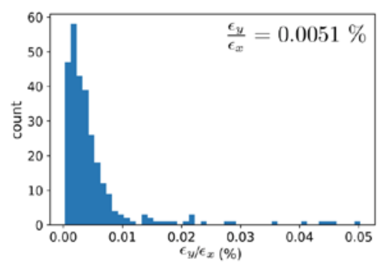

(c)

Fig. 3. Distribution of (a) horizontal emittance, (b) vertical emittance, and (c) coupling ratio of the corrected lattices. The errors that were introduced are summarized in Table 2, IP quadrupoles misaligned with $\sigma_x = \sigma_y = 100$ µm and $\sigma_\theta = 100$ µrad.

Figure 3 shows the distribution of horizontal and vertical emittances, when BPM errors were introduced. The offset of the BPMs were introduced relative to the adjacent quadrupole, with an rms value 20 µm in both in *x* and *y* planes, and with the roll angle of 1000 µrad (see Table 4). With this inclusion of BPM errors, the mean final vertical emittance achieved was 0.431 pm rad, and the mean final horizontal emittance was 3.50 nm rad. The ratio of the emittances (or the coupling ratio), $\varepsilon_y / \varepsilon_x = 0.014$ %.

TABLE 3
MISALIGNMENT AND ROLL ERRORS INTRODUCED INTO THE LATTICE. THE CORRECTED LATTICE RESULTS CORRESPONDING TO THESE ERRORS ARE SUMMARIZED IN FIG. 3. BPM ERRORS PLACED ARE RELATIVE TO QUADRUPOLES.

Magnet element	σ_x (µm)	σ_y (µm)	σ_θ (µrad)
Arc quadrupoles	100	100	100
IP quadrupoles	100	100	100
Sextupoles	100	100	100
Dipoles	100	100	100
BPM	20	20	1000

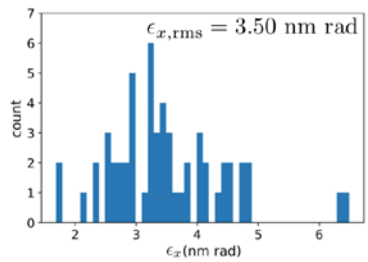

(a)

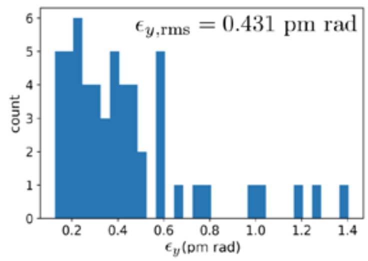

(b)

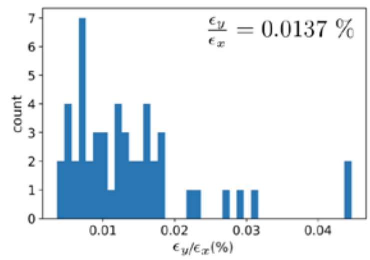

(c)

Fig. 4. Distribution of (a) horizontal emittance, (b) vertical emittance, and (c) coupling ratio of the corrected lattices. The errors that were introduced are summarized in Table 4, which include BPM misalignments distribution with $\sigma_x = \sigma_y = 20$ µm and $\sigma_\theta = 1000$ µrad.

CONCLUSION

FCC-ee presents unique challenges when it comes to emittance tuning. The small vertical emittance and the low coupling ratio makes the FCC-ee design particularly susceptible to misalignment and field errors. This summary outlines the correction strategy approach, which includes orbit corrections, Dispersion Free Steering, linear coupling correction based on Resonant Driving Terms and beta-beat correction using response matrices. For misalignments of 100 µm in x and y and a roll angle error of 100 μrad of all magnet types, and with relative BPM errors of 20 μm and 1000 μrad, the final vertical emittance achieved was 0.202 pm rad, and a coupling ratio of $\varepsilon_y / \varepsilon_x$ = 0.01 %.

REFERENCES

[1] K. Oide, et al, "Design of beam optics for the future circular collider e+e- collider rings," Phys. Rev. AB, **19**, 111005, 2016.

[2] Abada, A., et al. "Conceptual Design Report, Vol. **2**: The Lepton Collider (FCC-ee)", Eur. Phys. J. Spec. Top. (2019) 228: 261. https://doi.org/10.1140/epjst/e2019-900045-4

[3] K. Oide, "Optics Choices for High Luminosity IR Including Crab Waist Scheme" eeFACT 2018, Hong Kong

[4] A. Franchi, L. Farvacque, J. Chavanne, F. Ewald, B. Nash, K. Scheidt, and R. Tomás, "Vertical emittance reduction and preservation in electron storage rings via resonance driving terms correction," Phys. Rev. ST AB, **14**, 034002, 2011.

[5] "Methodical Accelerator Design Manual," https://madx.cern.ch

[6] B. Haerer, A. Doblhammer, and B. J. Holzer, "Tapering Options and Emittance Fine Tuning for the FCC-ee Collider", in *Proc. 7th Int. Particle Accelerator Conf. (IPAC'16)*, Busan, Korea, May 2016, pp. 3767-3770. doi:10.18429/JACoW-IPAC2016-THPOR003

[7] A. Chao, "Evaluation of Beam Distribution Parameters in an Electron Storage Ring," J.Appl.Phys., **50**, 595, pp. SLAC–PUB–2143, 1979.

Dynamic aperture in low emittance storage rings

Alexander Papash*
Karlsruhe Institute of Technology, Germany

***Abstract*— Nonlinearities arising from the chromatic perturbations and sextupoles in circular accelerators limit stable area of beam oscillations in light sources and lead to the reduction of beam life time. The dynamic aperture problem is one of the most challenging research topics for accelerator physicists. New generation diffraction limited light sources designed for ultimate small beam emittance are based on multi-bend achromat lattice with strong focusing. High chromaticity accompanied by small dispersion (to ensure ultra-low beam emittance) requires strong sextupoles. As a consequence the particles might fall into unstable phase space even at small deviations off reference orbit. Optimization methods of lattice de sign and dynamic aperture required to ensure efficient injection and long Touschek lifetime, are discussed here.

***Keywords*—accelerator, low emittance storage ring, dynamic aperture, non-linear beam dynamics, sextupoles**

I. INTRODUCTION. LINEAR EQUATIONS OF MOTION IN CIRCULAR ACCELERATORS

Concept of dynamic aperture was widely described, in particular, in original publications, Proceedings of CERN Accelerator Schools, Accelerator Conferences [**1,2,3,4**...]. "Original incentive to study the stability of the motion in non-linear dynamic systems has been prompted by development of Celestial Mechanics in XIX century to describe the orbital motion of Planets" [**1**]. Let's us remind some basics of particle motion. Trajectory of charged particles in a storage ring with periodic magnetic structure is described by Lorentz equation [**2**]

$$m\vec{R}'' = -\frac{e}{c}\left[\vec{R}' \times \vec{B}\right] \qquad (1)$$

Particles are focused by quadrupole lenses. We simplify the problem and neglect focusing by gradient field of bends and by magnet edges. Beam focusing in transverse direction is defined by quadrupole strength which is energy independent parameter. Strength is essentially the lens gradient $\frac{\partial B_z}{\partial x} = \frac{\partial B_x}{\partial z}$ normalized by magnetic rigidity

$$k_x = -k_z = \frac{1}{B_0 \cdot \rho_0}\left(\frac{\partial B_z}{\partial x}\right) \qquad (2)$$

At high energies relativistic factor $\gamma \gg 1$. Thus, beam energy and magnetic rigidity are equivalent

$$pc = B_0 \qquad (3)$$

Ring lattice is periodic structure and composed of N cells each of length L. Ring circumference is C=N·L. Restoring forces

$$K_{x,z}(s+L) = K_{x,z}(s) \qquad (4)$$

are periodic with same period L. Particle oscillations in transverse to the beam motion direction are fast with respect to the slow synchrotron oscillations of particle energy and phase in longitudinal direction (along the trajectory of motion). Thus, equations of motion might be split between transverse 4D phase space and longitudinal synchrotron 2D phase space [**3**]. Applying conditions of paraxial beam

- horizontal deviation of particle from reference orbit $X = R - R_0 \ll R_0$ and vertical deviation
- from median plane $z \ll R_0$ are small, angular deviations in radial $x' = dx/ds \ll 1$ and axial $z' = dz/ds \ll 1$ planes are small,

we neglect high order terms and derive linear HILL equations of harmonic oscillations in radial (x) and axial (z) planes

$$\frac{d^2x(s)}{ds^2} + K_x(s)x(s) = \frac{1}{\rho_0(s)}\frac{\delta p}{p_0} \qquad (5a)$$

$$\frac{d^2z(s)}{ds^2} + k_z(s)z(s) = 0 \qquad (5b)$$

If periodic restoring forces acting on on-momentum particle of reference energy $\boldsymbol{p_0 c}$ are perfectly linear, stable particle oscillations are described by second order homogeneous differential equations (quasi-harmonic oscillator) with periodic restoring force [**4**]. Radial focusing term in bending magnets $\frac{1}{\rho_0^2}$ should be taken into account [**5**]

$$K_x(s) = \frac{1}{\rho_0^2(s)} - k_x(s) \qquad (6)$$

Off-momentum particles are shifted from reference orbit in horizontal plane (dispersion plane of bending) by

$$x_D = D \cdot \left(\frac{\Delta p}{p_0}\right) = D \cdot \delta \qquad (7)$$

and off-momentum particles motion is described by linear equation for dispersion (D)

$$\frac{d^2D(s)}{ds^2} + K_x(s)D(s) = \frac{1}{\rho_0(s)} \qquad (8)$$

Solution of linear differentiation equation is LINEAR combination of initial coordinates and momentum and might be written in matrix form [**6**]

$$\vec{Y}(s) = M(s/s_0) \cdot \vec{Y}(s_0) \qquad (9)$$

where $\vec{Y}(s_0) = (x_0, p_{x0}, z_0, p_{z0}, \varphi_0, \delta)$ is vector of initial coordinates and momentums in 6D phase space. Transfer matrix

* alexander.papash@kit.edu

for full revolution must repeat itself in order for motion to be stable

$$M(s+L) = M(s+N\cdot L) = M(s) \quad (10)$$

Necessary and sufficient condition of stable motion – transfer matrix $[M]^{n\cdot N}$ should be bounded at any $n \to \infty$. Solutions of linear equations are real part of periodic quasi-harmonic function of orbit trajectory [**7**]. "Y" stay here for horizontal "x" either vertical "z" coordinate

$$y(s) = Re\left(\sqrt{\epsilon\beta_y} exp\left(\pm i\mu_y\right)\right) = \sqrt{\epsilon\beta_y(s)} cos\left(\mu_y(s)\right) \quad (11)$$

$$p_y\,(s) = -\sqrt{\frac{\epsilon}{\beta_y(s)}}\cdot\left[sin\left(\mu_y(s)\right) - \frac{\beta_y'(s)}{2} cos\left(\mu_y(s)\right)\right] \quad (12)$$

Betatron function has periodicity of lattice cell $\beta_y(s+L) = \beta_y(s)$ and there is no limit on amplitude of oscillations in linear approximation. Phase advance (μ) and Trace of transfer matrix (M) related as

$$cos(\mu) = \frac{1}{2}Tr(M) = \frac{1}{2}(m_{11} + m_{22}) \quad (13)$$

Betatron oscillations are bounded if phase advance (μ) has REAL values, i.e. $cos(\mu) < 1$. Main condition of stable motion in linear approximation is [**8**]

$$|Tr(M)| \leq 2 \quad (14)$$

Integrable motion of particles in accelerators and rings is stable. Deviations in all 3D planes with respect to central trajectory are finite and limited. Particles oscillate around reference orbit while asymptotic unbounded growth of particle coordinates represents unstable behavior. In linear conservative systems, where strengths are dependent on particle coordinate but not on velocity, the energy conservation law is obeyed and transfer matrix satisfies symplectic conditions [**9**]

$$M^T\cdot S\cdot M = S \quad (15)$$

Symplectic conditions are realized "if" and "when" determinant of transfer matrix is unit

$$det\ M = m_{11}m_{22} - m_{12}m_{21} \quad (16)$$

Equations of harmonic oscillations might be derived also from the unperturbed Hamiltonian function (H_1) where second order terms $(x\cdot\delta)$ and (δ^2) etc. are omitted

$$H_1 = \frac{p_x^2 + p_z^2}{2} + \frac{K(s)}{2}(x^2 - z^2) \quad (17)$$

First term of linear Hamiltonian is kinetic energy while second term is potential energy proportional to quadrupole strength. Providing there is no explicit dependence on time $\frac{\partial H}{\partial t} = 0$ the Hamiltonian of system as function of canonical variables $\dot{q}_k = \frac{\partial H}{\partial p_k}$ and $\dot{p}_k = -\frac{\partial H}{\partial q_k}$ is integral of motion and describes energy conservation law [**10**]

$$dH(q,p,t) = \frac{\partial H}{\partial t} + \sum_k\left\{\frac{\partial H}{\partial q_k}\dot{q} + \frac{\partial H}{\partial p_k}\dot{p}\right\} = 0 \quad (18)$$

Applying Lie algebra formalism [**11**] one can express transfer matrix of an element of length L in symplectic form where Lie operator acts on particle as Poisson brackets

$$M_{s0\to s1} = exp\!:\left(:-\int_{s0}^{s1} H(s)ds\right) = exp(:-LH:) \quad (19)$$

Canonical transformations with different types of generating functions (F) [**12**] are applied in order to eliminating explicit dependence of Hamiltonian on time and build new Integral of motion with $\frac{\partial H\prime}{\partial t} = 0$

$$dF = \sum_k(p_k\,dq_k - P_k dQ_k) + (H - H')dt \quad (20)$$

II. NONLINEAR BEAM DYNAMICS

Introduction of non-linear elements into ring lattice will cause oscillations about the closed reference orbit to grow in amplitude for particular betatron tunes [**13**]. High order terms of magnetic fields cause perturbations of linear lattice and leads to restriction on beam stability:

- resonances
- dependence of betatron tunes on beam energy offset (chromatic effects)
- amplitude dependent tune shifts (ADSTS) etc.

Canonical perturbation theory is applied to deal with non-linear beam dynamics away of resonances [**14**]. In particular, to describe mechanism of betatron tunes shifts with momentum deviation (linear, quadratic, cubic chromaticity terms), mechanism of ADTS, resonance conditions, resonance width, stopband.

Non-linear Hamiltonian in 2D transverse phase space includes contributions from bending magnet, quadrupole, sextupole and octupole and might be written in a form [**15,16,17,18**]

$$H = \overbrace{\frac{p_x^2 + p_z^2}{2(1+\delta)}}^{kinematic} - \overbrace{\frac{x}{\rho}\delta + \frac{x^2}{2\rho^2}}^{bend} + \overbrace{\frac{k_1}{2}}^{quad}(x^2 - z^2) \; +$$

$$\overbrace{\frac{k_2}{3}}^{sextupole}(x^3 - 3xz^2) + \overbrace{\frac{k_3}{4}}^{octupole}(x^4 - 6x^2y^2 + y^4) \quad (21)$$

Quadrupole k_1, sextupole k_2 and octupole k_3 strengths essentially are first, second and third order terms of Tailor expansion of magnetic field distribution normalized by magnetic rigidity

$$k_1 = \frac{1}{B_0\cdot\rho_0}\left(\frac{\partial B_z}{\partial x}\right) \quad (22a)$$

$$k_2 = \frac{1}{B\cdot\rho}\left(\frac{\partial^2 B_z}{\partial x^2}\right) \quad (22b)$$

$$k_3 = \frac{1}{B\cdot\rho}\left(\frac{\partial^3 B_z}{\partial x^3}\right) \quad (22c)$$

Hamiltonian of a ring includes contributions from each magnetic element and after canonical transformations [**8,19**] might be represented in Action-Angle variables

$(J_x, \psi_x, J_z, \psi_z)$ by combination of linear part and NON-linear contributions (kicks) of quads (H_2) , sextupoles (H_3) and higher order elements

$$H(\psi_x, J_x, \psi_z, J_z, s) \propto Q_x J_x + Q_z J_z + \int [H_2(s) + H_3(s)] \quad (23)$$

Linear part is a product of betatron tunes $(Q_{x,z})$ and Courant Snyder Invariants $(J_{x,z})$

$$2J_x = \varepsilon_x = \gamma x^2 + 2\alpha x x' + \beta x'^2 \quad (24)$$

Phase space plot of beam motion in Action-Angle variables (J, Ψ) with sextupole term (H_3) is shown in Fig. 1 [**12**]. Unperturbed motion $(H_3 = 0)$ would be represented by circle of radius (J). Non-linear Hamiltonian term is proportional to sextupole strength K_S and depends on phase advance as (3ψ)

$$H_{SXT} \sim \frac{J^{3/2}\beta^{3/2}(s)}{3!} K_S \cos^3\psi \rightarrow K_S \cos 3\psi \quad (25)$$

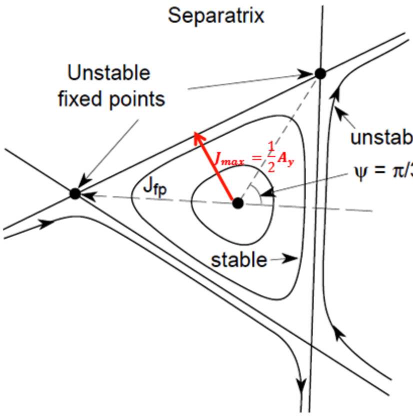

Fig. 1. Phase space plot in Action-Angle coordinates (J, Ψ) with non-linear sextupole term (H_3). Unperturbed motion would be represented by circle of radius (J). Picture taken from [**12**].

Non-linear Hamiltonian for octupole term is proportional to octupole strength K_{OCT} and depends on phase advance as (4ψ) [**20**]

$$H_{OCT} \sim \frac{(2J\beta_y(s))^{4/2}}{4!} K_{OCT} \cos^4\psi \rightarrow K_{OCT} \cos 4 \quad (26)$$

Amplitude of stable oscillations is limited and phase space is distorted at large amplitudes. One stable fixed point in the center corresponds to the reference orbit. Three unstable fixed points are connected by separatrix and define ring Acceptance $A_{x,z}$ – maximum value of action variable $(J_{x,z}^{max})$ where motion is still stable. Separatrix divide stable area around reference orbit and area of unstable motion represented by hyperbolic curves with asymptotic behavior. Dynamic aperture is a cross-section of ring Acceptance at certain position (s) in a ring

$$DA_{x,z}(s) = \sqrt{2J_{x,z}^{max} \cdot \beta_{x,z}(s)} = \sqrt{A_{x,z} \cdot \beta_{x,z}(s)} \quad (27)$$

At very large amplitude of particle oscillations islands of stability are present but could not be count for dynamic aperture because ring acceptance is an area of closed curves around reference orbit while there are open asymptotic unstable curves in phase space between region of main stability and closed stability islands. Analytical expressions have been derived for single magnetic elements in a ring. Sinlge sextupole of length (L_S) and integrated strength $(K_S \cdot L_S)$ located at position (s_1) limits Dynamic Aperture at position (s) according to the formula

$$DA_x^{sxt}(s) = \sqrt{2J_{max}\,\beta_x(s)} = \frac{\sqrt{2\beta_x(s)}}{\sqrt{3}\,\beta_x(s_1)^{3/2}}\left(\frac{1}{|K_S L_S}\right) \quad (28)$$

Sinlge octupole of integrated strength $(K_{OCT} \cdot L_{OCT})$, located at position (s_2), limits Dynamic Aperture at position (s)

$$DA_x^{oct}(s) = \sqrt{2J_{max}\,\beta_x(s)} = \frac{\sqrt{\beta_x(s)}}{\beta_x(s_2)}\sqrt{\frac{1}{|K_{OCT}|L_{OCT}}} \quad (29)$$

Dynamic aperture of single sextupole in axial plane is maximum at reference orbit (x=0) and smoothly reduced to zero at maximum horizontal deviation of particle $DA_x^{sxt}(s)$

$$DA_z^{sxt}(s) = \sqrt{\frac{\beta_z(s_1)}{\beta_x(s_1)}(DA_x^2 - x^2)} \quad (30)$$

General formula for Dynamic aperture limited by single multipole $(2m)$ lens, where m>3, is

$$DA_x^{2m}(s) = \sqrt{2\beta_x(s)}\left(\frac{1}{m\beta_x^m(s_{2m})}\right)^{\frac{(m-2)}{2}}\left(\frac{1}{|K_{m-1}|L}\right)^{\frac{1}{(m-2)}} \quad (31)$$

One can see that Dynamic Aperture is inversely proportional to integrated sextupole strength, to square root of integrated octupole strength etc. Also high value of horizontal $\beta_x(s)$ function at position of injection septum opens Dynamic Aperture and benefits injection efficiency. Same concerns vertical $\beta_y(s)$ function if injection is realized in axial plane. High value of dispersion at location of lens reduces sextupole strength and helps to open dynamic aperture. Dispersion bumps are applied at ESRF-2 to limit sextupole strength [22].

Small value of betatron function at location of sextupole might, in theory, improve dynamic aperture because DA opens as $\beta_x(s_1)^{-3/2}$ while increasing of sextupole strength to compensate reduction of betatron function is proportional only to $\beta_x(s_1)$. One should take into account that at smaller beta higher sextupole strength is required and benefit of small betatron function at lens location is limited.

If non-linear elements are located in a ring independently the dynamic aperture shrinks because it is inversely proportional to number of sextupoles/octupoles etc.

$$\frac{1}{DA_{total}} = \sum_i^{N_{SXT}}\left(\frac{1}{DA_{SXT}}\right) + \sum_i^{M_{OCT}}\left(\frac{1}{DA_{OCT}}\right) \sim \frac{N_{SXT}}{DA_{SXT}} + \frac{N_{OCT}}{DA_{OCT}} \quad (32)$$

Natural emittance in high energy electron storage rings is defined by equilibrium between synchrotron damping and quantum fluctuations. Emittance is proportional to fifth synchrotron integral I_5 and inversely proportional to second synchrotron radiation integral I_2 and damping partition number j_x [3]

$$\epsilon_{nat} = C_q \gamma^2 \frac{I_5}{j_x I_2} \quad (33)$$

Constant C_q equal to $C_q \approx 3{,}832 \cdot 10^{-13}\, m$. The Fifth Synchrotron Radiation integral essentially is dispersion invariant [23]

$$H_x(s) = \gamma \cdot D(s)^2 + 2\alpha_x \cdot D(s) \cdot D(s)' + \beta_x D'(s)^2 \quad (34)$$

integrated along ring circumference

$$I_5 = \oint \frac{H_x(s)}{|\rho|^3} ds \quad (35)$$

In approximation of small phase advance between two sextupole one can estimate stable area in phase space for ultra-low emittance synchrotron light sources and derive some kind of scaling "law" [24]

$$DA_x^{sxt}(s) \sim \frac{\sqrt{\epsilon_x^{nat}}}{|\xi_{cell}|} \sim \frac{D_x^{max}}{|\xi_{cell}|} \quad (36)$$

and for vertical plane

$$DA_z^{sxt}(s) \sim \frac{DA_x}{|\xi_{cell}|} \sqrt{\frac{\beta_z(s)}{\beta_x(s)}} \quad (37)$$

Dynamic aperture is proportional to Dispersion function and inversely proportional to chromaticity per cell. In ultra-low emittance ($\epsilon_{nat} \leq 100\ pm$) electron storage rings the high natural chromaticity due to strong lattice and reduced dispersion, required to keep small emittance, would lead to unacceptable low level of Dynamic Aperture, if some special measures will not be taken. Ring lattice of 4th generation Diffraction Limited Light Sources (DLLS) must include special features to provide self-compensation of sextupole aberrations in order to keep dynamic aperture reasonable large.

III. RESONANCE DRIVING TERMS

The concept of resonance Driving Terms is successfully applied when effect of nonlinear components depends on its position – special phase and amplitude relations are introduced to cancel or limit high order aberrations [8,19,25,26]. Non-linear forces of magnetic elements are represented by kicks in transverse momentum while particle position is fixed during kick Thin lens approximation for high order components of magnetic fields is applied.

Contributions of high order components into symplectic form of ring Hamiltonian are composed from individual Hamiltonians of each quadrupole H_{2m}, sextupole H_{3n} etc. and might be approximated by a Sum of different modes – Resonance Driving Terms (RDT)

$$\int [H_2(s) + H_3(s)]\, ds = h_3 \propto \sum h_{jklmp} \quad (38)$$

Hamiltonian coefficients h_{jklm} contain the contribution from all the multipoles of order $(n = j + k + l + m)$ where $j, k, l, m, p = 0,1,2,3$. Even sum $(j + k)$ corresponds to normal multipoles (B_n) while odd sum $(l + m)$ - to skew multipoles (A_n) of magnetic field distribution. Driving terms are derivatives of Lie operator over action variables

$$h_{jklmp} = \frac{\partial h_3}{\partial J_{x,y}} \quad (39)$$

Ten first order Hamiltonian modes and their complex conjugates (*) are linear and proportional to the first order of integrated sextupole strength $(K_S L_S)$

$$h_{jklmp} = -h^*_{jklmp} = \sum_n^{N_{SXT}} (K_S \cdot L_S)_n \beta_{xn}^{\frac{j+k}{2}} \cdot \beta_{yn}^{\frac{l+m}{2}} \cdot D_n^p e^{i(j-k)\mu_{xn} + i(l-m)\mu_{yn}} - \left[\sum_n^{M_{QUAD}} (K_Q \cdot L_Q)_n \beta_{xn}^{\frac{j+k}{2}} \cdot \beta_{yn}^{\frac{l+m}{2}} \cdot \quad e^{i(j-k)\mu_{xn} + i(l-m)\mu_{yn}} \right]_{p \neq 0} \quad (40)$$

First order Resonance Driving Term and their complex conjugative (*) is a SUM of integrated strengths of N_{SXT} sextupoles and M_{QUAD} quadrupoles with scaling factors ("lever of arm") over different frequencies multiple to betatron phase advance μ_{xn}, μ_{zn} at element location.

- quadrupoles at dispersive sections $(D \neq 0)$ contribute to chromatic driving modes of Hamiltonian $(p \neq 0)$,
- quads in achromatic sections $(D = D' = 0)$ do not contribute to RDT (in theory),
- sextupoles contribute to both chromatic RDT $(p \neq 0)$ in dispersive sections $(D \neq 0)$ and geometric RDT$(p = 0)$ in achromatic sections $(D = D' = 0)$
- chromatic sextupoles strength is fixed to compensate natural negative chromaticity
- additional harmonic sextupoles in achromatic sections compensate shrinking of stable oscillations are (reduction of Dynamic Aperture) due to main chromatic sextupoles
- Driving modes ideally should be SUPPRESSED either CANCELLED because they are the source of ALL the resonances considering long term behavior by multiple repetition of the lattice structure [27,28]

$$\left| h^{\infty}_{jklmp} \right| = \frac{|h_{jklmp}|}{2 sin\{\pi[(j-k)Q_x^{cell} + (l-m)Q_y^{cell}]\}} \quad (41)$$

Two real terms h_{11001} and h_{00111} driving horizontal (j=k) and vertical (l=m) linear chromaticities $\xi^{(1)}_{x,y}$ are independent on phase advance μ

TABLE I
FIRST ORDER RESONANCE DRIVING TERMS AND THEIR EFFECT

N	Linear Driving terms	Effect	Comments	Phase dependence	
1	$h_{11001} \quad (CrX\_lin)$	$\partial Q_x / \partial\delta$	Linear Chromaticity (hor) $\xi_x^{(1)}$		chromatic
2	$h_{00111} \quad (CrY\_lin)$	$\partial Q_y / \partial\delta$	Linear Chromaticity (vert) $\xi_y^{(1)}$		chromatic
3	$h_{20001} = -h^*_{02001}$	$2Q_x \pm Q_s$	parametric half-integer resonance synchro-betatron coupling	$e^{i\cdot 2\mu_x}$	chromatic
4	$h_{00201} = -h^*_{00021}$	$2Q_y \pm Q_s$	parametric half-integer resonance synchro-betatron coupling	$e^{i\cdot 2\mu_y}$	chromatic
5	$h_{10002} = -h^*_{01002}$	$\partial D / \partial\delta$	Second order dispersion $D^{(1)} \equiv \partial D / \partial\delta$	$e^{i\cdot\mu_x}$	chromatic
6	$h_{21000} = -h^*_{12000}$	Q_x		$e^{i\cdot\mu_x}$	geometric
7	$h_{10110} = -h^*_{01110}$	Q_x		$e^{i\cdot\mu_x}$	geometric
8	$h_{30000} = -h^*_{03000}$	$3Q_x$		$e^{i\cdot 3\mu_x}$	geometric
9	$h_{10200} = -h^*_{01020}$	$Q_{xy} + 2Q_y$		$e^{i\cdot(\mu_x + 2\mu_y)}$	geometric
10	$h_{10020} = -h^*_{01200}$	$Q_{xy} - 2Q_y$		$e^{i\cdot(\mu_x - 2\mu_y)}$	geometric

$$h_{11001} = \xi_x^{(1)} = -\frac{1}{4\pi}\sum_n^{N_{QUAD}}\left(K_Q L_Q\right)_n \beta_{xn} + \frac{1}{4\pi}\sum_m^{M_{SXT}}(K_S L_S)_m \beta_{xm} D_m \quad (42)$$

Linear RDT and their effects are shown in Table 1.

Second order driving terms depend on square of integrated sextupole strength $h^{(2)} \sim (K_S \cdot L_S)^2$ and drive synchrotron sidebands of linear modes. When linear RDT are vanished either reduced the second order RDT (sidebands) are week and might be ignored. One must suppress or minimize first order modes in order to reduce second order resonances. Second and third order chromaticies driven by high order RDT are independent on phase advance.

Cross-talks of different first order RDT in sextupoles as well as between different sextupoles produce phase independent second order RDT generating Amplitude Dependent Tune Shifts (ADTS). ADTS are originated from an amplitude or momentum dependent shift of the closed orbit in sextupole. Orbits must be corrected to the magnetic axis of a sextupole in order to minimize ADTS. Beam Position Monitors should be located as close as possible to each sextupole in order to control beam centroid.

$$\delta Q_x^{ADTS} = \frac{\partial h^{(2)}}{\partial J_X} \approx \alpha_{xx} J_X + \alpha_{yx} J_Y \quad (43a)$$

$$\delta Q_y^{ADTS} = \frac{\partial h^{(2)}}{\partial J_Y} \approx \alpha_{xy} J_X + \alpha_{yy} J_Y \quad (43b)$$

Octupoles effectively (in a first order of octupole strength) compensate ADTS as well as second order chromaticiy $\xi_{x,y}^{(2)}$. Nevertheless, octupole strength must be limited otherwise Dynamic Aperture could be reduced

$$\alpha_{xx} = +\frac{1}{16\pi}\left(\sum_n^{N_{oct}}(K_{oct} \cdot L_{oct}) \cdot \beta_{xn}{}^2\right) \quad (44a)$$

$$\alpha_{zz} = +\frac{1}{16\pi}\left(\sum_n^{N_{oct}}(K_{oct} \cdot L_{oct}) \cdot \beta_{zn}{}^2\right) \quad (44b)$$

$$\alpha_{xz} = -\frac{1}{8\pi}\left(\sum_n^{N_{oct}}(K_{oct} \cdot L_{oct}) \cdot \beta_{xn} \cdot \beta_{zn}\right) \quad (44c)$$

Chromatic sextupoles are located in dispersive sections of a ring and control linear chromaticity $\xi_{x,y}^{(1)}$. Its strengths are fixed. Hamiltonians of chromatic sextupoles are added either subtracted additively regardless of phase advance (μ). Harmonic sextupoles and quadrupoles are located at achromatic sections of a ring ($D = D' = 0$) and do not contribute to $\xi^{(1)}$.

Eight first order modes and its complex conjugative modes are phase dependent and experience resonance behavior. One might consider RDT as a sum of complex vectors. Each complex vector represents local Hamiltonian of sextupole either quadrupole with amplitude proportional to integrated strength of element. Phase of each vector is multiple of betatron phase advance at element location. By choosing proper phase advance between non-linear elements one could minimize and even diminish certain driving terms.

Nine families of harmonic sextupoles could be enough to compensate all excitation modes but at phase advance of cell close to $\mu_x = \pi$ resonance terms proportional to $(2\mu_{x,y})$ will be amplified coherently by all sextupoles. Linear system of 9 equations degenerates down to rank 8. It will be no solution to suppress all driving modes [27]. Linear lattice optics should be adjusted at design stage to cancel either minimize resonance terms by proper choice of phase advance between sections of a ring. One may apply mirror symmetry conditions and phase advance between cells close to quarter of integer

$$\mu_{x,z} \approx (k \pm 0.25) \cdot 2\pi \quad (45)$$

Phase dependent resonances associated with $2\mu_{x,y}$ will be cancelled between cells $2\mu_{x,z} = \pi$. Also phase dependent resonances (μ_y , $3\mu_y$) and coupling resonances ($\mu_x \pm 2\mu_z$) will be cancelled between two pairs of cells. One can use periodicity condition [27]

$$\Delta Q_{x,z} = N \cdot \mu_{x,z}^{cell} \left[2\Delta Q_{x,z}\ 3\Delta Q_x\right] \rightarrow integer \quad (46)$$

and cancel RDT between each N cells

$$N = (2n_{x,z} \pm 1)\pi/\mu_{x,z}^{cell} \quad (47)$$

Location of sextupoles in sequence of equal phase advance steps $\Delta\mu_{x,z}$ also might limit resonance driving terms due to partly cancellation.

To compensate linear chromaticity the "*–I*" condition is applied to pairs of not-interleaved sextupoles of equal strength $S_{X1} = S_{X1}$ located at mirror symmetry points of lattice sections of a ring (Fig.2).

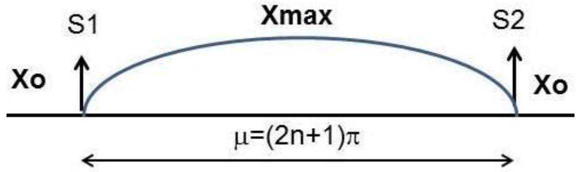

Fig. 2. Compensation of linear chromaticity by applying "–I" condition with non-interleaved sextupoles [24].

Phase advance between sextupoles S_1 and S_2 is multiple to odd integer $\mu_{x,z} = (2n \pm 1)\pi$ while Twiss parameters are mirror reflected

$$\beta_{x1} = \beta_{x2} \qquad \alpha_{x1} = -\alpha_{x2} \quad (48a)$$

$$D(s_1) = D(s_2) \qquad D'(s) = -D'(s_2) \quad (48b)$$

In approximation of thin lenses full cancellation of sextupole aberrations is achieved outside of region between non-linear elements while inside particles are moving on asymptotic trajectories. It is important to foresee enough space in transverse direction in order to accommodate disturbed trajectories between sextupoles [24].

General conditions for full cancellation of non-linear terms from two thin sextupoles of S_{X1} and S_{X2} strength each might be expanded for odd and even integer phase advance $n = 1,2,3$ ... [29]

$$\Delta\mu_{2-1} = n\pi \qquad \beta_{Z1}/\beta_{X1} = \beta_{Z2}/\beta_{X2} \quad (49a)$$

$$(S_{X1})\beta_{X1}^{3/2} = -(-1)^n(S_{X2})\beta_{X2}^{3/2} \qquad D_1 = -(-1)^n D_2 \quad (49b)$$

IV. Applications

Frequency analysis maps and Diffusion maps are powerful tools to simulate and optimize dynamic aperture of low emittance electron storage rings [30,31,32,33]. Nevertheless it might be of scientific interest to mention here one project of Diffraction Limited Light Source (DLLS) with large Dynamic Aperture [24, 34, 35]. Split magnet TME cell is considered as basic element of future ultimate storage ring of DLLS project of Budker Institute, Novosibirsk (Fig.3). Non-interleaved pairs of horizontal (either vertical) sextupoles are located at the beginning and end of cell at position of Dispersion bumps. Split bend with horizontal focusing quadrupole in–between is required to adjust phase advance between sextupoles and provide "**–I**" condition.

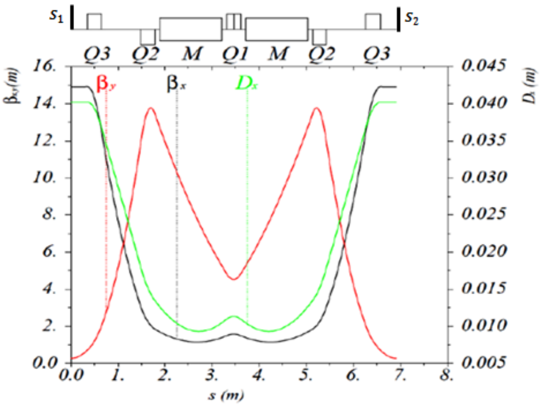

Fig. 3: Split magnet TME cell for ultimate storage ring. Picture taken from [35].

Five-cells (either seven-cells) with two non-interleaved horizontal sextupole pairs (denoted X) and two vertical sextupole pairs (denoted Y) form one supercell (Fig. 4). Dispersion suppressors at supercell edges are not shown.

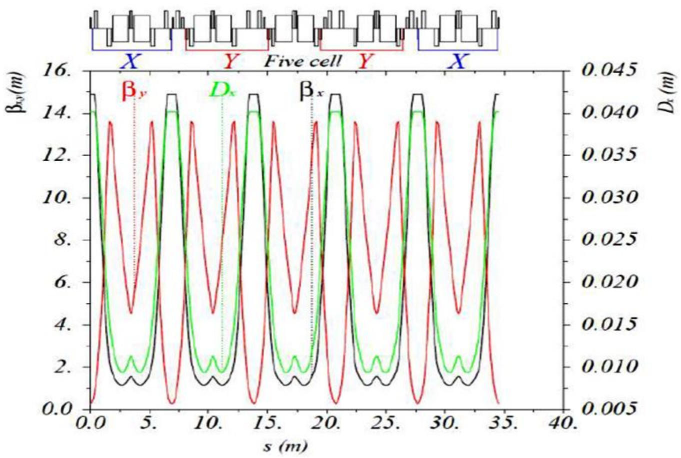

Fig. 4. Five-cell superperiod with two non-interleaved horizontal sextupole pairs (denoted X) and two vertical pairs (denoted Y). [35].

Adjusting of phase advance of split TME cell helps to realize self-compensation conditions between non-interleaved pairs of sextupoles, thus, the Dynamic Aperture will be enlarged in few times. Area of stable motion in an ultimate storage ring with natural beam emittance of 10 pm might be as large as $\pm(20\times20)mm^2$ (corresponds to value of horizontal and vertical betatron functions $\beta_{x,y} = 10\ m$), see Fig. 5. Momentum acceptance of ultimate storage ring $\mathrm{MA} = \pm 1{,}5\%$ should guarantee the beam life time of about 10 hours for 100 mA beam.

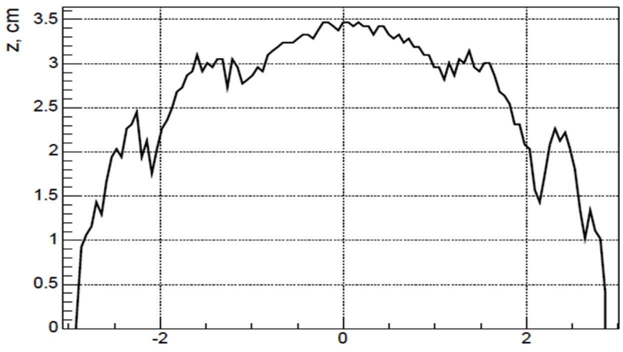

Fig. 5: Dynamic aperture of ultimate storage ring with 10 pm emittance. $\beta_x = 10\ m.$ Picture taken from [34].

Acknowledgements

I'm very grateful to Prof. Anke-Susanne Müller and Dr. Sara Casalbuoni for kind invitation to present this talk.

References

[1] W.Scandale, "Dynamic aperture", in *Proc. CERN Accelerator School* CAS-95-06, 1995.

[2] K.Steffen, "Basic Course on accelerator Optics", in *Proc. CERN Accelerator School* CAS-85-19, 1985.

[3] A.Wolski, "Design of electron storage rings", in *Proc. US Particle Acceleratro School* USPAS-2013, 2013.

[4] E.Courant and H.Snyder, "Theory of the alternating-gradient synchro-tron". *Annual Phys.* 3, 1958.

[5] J.Livingood, "Principles of Cyclic Accelerators", Interscience Publishers 1954.

[6] K.Steffen, "High energy Beam Optics", Interscience Publishers, 1965.

[7] A.Kolomensky and A.Lebedev, "Theory of Cyclic Accelerators", Nauka, 1966.

[8] G.Guignard, "Nonlinear dynamics", *Particle Accelerators*, v.18, pp.129-165, 1986.

[9] J.Rees, "Symplecticity in Beam Dynamics: An Introduction", *SLAC-PUB*-9939, 2003.

[10] B.Montague, "Basic Hamiltonian mechanism", in *Proc. CERN Accelerator School* CAS-95-06, 1995, pp.1-17.

[11] A.Dragt, "An Overview of Lie Methods for Accelerator Physics", in *Proc. Part. Accel. Conf*. PAC-2012, USA, 2012.

[12] E.Wilson, "Non-linear resonances", in *Proc. CERN Accelerator School* CAS-95-06, 1995.

[13] A.Wolski, "Beam Dynamics in High Energy Particle Accelerators", World Scientific, p.1-608, 2014.

[14] L.Nadolski, "Non-linear Beam Dynamics", in *Proc. 2nd Non-linear Beam Dynamic Workshop*-2009, Diamond, UK, v2.2, NPA-2011-2012.

[15] A.Verdier, "Longitudinal beam dynamics", in *Proc. CERN Accelerator School* CAS-95-06, 1995.

[16] W.Herr, "Mathematical and numerical methods for non-linear beam dynamics", in *Proc. CERN Accelerator School CAS-2013* (CERN-2014-009), 2014.

[17] P.Streun, "Lattices for Light Sources", in *Proc. CERN Accelerator School CAS-2003* (CERN-2006-002), 2006.

[18] Y.Cai, "Single particle beam dynamics in electron storage rings with extremely low emittance", *NIM-A*, Volume 645, Issue 1, p.168-174, 2011.

[19] J.Bengtsson, "The sextupole scheme for the Swiss Light Source(SLS): an analytical approach", Internal report *SLS-TME-TA-1997-0009*. PSI, Swiss, 1997.

[20] L.Evans, "Effect of Octupole near a fourth-order resonance", in *Proc. CERN Accelerator School* CAS-CERN 84-15, 1985.

[21] J.Cao, "Analytical estimation of the dynamic aperture of circular accelerators", Orsay, France, LAL/RT 00-02, 24 p., 2000.

[22] A.Ropert, "Dynamic aperture studies at ESRF", in *Proc. European Particle Accelerator Conference EPAC*-98, 1998.

[23] R.Bartolini, "Review of lattice design for low emittance rings", *Beam Dynamics News*, No.57, 2012.

[24] E.Levichev, P.Piminov et al. "Beam optics and dynamics in electron storage rings with ultralow emittance", *Physics of Particles and Nuclei Letters*, v.13, issue 7, pp.884-889, 2016.

[25] J.Bengtsson, "Control of dynamic aperture for synxhrotron light sources", *Beam Dynamics Newsletter*, No.57, 2012, in *Proc. Part. Acc. Conf.*, Knoxville, USA, p.1670-1672. 2005.

[26] J.Bengtsson, W.Joho, A.Streun et al, "Increasing the energy acceptance of high brifhtness synchrotrobn light source", *Nucl. Inst. and Meth*. A404, p.237-247, 1998.

[27] P.Streun, "Non-linearities in Light Sources", in *Proc. CERN Accelerator School CAS-2003*, SLS-TME-TA-2005-0282.2005.

[28] R.Bartolini et al, „Correction of multiple nonlinear resonances in storage rings", Phys. Rev. ST-Accel. Beams 11, 104002, 2008.

[29] G.Xu, "General conditions for self-cancellation of geometric aberrations in a lattice", Phys. Rev. ST- Accel. Beams 8, 104002, 5 p., 2005.

[30] C.Steier, L.Nadolski et al, "Lattice model calibration and frequency map measurements at ALS", in *Proc. Europ. Part. Acc. Conf.* EPAC-2000, Vienna, Austria, 2000.

[31] D.Robin, L.Nadolski et al, "Understanding the dynamic aperture of the advanced Light Source", *Phys. Rev. Lett.* 85, 3, pp.558-561, 2001.

[32] J.Laskar, "Frequency Map Analysis and particle accelerators", in *Proc. Part. Acc. Conf.* PAC-2003, Portland, Oregon, USA, pp.378-382, 2003.

[33] L.Nadolski, "Methods and tools to simulate and analyze non-linear dynamic in electron storage rings", in *Proc. Int. Part. Acc. Conf*. IPAC-2011, San-Sebastian, Spain, pp.937-941, 2011.

[34] A.Bogomyagkov, E.Levichev, P.Piminov, "Low emittance lattice cell with large dynamic aperture", in *Proc. Int. Part. Acc. Conf*. IPAC-2014, Dresden, Germany, pp.99-101, 2014.

[35] E.Levichev et al. "Diffraction limited electron storage ring with large dynamic aperture", Budker Institute Proposals, Novosibirsk, Russia, 2013.

Session 7: Optics Design, Measurements and Correction

Optics Measurements using Fast Orbit Feedback Data

I.P.S.Martin
Diamond Light Source, Oxfordshire UK

***Abstract*—An overview of beam optics measurements taken using fast orbit feedback data is presented. The benefits of improved measurement precision and reduced data acquisition time are discussed, and examples of how to further reduce the time to correct the linear optics are discussed. Examples of how the technique can be extended to study the nonlinear lattice are provided.**

I. Introduction

For the latest generation of light sources, excellent control of the linear optics is mandatory. The optics underpins all aspects of operation, from source size to tune-stability, resonance control and coupling and vertical dispersion correction, all of which impact on the final lifetime and injection efficiency.

Many techniques have been developed for this purpose, however, LOCO-style [1] algorithms based on closed orbit response matrix (ORM) measurements are typically applied. LOCO has been demonstrated to be very successful, with the ability to control the optics to the percentage level. However, there are still issues, including:

- the ORM is typically very large. For Diamond-II, it is proposed to have 252 BPMs and correctors per plane. It can take up to 1h for a complete correction cycle.
- Significant orbit drift can occur during measurement due to thermal or hysteresis effects (particularly after fresh injection).
- Orbit stability or beam vibrations can affect the measurement accuracy.
- it is invasive, so cannot be carried out during user time.

The use of fast orbit data can help to address some of these shortcomings.

II. Fast LOCO

At Diamond Light Source, a fast optics correction tool has been developed, based around the existing matlab-LOCO code and a fast orbit response matrix measurement [1]–[3]. The package has been wrapped with a python user interface, such that the process is initially configured by the user, then the measurement, optics-fitting and machine correction stages are all automated.

The application makes the following steps:

- Measure the ORM using the fast orbit feedback network. A programmed sine-wave excitation is applied to each corrector in turn, and orbit data is taken from the fast acquisition (FA) BPM data and post-processed.
- At the end of the measurement, the data is converted into a LOCO-compliant matlab input file.
- The standard LOCO analysis is completed in batch mode using the matlab parallel computing tool kit.
- the user is queried at the end whether they would like to apply the results.

The new measurement and correction procedure has reduced the typical times for a complete correction cycle from around 20 minutes to around 5 minutes.

A. Response matrix measurement

Each of the fast orbit feedback nodes at Diamond can produce sine-wave excitations on each corrector with programmable amplitude, frequency, duration and synchronised start time. The new fast LOCO application configures this excitation using a Python script, and the orbit data is then extracted from the 1 kHz live FA data stream. Once the excitation has been completed, the amplitude at the excitation frequency is extracted from the measured orbit at BPM m and corrector n using:

$$\begin{aligned} A_{m,n} &= < 2 \times z_m(t) \times sin(2\pi f t) > \\ R_{m,n} &= A_{m,n}/\Delta\theta_n \end{aligned} \tag{1}$$

The number of excitation cycles for each corrector, the excitation frequency, choice of correctors and delay between corrector all configurable. The particular choice depends on context (e.g. low alpha mode, fast coupling correction, ...). An example of using single-cycle excitation is shown in Fig. 1.

B. Choice of excitation frequency

The choice of excitation frequency is a trade off between reducing the measurement time and improving the accuracy of the measurement. Shown in Fig. 2 is the displacement power spectral density for the electron beam at Diamond at a single BPM. There is a clear dip in the beam motion at 8 Hz, suggesting that exciting the correctors at this frequency will lead to the lowest noise / highest precision data.

Another consideration is the impact of attenuation and phase delay for the corrector field. This is shown in Fig. 3. These depend on the whole system (i.e. the magnet, power supply, vacuum chamber, cabling, etc.), and show that above a few tens of Hz, attenuation and phase delay can become significant, impacting the measurement. Taking all these aspects into account, it was decided to use 8 Hz for the embedded correctors on sextupoles, and 1 Hz for discrete correctors in mini-beta straights.

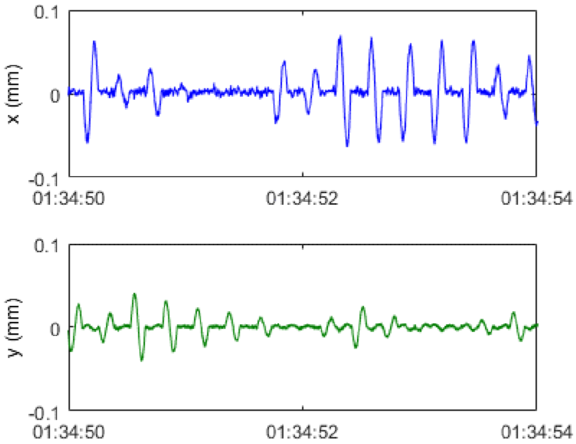

Fig. 1. Horizontal (top) and vertical (bottom) orbit at a single BPM as different correctors have their single-cycle excitation applied.

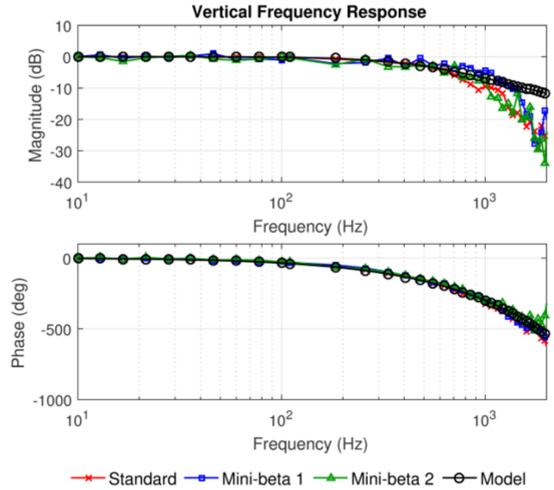

Fig. 3. Attenuation and phase delay for the different corrector types.

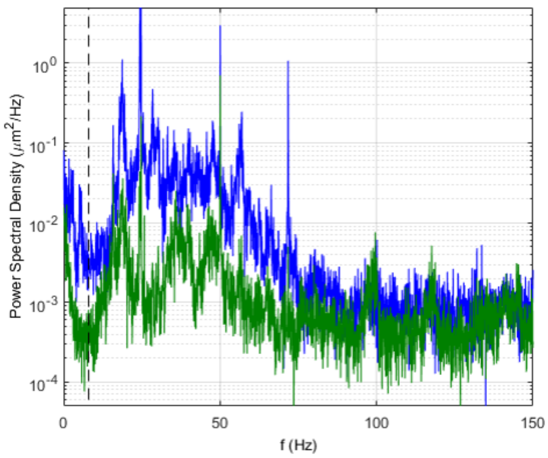

Fig. 2. Displacement power spectral density measurement for the electron beam at a single BPM .

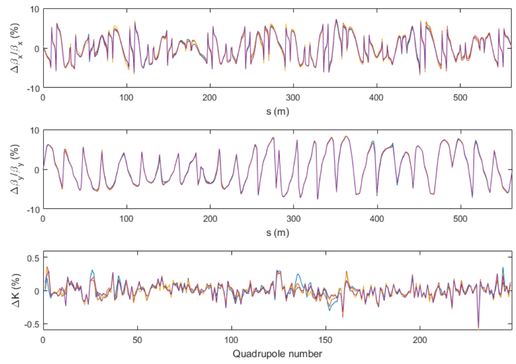

Fig. 4. Results of optics fitting on three consecutive data sets. The measurement in blue was taken using the standard LOCO application for reference.

C. Results

An example of the results of the new application are shown in Fig. 4. In this figure, three consecutive data sets were taken and compared to one data set measured using the standard LOCO application. Clearly, a high degree of consistency is achieved, both in terms of the fitted machine optics and the quadrupole corrections required.

The new LOCO application has been in routine operation since 2014 and can be used by anyone (no specialist knowledge is required). The ease of use means it is now applied for many situations where previously it would have been impractical, including:

- Normal and skew quadrupoles for ID compensation.
- Re-correcting the coupling after a beam trip.
- Correcting the machine for machine development studies (e.g. injection studies, resonant spin, pinhole calibration, ID studies, tune scans, ...).

Different configurations of the fast LOCO application are in use for different operating modes. For example, for the standard user optics it is sufficient to have a single cycle for each corrector and 100 orbit samples for the BPM noise measurement. However, during low alpha (where the beam stability is much worse), we found it necessary to have five cycles for each corrector, and 200 samples for the BPM noise.

The parallelisation in Matlab also allows an increased number of iterations during the LOCO fit which can help to improve the convergence. Tests with higher excitation frequencies have shown comparable results to the above for the nominal optics. The main impact is a reduced fitted gain for the correctors (attenuation / phase delay). The acquisition and fit times can be further reduced by using fewer correctors, where again the main impact is on the gain and roll values for correctors. Using multiple excitations in parallel at different frequencies has also been demonstrated. A complete ORM can be measured in less than 10 s, however, it is the post-processing of the measured data that is limiting factor at present.

III. Examples from other facilities

A. NSLS-II

At NSLS-II extensive studies have been carried out [4] to understand how fast LOCO measurements compare to standard LOCO [1], [2], [9] and to turn-by-turn data methods [5]–[8]. In these studies, the machine was initially 'spoiled' by applying random errors to the quadrupoles, then the various algorithms were run to establish the relative accuracy of correction and the time taken. Overall, the fast LOCO measurements were found to be the most accurate, with the total acquisition times comparable (but still slightly slower than) the turn-by-turn methods. The results of the comparison are shown in Fig. 5.

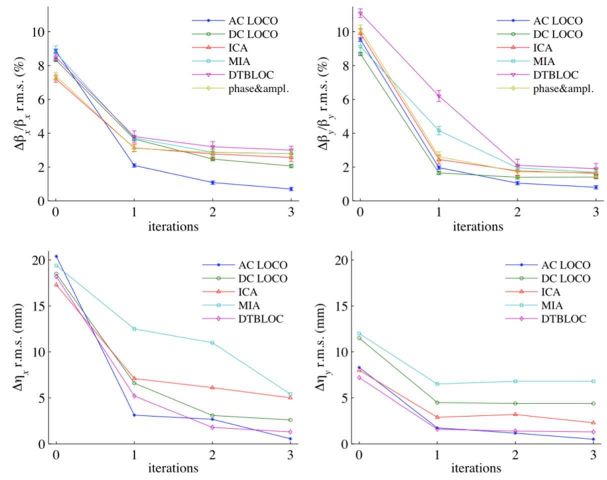

Fig. 5. Comparison of beta and dispersion fitting for the different linear optics algorithms.

Experiments have also been conducted to see if several correctors can be excited simultaneously but at different frequencies (see Fig. 6). The choice of frequency can be made based on the signal bandwidth (0.2 Hz for a 5 second measurement) and minima in the Fourier transform. A 2 Hz separation was tested for 23 simultaneous excitations. The results showed an r.m.s. noise floor of 20 nm, comparable to the single corrector results.

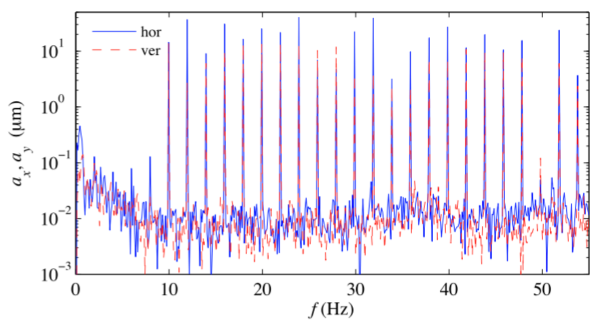

Fig. 6. Horizontal and vertical orbit spectrum during the multi-corrector excitation.

B. ALBA

At ALBA, various tests have been made to study the nonlinear machine optics [10]. The increased accuracy of the fast LOCO measurement allows the variation of each ORM element with beam energy to be evaluated by taking data at several values of RF frequency. This allows the nonlinear lattice to be probed for regions where the sextupoles are occupying dispersive locations. This measurement data can then be compared to the machine model in the same way as the quadrupoles are fitting for the linear optics.

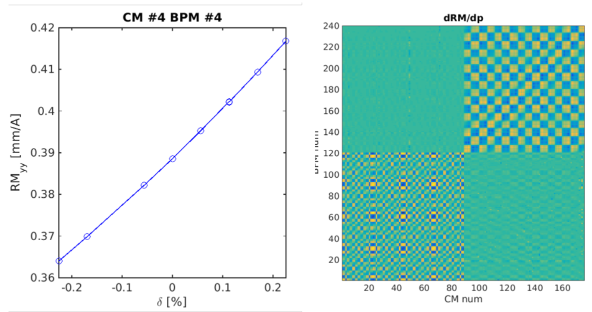

Fig. 7. ORM matrix element as a function of energy for a single corrector/BPM pair (left). Full matrix of off-energy ORM elements (right).

Similarly, the nonlinear lattice can be investigated by studying the amplitude of orbit motion at harmonics of the corrector excitation frequency. This can be seen, as if the beam is excited at f_x and f_y in each plane, then harmonics will appear as:

- $B_y = m(x^2 - y^2)$ (horizontal orbit contains $2f_x$ and $2f_y$).
- $B_x = 2mxy$ (vertical orbit contains $f_x - f_y$ and $f_x + f_y$).

where m is the sextupole strength. An example of one such measurement is shown in Fig. 8. The main difficulty with this measurement lies in having to drive the beam motion to large amplitudes in order to see the line in the spectrum with sufficient precision.

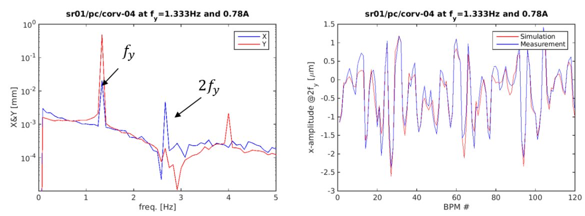

Fig. 8. FFT of BPM signals for excitation with a single vertical corrector (left). Amplitude of $2f_y$ line around the ring and comparison to the machine model (right).

C. ESRF

Lastly, the technique of fast LOCO has also been investigated at ESRF. One example of this is in the use of fast LOCO to calibrate skew quadrupole trim magnets, then to use these magnets to compensate for ID gap changes. An example of this is shown in Fig. 9, demonstrating that a substantial reduction in the impact of this insertion device on the vertical emittance can be easily achieved. Without the skew compensation the vertical emittance was changing by few pm as the ID was closed. After compensation, this was reduced to 0.2 pm, with the tests being completed during around 2 hours of beam time.

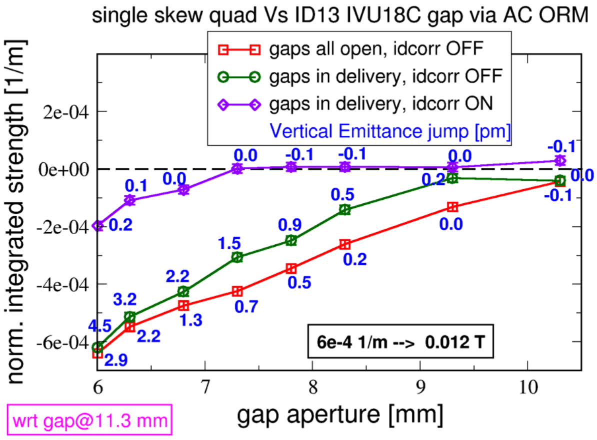

Fig. 9. Skew quadrupole strength and vertical emittance as a function of gap for ID 13 at ESRF.

IV. Conclusions

Beam optics measurements taken with fast orbit data have many benefits:

- a substantial reduction in measurement / correction time.
- minimises impact from machine drift and / or hysteresis effects.
- improved accuracy compared to DC LOCO or TBT-based algorithms.
- enables frequent optics correction and use by non-experts.
- enables new types of measurement (off-energy ORM, nonlinear ORM).

In particular, by integrating the fast ORM measurement with the fast orbit feedback, this technique has the potential to provide low noise measurements of the nonlinear lattice and allow accurate corrections to be made to the sextupoles.

V. Acknowledgements

It is a pleasure to acknowledge the contributions to the work conducted at Diamond by G. Rehm and M. Furseman. The author to also grateful to V. Smaluk, Z. Marti and A. Franchi for providing material shown during the presentation and in this manuscript.

References

[1] J. Safranek, Nucl. Inst. and Methods A, vol. 388, p. 27-36, (1997).
[2] I.P.S. Martin *et al.*, in Proc. IPAC'14, Dresden, Germany, TUPRI083, (2014).
[3] G. Rehm *et al.*, in Proc. BIW'10, Santa Fe, U.S.A, MOCNB01, (2010).
[4] V. Smaluk *et al.*, in Proc. IPAC'16, Busan, Korea, THPMR008, (2016).
[5] G. Wang *et al.*, BNL Tech. Note 168, (2015).
[6] X. Huang *et al.*, Phys. Rev. ST Accel. Beams, 8, 064001, (2005).
[7] J. Irwin *et al.*, Phys. Rev. Lett., 82, 1684, (1999).
[8] Y. Hidaka *et al.*, in Proc. NA-PAC'16, Chicago, USA, TUPOB52, (2016).
[9] X. Yang *et al.*, Phys. Rev Accel. Beams, 20, 054001, (2017).
[10] Z. Marti *et al.*, in Proc. IPAC'17, Copenhagen, Denmark, MOPAB102, (2017).

Diamond-II storage ring tuning - Design to commissioning

AH. Ghasem, M. Apollonio, F. Bakkali Taheri, R. Bartolini, J. Bengtsson, R. Fielder, J. Kennedy, M. Korostelev, I. Martin, T. Olsson, B. Singh, R. Walker
Diamond Light Source, Oxfordshire, UK

***Abstract*—The Diamond Light Source (DLS) initiated a design study into the feasibility of replacing the existing electron storage ring with a next-generation, high-performance accelerator called as Diamond-II. A careful lattice design and nonlinear dynamics optimization are done to achieve the desired storage ring specifications with large dynamic and momentum apertures, enabling efficient injection of the incoming beams.**

***Keywords*—Storage ring, Optical functions, Dynamic aperture, Frequency map**

I. Introduction

The DLS is the UKs national synchrotron science laboratory which is located in Oxfordshire area. It is one of the most advanced operational scientific facilities in the world since 2007. As demanded by the users to have super bright photon beam and higher number of beam lines, the DLS started to study feasibility of replacing the existing electron storage ring with an ultra-low beam emittance ring called as Diamond-II.

II. Linear lattice

Following design trend of the modern accelerator facilities, a novel lattice has been designed for the Diamond-II storage ring. The ELEGANT [1], AT [2] and OPA [3] codes are used for the design and particle tracking. The optical functions in one super period of the ring are shown in Fig. 1 and main beam parameters are given in Table 1.

TABLE I
Main parameters of the storage ring.

Parameter	Unit	Value
Beam energy	GeV	3.5
Circumference	m	560.7
Beam emittance	pmrad	157.3
Hor./Ver. tune	-	57.16/20.24
Natural Hor./Ver. chromaticity	-	-75.6/-89.6
Momentum compaction factor	-	1.17E-4
Energy spread	-	7.76E-4
Radiation loss per turn	MeV	0.67
RF frequency	MHz	499.5
Harmonic number	-	934
Natural bunch length	ps	9.86

III. Nonlinear beam dynamics

To suppress transverse head-tail instabilities and to avoid large tune spread of the off energy electrons, the natural horizontal/vertical chromaticity has to be corrected close to zero. Three chromatic sextupoles have been used to control the chromaticity and additional three harmonic sextupole with one families of octupole magnet are employed to control the dynamic and momentum apertures and to confine the tune shifts with energy and amplitudes. The on/off energy dynamic aperture (DA) and corresponding frequency map (FM) of the bare lattice are displayed in Fig. 2.

IV. Commissioning simulation and errors effects

The impact of a realistic distribution of errors of the magnetic elements and beam position monitors (BPMs) on the performance of the ring has been assessed by means of a statistical analysis of the closed orbit, linear optics and the key performance parameters of the nonlinear beam dynamics [4]. In order to correct the errors effects, 252 BPMs, 252 combined horizontal and vertical correctors and 144 skew quadrupoles have been employed.

TABLE II
Machine errors used in the commissioning simulation.

Parameter	Value (μm/μrad)
Girder misalign. /roll	150/150
Dipole misalign. / roll within girder	50/100
Quad., Sext., Oct. misalign. /roll within girder	25/100
BPM misalign. /roll within girder	100/100
Dipole/Quad./Sext./Oct. fract. strength error	$5{\cdot}10^4/10^3/10^3/10^3$

The commissioning of the storage ring is based on the following steps [1]-[3]: 1) Establish the first turns with quads and dipole only and perform basic trajectory correction while the sextupoles have been switched off, 2) power on the sextupoles and RF to capture the beam, (fine tune and chromaticity if necessary) 3) Preliminary BPM calibration and quadrupole centering (also known as beam based alignment (BBA), 4) correct the closed orbit, 5) correction of the beta-beating, 6) correction of the vertical dispersion and coupling errors, 7) accumulation [5,6]. All the correction steps are based on the response matrix method and singular value decomposition (SVD) algorithm. After all corrections are done, particle tracking has been carried out for 30 random error seeds of Table 1 and the nonlinear beam dynamics has been investigated. The on/off momentum dynamic aperture (DA) is displayed in Fig. 3. For the on energy case, the dynamic aperture is on average $\pm$6 mm in the horizontal and $\pm$2 mm in the vertical planes which is sufficient for off axis injection. The corresponding frequency maps and tune diffusion plots are shown in Fig. 4 for one representative seed. An example of the impact of the

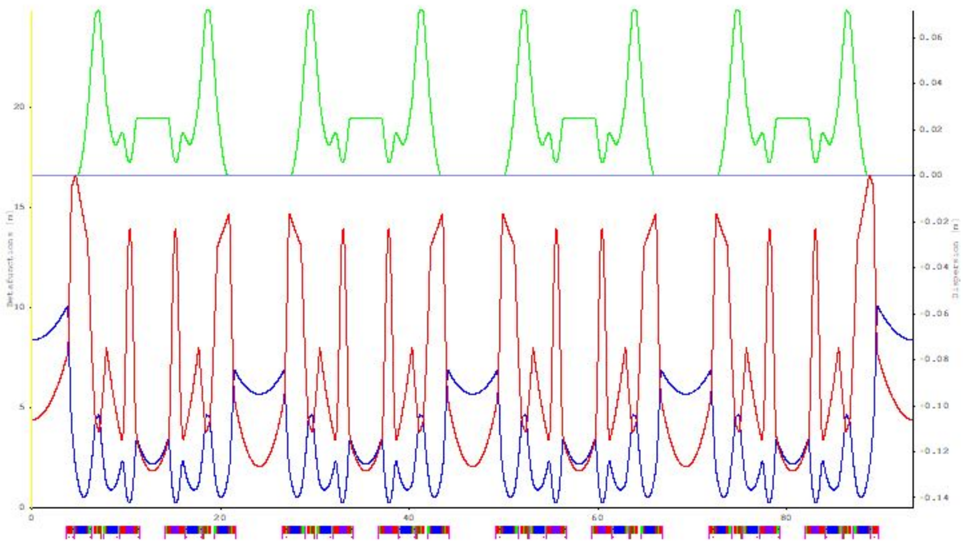

Fig. 1. The optic functions in one super period, β_x (blue), β_y (red) and dispersion function (green).

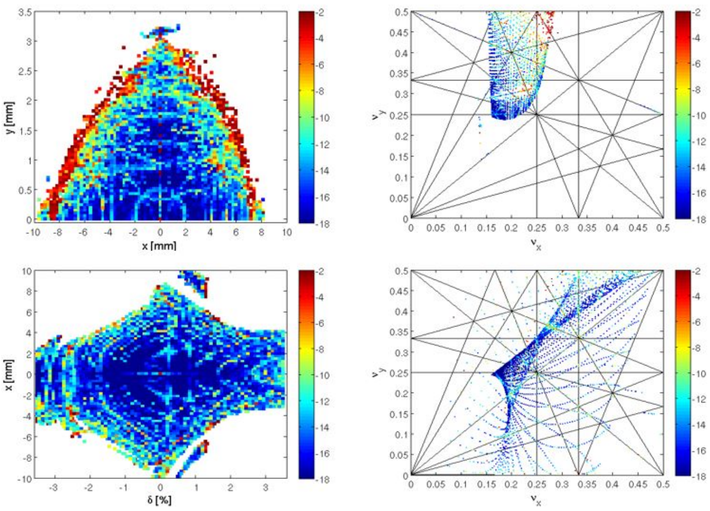

Fig. 2. The dynamic aperture for the on energy (top-left) and off energy (bottom-left) electrons. Corresponding frequency maps are given in the right side graphs.

errors on the momentum aperture (MA) is shown in Fig. 5. The resulting lifetime over 30 seeds is 0.95 h $\pm$ 0.12 h.

REFERENCES

[1] M. Borland, Elegant: a flexible sdds-compliant code for accelerator simulation, Advanced Photon Source, Argonne National Laboratory, USA, Report No. LS-287 (2000).

[2] A. Terebilo, Accelerator toolbox for MATLAB, in Proc. Workshop on Performance Issues at Synchrotron Light Sources Berkeley, California, October 2-4, 2000.

[3] A. Streun, OPA Lattice Design Code, https://ados.web.psi.ch/opa/

[4] R. Bartolini et al., Double-double bend achromat cell upgrade at the Diamond Light Source: From design to commissioning, PRAB 21, 050701 (2018).

[5] V. Sajaev, M. Borland, Commissioning simulations for the APS upgrade lattice, IPAC2015, Richmond, USA., p. 553-553 (2015).

[6] T. Hellert, et al., Simulation of trajectory correction in early commissioning of the Advanced Light Source upgrade, IPAC2018, Vancouver, BC, Canada, p. 4256-4258 (2018).

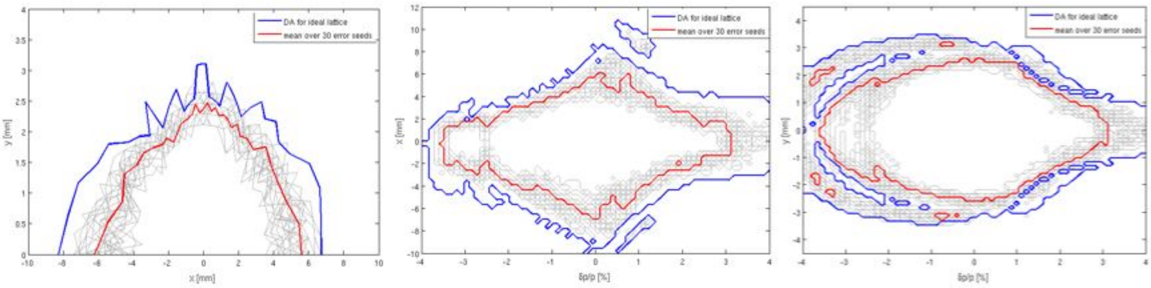

Fig. 3. On energy DA (left) and x amplitude dependence to energy deviation (middle), y amplitude dependence to energy deviation in the presence of errors in Table 1 after corrections.

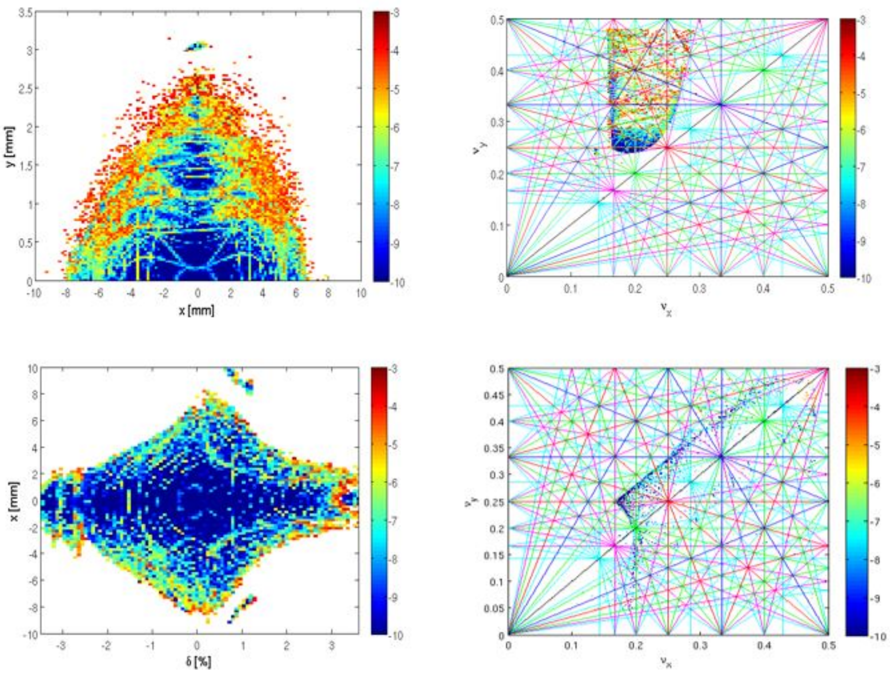

Fig. 4. The dynamic aperture after errors corrections for the on energy (top-left) and off energy (bottom-left) electrons. Corresponding frequency map (right) are given in the right side graphs.

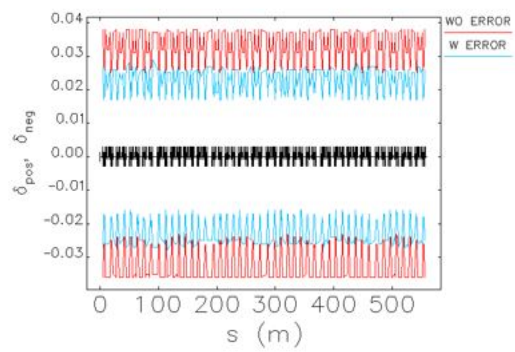

Fig. 5. Momentum aperture for the bare lattice and for one of the worse errors seed.

Low and Negative Alpha Commissioning at KARA Storage Ring

Akira Mochihashi, Tobias Boltz, Miriam Brosi, Bastian Härer, Benjamin Kehrer, Patrick Schreiber, Marcel Schuh, Johannes Leonhard Steinmann,
Alexander Papash, Robert Ruprecht and Anke-Susanne Müller
Karlsruhe Institute of Technology, Karlsruhe, Germany

***Abstract*—Lattice structures of electron storage rings with negative and positive low-momentum compaction factor are now drawing attention again as new promising ideas to achieve an ultra low emittance beam. In particular, the operation with negative momentum compaction factor (negative alpha) can lead to negative chromaticity operation in which sextupole magnetic field can be relaxed and thus an expansion of the transverse dynamic aperture can be expanded. In the KArlsruhe Research Accelerator (KARA), we proceed with negative alpha operation to investigate the strategy of beam commissioning as well as te collective beam instability in negative alpha operation mode.**

***Keywords*—Negative and low momentum compaction factor, beam commissioning**

I. Introduction

In electron storage rings, the equilibrium beam emittance ϵ_x is described as

$$\epsilon_x \propto \frac{\gamma^2}{J_x} \frac{\oint \frac{H}{|\rho_0|^3} ds}{\oint \frac{1}{\rho_0^2} ds}, \tag{1}$$

where γ is the Lorentz factor of the beam, J_x is the horizontal damping partition number and ρ_0 is the curvature radius of the beam orbit inside the bending magnets. The function H is determined by the lattice functions of the storage ring and is given by

$$H = \gamma_x \eta_x^2 + 2\alpha_x \eta_x \eta_x' + \beta_x \eta_x'^2, \tag{2}$$

where α_x, β_x and γ_x are the Twiss parameters and η_x, η_x' are the disperson function and its derivative. The equation shows that the emittance can be manipulated by changing the dispersion and its derivative, and which can lead to a change in the momentum compaction factor. Senichev [1] has discussed a possibility to get lower emittance by optimizing the dispersion function and setting momentum compaction factor to be negative, accordingly.

One of the benefits for the negative alpha operation can be the relaxation of sextupole magnetic field in storage rings. Normally the chromaticity value in storage rings is settled to be slightly positive to damp collective instabilities like the head-tail instability. Because the natural chromaticity of storage rings is normally negative, sextupole magnets are needed to make the chromaticity positive. However, the dynamic aperture of the beam can be drastically decreased because of a non-linear effect from the sextupole magnetic field. On the other hand, in negative alpha condition the chromaticity must be negative to suppress the head-tail instability, that can lead to relaxed sextupole field and to expanded dynamic aperture, accordingly.

In KARA, now we proceed with development of the negative alpha operation. To investigate this interesting operation mode at KARA, we have designed a negative alpha lattice and performed tracking simulation to estimate the injection efficiency under this operation mode. We have also performed real beam commissioning at beam energy of 500 MeV.

II. Lattice design

The KARA storage ring [2] with a circumference of 110 m can be operated with the beam energy range of 500 MeV $\sim$ 2.5 GeV. Because KARA is a compact storage ring, it has a typical double bend achromatic (DBA) lattice with 16 bending magnets. In normal KARA operation, we use the DBA lattice with non-zero dispersion in long straight sections. Figure1 shows the lattice functions for 1-cell under 500 MeV operation for the normal injection. If we get a negative alpha lattice we have to modify the dispersion function drastically to make the momentum compaction factor negative. Figure2 shows a designed negative alpha lattice for KARA. As seen in the figure, the dispersion function has large amplitude to realize a negative momentum compaction factor. This large amplitude of the dispersion could make the initial beam commissioning difficult.

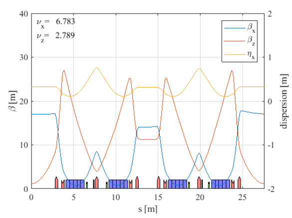

Fig. 1. Lattice functions for 500 MeV, normal operation at KARA. Momentum compaction factor is 0.0095.

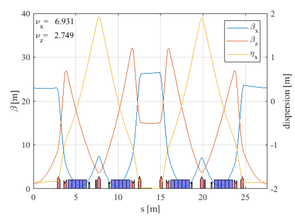

Fig. 2. Lattice functions for 500 MeV, negative alpha operation at KARA. Momentum compaction factor is -0.0081.

III. Tracking simulation

To evaluate the injection rate under manipulated alpha condition, we have peformed tracking simulations in which

e-mail: akira.mochihashi@kit.edu

we have assumed realistic conditions. The following is the conditions and values of the parameters used in the simulations.

- The simulation has been peformed in 6 dimensonal phase space considering couplings. For x-y coupling, we have introduced a skew quadrupole component for each quadrupole magnet by assuming random rotation errors whose distributions are Gaussian with $\sigma = 1$ mrad.
- We have assumed physical aperture with realistic size of the beam ducts. At the injection point, the septum wall is placed at -28 mm horizontally from the center of the physical aperture.
- The beam from the transport line passes through the injection septum and enters the storage ring. We assume a parallel beam whose horizontal position is -30 mm from the center of the physical aperture of the storage ring.
- We have 3 dipole kicker magnets for beam injection. We have assumed the waveform of the kicker excitation is half-sinusoidal with 1.94 μseconds (designed value) in full width. That means the beam can be kicked at least 3 times when we inject the beam at the peak timing of the kicker waveform.
- As the lattice parameters of the beam transport line into the storage ring, we have assumed designed values. At present, there is less measured data for the injection beam parameters. It would be one of the important tasks to investigate the injection process in the near future.
- We have settled the parameters for sextupole magnets to get the chromaticity of +1 for both directions.
- To consider the longitudinal motion of the beam, we have introduced synchrotron motion into the tracking code. In the simulation, we have assumed the RF accelerating voltage to be 330 kV which is the usual operation value at KARA for 500 MeV.
- We have ignored the radiation damping effect because it is very slow compared to the time range of the beam injection; longitudinal radiation damping time is 4.9×10^5 turns at KARA for 500 MeV.
- Initially we have prepared 1000 particles which have Gaussian distributions in 6 dimensional phase space. The tracking has been performed for a time period of 5 synchrotron oscillation periods.

Under the conditions and assumptions described above, we have performed tracking simulation for normal positive alpha, negative alpha and positive low alpha lattice conditions.

A. *Normal positive alpha lattice*

In the tracking, we have changed the amplitude of the bump orbit at the injection septum from -25 mm to -10 mm. Figure3 shows the beam loss rate for normal positive alpha lattice in Fig.1. As seen in this figure, the injection beam is completely lost at a bump orbit of -25 mm. The loss rate can be minimized with a bump orbit of -15 mm. The optimized bump orbit condition can get an injection rate of about 85%, according to the simulation.

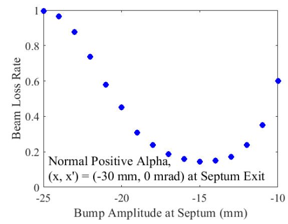

Fig. 3. Tracking result for beam loss rate at normal positive alpha condition for different bump orbit conditions.

B. *Negative alpha lattice*

Figure4 shows the result of beam loss rate for the negative alpha lattice in Fig.2. As seen in the figure, it is difficult to get a good enough and tolerable injection rate under these conditions; the maximum injection rate has been estimated to be only 30%. To improve the undesirable condition, we have adjusted the exit angle of the injection beam at the injection septum from 0 mrad (parallel beam) to -0.5 mrad. The result is shown in Fig.5. The injection rate can be improved up to 70% by adjusting the exit angle of the beam. The range of the adjustment is realistic and not drastic in our case.

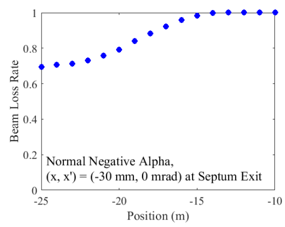

Fig. 4. Tracking result for beam loss rate at negative alpha condition for different bump orbit conditions with parallel injection beam.

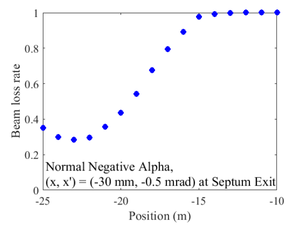

Fig. 5. Tracking result for beam loss rate at normal positive alpha condition for different bump orbit conditions with non-zero exit angle beam.

C. *Positive-low alpha lattice*

At KARA, we regularly investigate beam dynamics in short bunch operation [3] in-depth, especially for microbunching instability [4] with generation of coherent synchrotron radiation in the THz region. At present, we peform the short bunch operation by injecting the beam at 500 MeV under normal positive alpha optics, and after the injection we ramp up the energy to 1.3 GeV and perform a "beam squeezing" to change the lattice from the normal alpha to the positive-low alpha gradually. As one of the new attractive operation modes at KARA, we consider top-up operation under positive-low alpha at 500 MeV. As a trial for such operation mode, we have performed the tracking simulation under positive-low alpha lattice. To consider beam dynamics at the low alpha lattice, we have introduced both the first and second order of the momentum compaction factor. Here, we have calculated theoretically the second order momentum compaction factor from the second order dispersion function. Figure6 shows the lattice functions for a positive-low alpha for 500 MeV. The lattice has the first and second order momentum compaction factor of $(5.0 \times 10^{-4}, 0.0939)$. Figure7 shows the result of the beam loss rate under the positive-low alpha condition. An injection rate larger than 20% cannot be expected under this condition because of a mismatching of the longitudinal phase space distribution between the injection beam and the storage ring beam, e.g. a mismatching between the bunch length of the injection beam and the temporal acceptance of the storage ring at positive-low alpha mode. Some additional considerations would be needed to perform beam injection at positive-low alpha mode.

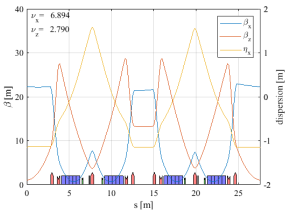

Fig. 6. Lattice functions for 500 MeV, positive low alpha operation at KARA. The first and second order of momentum compaction factors are $(0.000496, 0.0939)$.

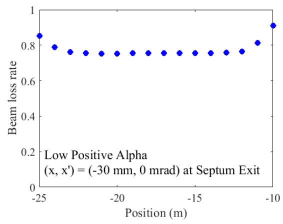

Fig. 7. Tracking result for beam loss rate at positive-low alpha condition for different bump orbit conditions.

IV. Beam commissioning at KARA in negative alpha condition

We have performed beam commissioning under negative alpha lattice at 500 MeV. As one of the basic strategies of the commissioning, we initially inject the beam under normal alpha lattice and gradually change the set values of the quadrupole magnets to approach positive low alpha with keeping beam injection. After we have reached positive-low alpha, we go across $\alpha = 0$ by changing slightly the quadrupoles and making an RF phase jump with $\sim$180 degree. The beam in the storage ring is lost when we go across $\alpha = 0$, and after the crossing we try the beam injection again.

According to this commissioning strategy, we have stored 500 MeV electron beam with negative momentum compaction factor. In the commissioning process, we have also adjusted the injection kicker bump and magnetic field strength of the bending magnets. Until February 2019, we have confirmed 2 mA of stored multibunch beam under negative alpha condition at 500 MeV. At present we continuously proceed with the beam commissioning under the negative alpha condition to increase the stored beam current and the beam injecton efficiency.

V. Next plan and interests

One of the main subjects is to get a better injection efficiency and a higher stored beam current under negative alpha condition. As seen in Fig.2, the dispersion function has a large amplitude in negative alpha condition at KARA. This large amplitude of the dispersion could cause beam loss very easily if mismatching of the beam energy between the injection beam and a central energy of the storage ring occurs. At present we consider additional simulations which can make clear the difference of the beam orbit between the injection beam and the stored beam when we have such an energy mismatching. An optimization of the injection magnets would be another subject which we should complete.

After getting enough stored beam current, we shift our main activity to the characterization of stored beam parameters such as the chromaticity. One of the main interests is to investigate the feasibility of negative alpha operation with negative chromaticity. In parallel, beam diagnostics to justify stability criteria for the head-tail instability would be the most important experiment. The other topics about collective phenomenon would be thorough investigation for the mode coupling (microwave) instability. Difference of the threshold beam current between the positive and negative alphas could become one of the hot topics in the field of collective beam instability.

References

[1] Yu. Senichev, Proceedings of Particle Accelerator Conference 2009 (May 2009, Vancouver), p. 677-679.

[2] Institute for Beam Physics and Technology (IBPT), http://www.ibpt.kit.edu

[3] A. Papash, E. Blomley, M. Brosi, J. Gethmann, B. Kehrer, A.-S. Müller, P. Schönfeldt, M. Schuh, J. L. Steinmann, Proceedings of International Particle Accelerator Conference 2018 (April-May 2018, Vancouver), p. 4235-4238.

[4] J. L. Steinmann, T. Boltz, M. Brosi, E. Bründermann, M. Caselle, B. Kehrer, L. Rota, P. Schönfeldt, M. Schuh, M. Siegel, M. Weber, A.-S. Müller, Physical Review Accelerator and Beams, 21 (11), 110705.

Editorial Series on ACCELERATOR SCIENCE

Vol. LIII
Eleonora Belli: Coupling Impedance and Single Beam Collective Effects for the Future Circular Collider (Lepton Option)

Vol. LII
Andrzej G. Chmielewski & Zbigniew Zimek (Eds): Electron Accelerators for Research, Industry and Environment – the INCT Perspective

Vol. LI
Carlotta Accettura: Ultra-high Vacuum Characterization of Advanced Materials for Future Particle Accelerators

Vol. L
Federico Carra: Thermomechanical Response of Advanced Materials under Quasi-Instantaneous Heating

Vol. XLIX
Janne Ruuskanen: Predicting Heat Propagation in Roebel Cable Based Accelerator Magnet Prototype

Vol. XLVIII
Liangliang Shi: Higher-Order-Mode-based Beam Phase and Beam Position Measurements in Superconducting Accelerating Cavities at the European XFEL

Vol. XLVII
Raphael Kleindienst: Radio Frequency Characterization of Superconductors for Particle Accelerators

Vol. XLVI
Sebastian Keckert: Optimizing a Calorimetry Chamber for the RF Characterization of Superconductors

Vol. XLV
Maurizio Vretenar (Ed.): Final EuCARD-2 Project Report

Vol. XLIV
Frank Zimmermann (Ed.): Strategy for Future Extreme Beam Facilities

Vol. XLIII
Mike Seidel (Ed.): The Energy Efficiency of Proton Driver Accelerators

Vol. XLII
Andrzej Rychter: Measurement Based Characterisation and Modelling of Micropixel Avalanche Photodiodes

Vol. XLI
Rafał Graczyk: Reliability and Performance Modeling of Configurable Electronic Systems for Unmanned Spacecraft

Vol. XL
Maciej Lipiński: Methods to Increase Reliability and Ensure Determinism in a White Rabbit Network

Vol. XXXIX
Antonella Chiuchiolo: Cryogenic Fiber Optic Sensors for Superconducting Magnets and Power Transmission Lines in High Energy Physics Applications

Vol. XXXVIII
Oscar Frasciello: Wake Fields and Impedance Calculations of LHC Collimators' Real Structures

Vol. XXXVII
Sławomir Wronka: Interlaced Energy Linac with Smooth Energy Regulation

Vol. XXXVI
Lucas Nathan Brouwer: Canted-Cosine-Theta Superconducting Accelerator Magnets for High Energy Physics and Ion Beam Cancer Therapy

Vol. XXXV
Nicholas C. Shipman: Experimental Study of DC Vacuum Breakdown and Application to High-Gradient Accelerating Structures for CLIC

Vol. XXXIV
Tiina Salmi: Optimization of Quench Protection Heater Performance in High-Field Accelerator Magnets Through Computational and Experimental Analysis

Vol. XXXIII
Thomas Flisgen: Compact State-Space Models for Complex Superconducting Radio-Frequency Structures Based on Model Order Reduction and Concatenation Methods

Vol. XXXII
Marija Cauchi: Thermo-Mechanical Studies of Large Hadron Collider Collimators in Accident Scenarios

Vol. XXXI
Daniele Mirarchi: Crystal Collimation for LHC

Vol. XXX
Grzegorz Korcyl: A Novel Data Acquisition System Based on Fast Optical Links and Universal Readout Boards

Vol. XXIX
Marcello Spera: Pinning Mechanisms in YBCO Tapes

Vol. XXVIII
Adrian Fiergolski: Hardware Implementation of the Track Identification Algorithm in the Scalable Readout System for the TOTEM Experiment

Vol. XXVII
Bartłomiej Juszczyk, Grzegorz Kasprowicz: MicroTCA Based Platform for Advanced Particle Accelerators Diagnostics

Vol. XXVI
Michał Kozieł: Development of Radiation Hardened Pixel Sensors for Charged Particle Detection

Vol. XXV
Ben Hall: Designing the Four Rod Crab Cavity for the High-Luminosity LHC Upgrade

Vol. XXIV
José Luis Abelleira Fernández: Optics Designs of Final-Focus Systems for Future LHC Upgrades

Vol. XXIII
César Octavio Domínguez Sánchez de la Blanca: Electron Cloud Studies for the LHC and Future Proton Colliders

Vol. XXII
Jean-Pierre Koutchouk and Agnes Szeberenyi (Eds): EuCARD Final Project Report

Vol. XXI
Tomasz Pławski: Digital RF Control System for Superconducting Cavity with Large Lorentz Force Detuning Coefficient

Vol. XX
Maciej Kwiatkowski: Methods for the Application of Programmable Logic Devices in Electronic Protection Systems for High Energy Particle Accelerators

Vol. XIX
Gianluca Valentino: Fast Automatic Beam-Based Alignment of the LHC Collimator Jaws

Vol. XVIII
Krzysztof Czuba: RF Phase Reference Distribution System for TESLA Technology Based Projects

Vol. XVII
Anna Wysocka-Rabin: Advances in Conformal Radiotherapy. Using Monte Carlo Code to Design New IMRT and IORT Accelerators and Interpret CT Numbers

Vol. XVI
Pei Zhang: Beam Position Diagnostics with Higher Order Modes in Third Harmonic Superconducting Accelerating Cavities

Vol. XV
Tobias Junginger: Investigation of the Surface Resistance of Superconducting Materials

Vol. XIV
Michał Dziewiecki: Measurement-based Characterization of Multipixel Avalanche Photodiodes for Scintillating Detectors

Vol. XIII
Matthew Alexander Fraser: Beam Dynamics Studies of the ISOLDE Post-Accelerator for the High Intensity and Energy Upgrade

Vol. XII
Claire Antoine: Materials and Surface Aspects in the Development of SRF Niobium Cavities

Vol. XI
Grzegorz Kasprowicz: Determination of Beam Intensity and Position in a Particle Accelerator

Vol. X
Wolfgang Weingarten: European Infrastructures for R&D and Test of Superconducting Radio-Frequency Cavities and Cryo-Modules

Vol. IX
Vasim Khan: A Damped and Detuned Accelerating Structure for the Main Linacs of the Compact Linear Collider

Vol. VIII
Paweł Gryboś: Front-end Electronics for Multichannel Semiconductor Detector Systems

Vol. VII
Tomasz Czarski: Complex Envelope Control of Pulsed Accelerating Fields in Superconducting Cavities

Vol. VI
Guido Sterbini: An Early Separation Scheme for the LHC Luminosity Upgrade

Vol. V
Helmut Mais: Some Topics in Beam Dynamics of Storage Rings

Vol. IV
Roy Aleksan and Olivier Napoly (Eds): Coordinated Accelerator Research in Europe. Summary of Project Achievements

Vol. III
Zbigniew Szadkowski: Triggers for the Pierre Auger Observatory, the Current Status and Plans for the Future

Vol. II
Krzysztof Poźniak: Detektorowe systemy pomiarowe typu TRIDAQ w eksperymentach fizyki wysokich energii (TRIDAQ Detector Systems for High Energy Physics Experiments)

Vol. I
Jacek Sekutowicz: Multi-cell Superconducting Structures for High Energy e^{+} e^{-} Colliders and Free Electron Laser Linacs